

AFML-TR-71-231

AD 742282

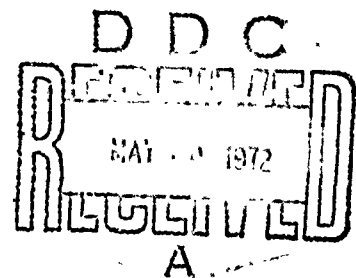
# MICROBUCKLING OF UNIDIRECTIONAL COMPOSITES

L. B. GRESZCZUK

McDONNELL DOUGLAS ASTRONAUTICS COMPANY

TECHNICAL REPORT AFML-TR-71-231

JANUARY 1972



Approved for public release; distribution unlimited.

Reproduced by  
NATIONAL TECHNICAL  
INFORMATION SERVICE  
Springfield, Va. 22151

AIR FORCE MATERIALS LABORATORY  
AIR FORCE SYSTEMS COMMAND  
WRIGHT-PATTERSON AIR FORCE BASE, OHIO 45433

105

NOTICE

When Government drawings, specifications, or other data are used for any purpose other than in connection with a definitely related Government procurement operation, the United States Government thereby incurs no responsibility nor any obligation whatsoever; and the fact that the government may have formulated, furnished, or in any way supplied the said drawings, specifications, or other data, is not to be regarded by implication or otherwise as in any manner licensing the holder or any other person or corporation, or conveying any rights or permission to manufacture, use, or sell any patented invention that may in any way be related thereto.

Source: per telecon  
by DDC-TCA;  
McDonnell Douglas Prime Contract  
is F33615-71-C-1090 (see  
forward). F33615-67-C-1569  
is Prime Contract with Ohio  
State Univ. Research Foundation,  
Columbus. Much work under  
this contract has been sub-  
contracted (See Contract Card,  
DOC files).

  
26 May 72

ACCESSION REF	
OFSTI	WHITE SECTION <input checked="" type="checkbox"/>
DDC	BUFF SECTION <input type="checkbox"/>
UNANNOUNCED	
JUSTIFICATION	
DISTRIBUTION AVAILABILITY CODES	
DIST.	AVAIL. and/or SPECIAL
A	

Copies of this report should not be returned unless return is required by security considerations, contractual obligations, or notice on a specific document.

UNCLASSIFIED

Security Classification

DOCUMENT CONTROL DATA - R & D

(Security classification of title, body of abstract and indexing annotation must be entered when the overall report is classified)

1. ORIGINATING ACTIVITY (Corporate author) McDonnell Douglas Astronautics Company <del>West</del> Huntington Beach, California		2a. REPORT SECURITY CLASSIFICATION Unclassified
3. REPORT TITLE Microbuckling of Unidirectional Composites		2b. GROUP
4. DESCRIPTIVE NOTES (Type of report and inclusive dates) Technical Report AFML-TR-71-231 - September 1969 - May 1971.		
5. AUTHOR(S) (First name, middle initial, last name) L. B. Greszczuk		
6. REPORT DATE January 1972	7a. TOTAL NO. OF PAGES 110	7b. NO. OF REFS 14
8a. CONTRACT OR GRANT NO.	9a. ORIGINATOR'S REPORT NUMBER(S)	
b. PROJECT NO.	9b. OTHER REPORT NO(S) (Any other numbers that may be assigned this report) AFML-TR-71-231	
c.		
d.		
10. DISTRIBUTION STATEMENT Approved for public release; distribution unlimited.		
11. SUPPLEMENTARY NOTES		12. SPONSORING MILITARY ACTIVITY Air Force Materials Laboratory Wright-Patterson Air Force Base Dayton, Ohio 45433
13. ABSTRACT A review is presented of the theories for microbuckling of unidirectional composites subjected to compressive loading parallel to the fiber direction. The results predicted by the various theories are compared. Large differences in predicted results are shown to exist for microbuckling in the extension mode. In the case of microbuckling in the shear mode, the various theories predict the same results. Nearly perfect (as compared to actual composites) model composites consisting of circular rods in an epoxy matrix are employed to obtain experimental data on failure of unidirectional composites subjected to compressive loading. The constituent materials used in preparation of model composites are characterized for their mechanical properties. Two types of reinforcement materials and four different resins are used in the experimental phase of the program. Anisotropic graphite rods with a modulus of elasticity of $\approx 12 \times 10^6$ psi and a degree of anisotropy of 10, and stainless steel rods with moduli of elasticity of $\approx 27 \times 10^9$ psi are used as the reinforcement materials. Resins with moduli of elasticity of approximately 2,000 psi, 100 ksi, 180 ksi, and 460 ksi are used as the matrix materials. Most of the tests are performed on composite specimens consisting of nine rods imbedded in a resin. The nominal volume fraction of the reinforcement is 50 percent. The test variables are specimen geometry, fiber diameter, and properties of constituents. In the case of low-modulus resin composites, the failures are by microbuckling in the shear mode. For intermediate-modulus resin composites, the failures are by inelastic microbuckling in the case of ductile reinforcement and by transverse tension in the case of brittle reinforcement. In the case of high-modulus resin composites, the failure is by compressive failure of the reinforcement. The experimental results for specimens that failed by microbuckling are shown to be higher		

DD FORM 1473  
1 NOV 68

Unclassified  
Security Classification

ABSTRACT (CONTINUED)

DOCUMENT CONTROL DATA - R & D  
(Continued)

than the theoretical results predicted from a two-dimensional microbuckling theory. A semi-empirical, three-dimensional theory shows an improved test-theory correlation. Data are also presented on the effect of shear modulus and Young's modulus of the matrix on the compressive strength of composites. Finally, preliminary results are presented on the effect of initial fiber deformation and repeated loading on the composite compressive strength. Possible reasons for the low compressive strength of composite: such as graphite epoxy are briefly discussed.

Unclassified

Security Classification

14. KEY WORDS	LINK A		LINK B		LINK C	
	ROLE	WT	ROLE	WT	ROLE	WT
Compression Failures Microbuckling Unidirectional Composites Model Studies						

Unclassified

Security Classification

AFML-TR-71-231

# MICROBUCKLING OF UNIDIRECTIONAL COMPOSITES

*L. B. GRESZCZUK*

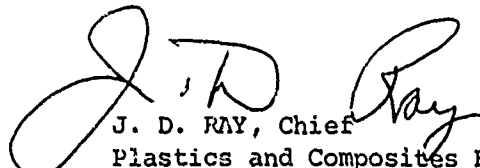
Details of illustrations in  
this document may be better  
studied on microfiche

Approved for public release; distribution unlimited.

FOREWORD

This report was prepared by L. B. Greszczuk of McDonnell-Douglas Astronautics Company, West, Huntington Beach, CA under USAF Contract Nrs. F33615-67-C-1559 and *new* F33615-71-C-1070, Project Nr. 7340, "Nonmetallic and Composite Materials", Task Nr. 734003, "Structural Plastics and Composites". The work was accomplished under the technical direction of N. J. Pagano (LNC), W-PAFB, Ohio 45433.

This report covers the research efforts of the period September 1969 - May 1971. This report was submitted in July 1971. This technical report has been reviewed and is approved.

  
J. D. RAY, Chief  
Plastics and Composites Branch  
Nonmetallic Materials Division  
Air Force Materials Laboratory

## ABSTRACT

A review is presented of the theories for microbuckling of unidirectional composites subjected to compressive loading parallel to the fiber direction. The results predicted by the various theories are compared. Large differences in predicted results are shown to exist for microbuckling in the extension mode. In the case of microbuckling in the shear mode, the various theories predict the same results. Nearly perfect (as compared to actual composites) model composites consisting of circular rods in an epoxy matrix are employed to obtain experimental data on failure of unidirectional composites subjected to compressive loading. The constituent materials used in preparation of model composites are characterized for their mechanical properties. Two types of reinforcement materials and four different resins are used in the experimental phase of the program. Anisotropic graphite rods with a modulus of elasticity of  $\approx 12 \times 10^6$  psi and a degree of anisotropy of 10, and stainless steel rods with moduli of elasticity of  $\approx 27 \times 10^6$  psi are used as the reinforcement materials. Resins with moduli of elasticity of approximately 2,000 psi, 100 ksi, 180 ksi, and 460 ksi are used as the matrix materials. Most of the tests are performed on composite specimens consisting of nine rods imbedded in a resin. The nominal volume fraction of the reinforcement is 50 percent. The test variables are specimen geometry, fiber diameter, and properties of constituents. In the case of low-modulus resin composites, the failures are by microbuckling in the shear mode. For intermediate-modulus resin composites, the failures are by inelastic microbuckling in the case of ductile reinforcement and by transverse tension in the case of brittle reinforcement. In the case of high-modulus resin composites, the failure is by compressive failure of the reinforcement. The experimental results for specimens that failed by microbuckling are shown to be higher than the theoretical results predicted from a two-dimensional microbuckling theory. A semi-empirical, three-dimensional theory shows an improved test-theory correlation. Data are

also presented on the effect of shear modulus and Young's modulus of the matrix on the compressive strength of composites. Finally, preliminary results are presented on the effect of initial fiber deformation and repeated loading on the composite compressive strength. Possible reasons for the low compressive strength of composites such as graphite epoxy are briefly discussed.

## CONTENTS

<u>Section</u>	<u>Title</u>	<u>Page</u>
	INTRODUCTION	1
1	THEORIES FOR MICROBUCKLING OF UNIDIRECTIONAL COMPOSITES	3
2	EXPERIMENTAL STUDIES ON MICROBUCKLING OF UNIDIRECTIONAL COMPOSITES	15
3	INFLUENCE OF FIBER DIAMETER ON COMPRESSIVE STRENGTH OF UNIDIRECTIONAL COMPOSITES	41
4	INFLUENCE OF CONSTITUENT PROPERTIES ON MICROSTABILITY OF UNIDIRECTIONAL COMPOSITES	57
5	FURTHER DISCUSSION OF RESULTS	73
6	CONCLUSIONS	79
	REFERENCES	81
Appendix	COMPOSITE SPECIMEN TEST DATA	83

## ILLUSTRATIONS

<u>Figure</u>	<u>Title</u>	<u>Page</u>
1	Possible Buckling Patterns for Unidirectional Composites	4
2	Microbuckling Failure Domains [4]	6
3	Comparison of Microbuckling Solutions for Composites With Low Fiber Volume Fraction ( $k=1.64$ percent)	10
4	Comparison of Exact and Approximate Buckling Solutions of Sadowsky [5] and Herrmann [6, 7] for Composites with Low Fiber Volume Fraction	11
5	Comparison of Buckle Wave Lengths in Composites With Low Fiber Volume Fraction	12
6	Comparison of Solutions for Buckling in the Shear Mode	13
7	Failure Domains for Composite Compression Specimens	16
8	Typical Stress-Strain Curves for Resins	18
9	Typical Compressive Stress-Strain Curve for 0.076-In. - Diameter Graphite Rod	19
10	Graphite Rod Axial Compression Specimen and Several Failed Specimens (5X)	20
11	Transverse Compression Specimen and Specimen After Failure (5X)	21
12	Five-Rod Composite Compression Specimens Used in Preliminary Testing (2X)	23
13	Test-Theory Correlation for Compressive Strength of Five-Rod Composite Specimens	24
14	Compression Failure of Urethane Resin Composite Specimen (5X)	25

<u>Figure</u>	<u>Title</u>	<u>Page</u>
15	Compression Failure of Hysol Resin Composite Specimen (5X)	26
16	Compression Failure of RTC Resin Composite Specimen (5X)	27
17	Compression Load Versus Machine Head Travel for Five-Rod Urethane Resin Composites	29
18	Typical Nine-Rod Compression Specimens Made of Graphite Rods and Urethane Resin	30
19	Test-Theory Correlation for Compressive Strength of Nine-Rod Composite Specimens	31
20	Nine-Rod Urethane Resin Compression Specimens After Failure (2.5X)	34
21	Nine-Rod Hysol Resin Compression Specimens After Failure (3X)	35
22	Twenty-Five Rod Urethane Resin Composite Specimen After Failure	36
23	Typical Stress-Strain Curves for Urethane Resin Composites	37
24	Load-Deflection Curves for Specimens that Did Not Fail by Microbuckling	38
25	Load-Deflection Curve for Twenty-Five-Rod Graphite-Urethane Composite That Failed by Microbuckling	39
26	Compressive Strength Versus Fiber Diameter for Fiber Glass Composites [12]	42
27	Experimental Results for Fiber Buckling Wave Length as a Function of Fiber Diameter [3]	42
28	Aluminum Molds for Preparation of Composites	45
29	Resin Casting and Typical Unidirectional Graphite Fiber-Hysol Resin Composites made with 0.079-, 0.060-, 0.045-, and 0.030-In. -Diameter Rods	47

<u>Figure</u>	<u>Title</u>	<u>Page</u>
30	Effect of Fiber Diameter on the Compressive Strength of Composites and Fiber Failure Stresses	49
31	Effect of Fiber Diameter and L/W Ratio on the Compressive Strength of Graphite Fiber-Hysol Resin Composites	50
32	Typical Load-Deflection Curves for Hysol Resin Composites That Failed by Compressive Failure of the Reinforcement	51
33	Typical Stress-Strain Curves for Hysol Resin Composites Subjected to Compressive Loading	52
34	Typical Compression Stress-Strain Curve for Urethane Resin Cured According to the Modified Cure Cycle	53
35	Compression Stress-Strain Curves for Resins A and B	59
36	Effect of Resin Properties on Compressive Failure of Composites Made With Steel Fibers	61
37	Effect of Repeated Loading on Microbuckling of Steel-Urethane Unidirectional Composite	62
38	Compression Failure Modes of Composites Made with Graphite Fibers and Epoxy A	63
39	Failed Composite Specimens made of S, Steel Fibers and Urethane, Epoxy B, and Epoxy A Resins (L = 1.5 In.)	65
40	Failed Composite Specimens Made of S, Steel Fibers and Urethane, Epoxy B, and Epoxy A Resins (L = 2.5 In.)	66
41	Test-Theory Comparison of Compressive Strength of Urethane Resin Composites Reinforced With Graphite and Stainless Steel Fibers	67
42	Effect of Resin Shear Modulus on the Compressive Strength of Graphite Fiber Composites	68
43	Effect of Resin Shear Modulus on the Compressive Strength of Stainless Steel Fiber Composites	69
44	Effect of Initial Deformation on Microbuckling	71

<u>Figure</u>	<u>Title</u>	<u>Page</u>
45	Comparison of Test Data for Graphite Fiber Composites With the Results Predicted by Two-Dimensional and Semi-Empirical Three-Dimensional Microbuckling Theory	74
46	Effect of Young's Modulus of the Resin on the Non-Microbuckling Compressive Strength of Graphite Fibers at Failure of Composites	76

## TABLES

<u>Table</u>	<u>Title</u>	<u>Page</u>
I	Values of $\delta_f^*$ (for $\nu_r = 0.4$ )	7
II	Average Properties of Graphite Rods	17
III	Average Properties of Resins	17
IV	Effect of Diameter on the Flexure Strength and Modulus of Graphite Rods	46
V	Test-Theory Comparison of Composite Microbuckling	55
VI	Mechanical Properties of Reinforcement Materials	58
VII	Mechanical Properties of Resins Used in Models	58
VIII	Test-Theory Comparison Assuming Elastic and Inelastic Microbuckling	70

## SYMBOLS

$A_f$	=	Cross-sectional area of the fiber
$a_s$	=	Beam shear deformation coefficient of the fiber
$2c$	=	Thickness of the matrix between fibers (see Figure 1)
$E$	=	Young's modulus
$G$	=	Shear modulus
$G_{LT}$	=	Shear modulus of composite with circular fibers
$h$	=	Fiber diameter or reinforcement thickness (see Figure 1)
$I_f$	=	Moment of inertia of fiber's cross section
$k$	=	Volume fraction of fibers
$k_1$	=	Modulus of foundation associated with extension
$k_2$	=	Modulus of foundation associated with rotation
$K_0(\beta r_0), K_1(\beta r_0)$	=	Modified Bessel functions of the second kind
$l, l_{cr}$	=	Buckle wave length
$L$	=	Length of composite specimen
$m$	=	Number of buckle waves

$P$	= Compressive load
$r_0$	= Fiber diameter
$w$	= Width of the composite specimen
$\alpha_1$	= $\pi h/l$
$\alpha_2$	= $\pi c/l$
$\beta$	= $2\pi/l$
$\delta_f^*$	= Critical dimensionless contraction of the fiber during microbuckling
$\delta_E^*$	= Critical dimensionless contraction of the microfibers for microbuckling in the extension mode
$\delta_S^*$	= Critical dimensionless contraction of the microfibers for microbuckling in the shear mode
$\sigma_{CE}$	= Critical composite stress for buckling in the extension mode
$\sigma_{CS}$	= Critical composite stress for buckling in the shear mode
$\nu$	= Poisson's ratio

#### Subscripts

$c, C$	Denotes composite
$E$	Denotes microbuckling in extension mode
$f$	Denotes fiber
$r$	Denotes resin or matrix

S Denotes microbuckling in shear mode

$(\sigma_{CS})_n$   $(\sigma_{CE})_n$  Subscripts 1, 2, 3, —denote solutions obtained by various  
 $(n = 1, 2, 3)$  authors

## INTRODUCTION

The compressive strength of filamentary composites such as graphite-epoxy has been found to be significantly lower than the theoretical values predicted by the microbuckling theory. Whereas the predicted compressive strength values of unidirectional composites are in the range of 350 to 550 ksi, the experimentally obtained values fall around 60 to 180 ksi. For boron-epoxy composites, a somewhat closer correlation exists between experiments and theory. Compressive composite strength as high as 370 ksi has been measured experimentally, while the theory predicts strengths of the order of 400 ksi.

The low experimental compressive strength values of graphite-epoxy composites and the large discrepancies between test and theory have led to AFML-initiated studies on behavior of composites subjected to compressive loading. The primary objectives of these studies were (1) to establish, through testing of nearly perfect composite models, if microbuckling is a valid failure mode; (2) to verify the accuracy of the two-dimensional microbuckling theory and/or establish its inadequacies; and (3) to identify some of the more important parameters influencing the compressive strength of composites.

Although the studies were primarily experimental, an extensive review has also been conducted of the theoretical work on microbuckling of composites. Following the literature survey and comparison of results predicted by various microbuckling theories, tests were performed on model composites consisting of various combinations of reinforcement and matrix materials. Composites that were selected for experimental evaluation included those designed to fail by microbuckling and those designed to fail by compressive failure of the reinforcement (no microbuckling). The experimental results were compared

with the theoretically predicted values. The experimental results were used to arrive at preliminary conclusions relevant to the primary objectives of the study.

Section 1  
THEORIES FOR MICROBUCKLING OF  
UNIDIRECTIONAL COMPOSITES

A number of papers have been devoted to studying microbuckling as a possible failure mechanism for unidirectional composites subjected to a compressive force in the fiber direction. Fiber microbuckling as a failure mode was apparently first suggested by Dow [1]. Using Timoshenko's column-on-elastic-foundation approach [2], Rosen has obtained the equation for predicting the external loads at which fiber microbuckling takes place [3]. The two possible buckling patterns for which equations were derived by Rosen were the "extension" mode and the "shear" mode. They are illustrated in Figure 1. In the case of the extension mode, the following equation gives the composite stress,  $\sigma_{CE}$ , at which microbuckling takes place.

$$(\sigma_{CE})_1 = 2k \left[ \frac{E_f E_r k}{3(1-k)} \right]^{1/2} \quad (1)$$

where

$$k = \text{fiber volume fraction} \left[ k = h/(h + 2c) \right]$$

$E_f$  = modulus of elasticity of the fiber

$E_r$  = modulus of elasticity of the resin

This equation was derived for a two-dimensional model and applies to composites with low fiber volume fractions ( $k < 20$  percent) and having large numbers of buckle wave lengths. If the number of wave lengths is small, then the following equation applies [3].

$$(\sigma_{CE})_1^* = \frac{\pi^2 E_f h^2 k}{12L^2} \left[ m^2 + \frac{24L^4 E_r}{\pi^4 c h^3 E_f} \left( \frac{1}{m^2} \right) \right] \quad (2)$$

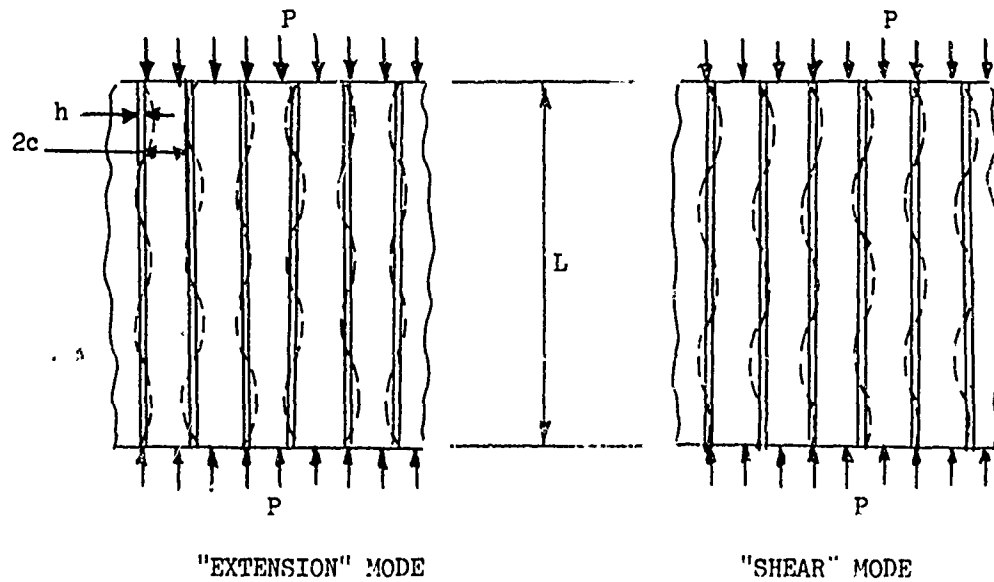


Figure 1. Possible Buckling Patterns for Unidirectional Composites

where  $m$  is the number of buckle waves and the remaining terms are defined in Figure 1. In the case of buckling in the shear mode, Rosen gives the following equation for the composite stress that will cause microbuckling.

$$(\sigma_{CS})_1 = \frac{G_r}{(1-k)} \quad (3)$$

where  $G_r$  is the shear modulus of the resin. Equation (3) was also derived for a two-dimensional model and applied to composites with large numbers of buckling waves. The more complete equation for any number of wave lengths was given as

$$(\sigma_{CS})_1 = \frac{G_r}{1-k} + \frac{\pi^2 E_f k}{12} \left( \frac{mh}{L} \right)^2 \quad (4)$$

Results similar to those of Rosen were also obtained by Schuerch [4], who also used Reference 2 as a basis for obtaining the microbuckling equations. In the present notation, the equations given by Schuerch for the critical composite stresses for the two buckling modes are

$$(\sigma_{CE})_2 = \left[ \frac{2}{(3)^{1/2}} \right] [kE_r] \left( \frac{k E_f}{1 - k E_r} \right)^{1/2} \left[ 1 + \frac{1 - k E_r}{k E_f} \right] \quad (5)$$

for the extensional mode and

$$(\sigma_{CS})_2 = \frac{G_r}{1 - k} \quad (6)$$

for the shear mode. The above equations also apply to a two-dimensional problem. Equation (6) is identical to that given by Rosen. Equation (5) differs from the corresponding equation given by Rosen [Equation (1)] by the presence of the underlined term in brackets in Equation (5). Since for practical composites  $(1 - k)E_r/E_f k \ll 1$ , therefore, with this condition, a complete agreement is obtained between the results of Rosen and Schuerch.

In addition to obtaining the equations for microbuckling of composites, Schuerch has also established the boundary where each buckling mode predominates. It is given by the following equation.

$$\frac{E_f}{E_r} = \left[ \frac{16}{3} (1 + \nu_r)^2 (1 - k)k^3 \left( 1 + \frac{E_r}{E_f} \frac{1 - k}{k} \right)^2 \right]^{-1} \quad (7)$$

where in addition to the previously described terms,  $\nu_r$  is the Poisson's ratio of the resin. The domains according to Equation (7) are shown in Figure 2. This graph shows that for composites with  $k > 0.2$  and  $E_f/E_r > 5$ , the shear buckling mode will prevail.

The results of both Rosen and Schuerch are for two-dimensional models and must be regarded as only a first approximation to actual composites.

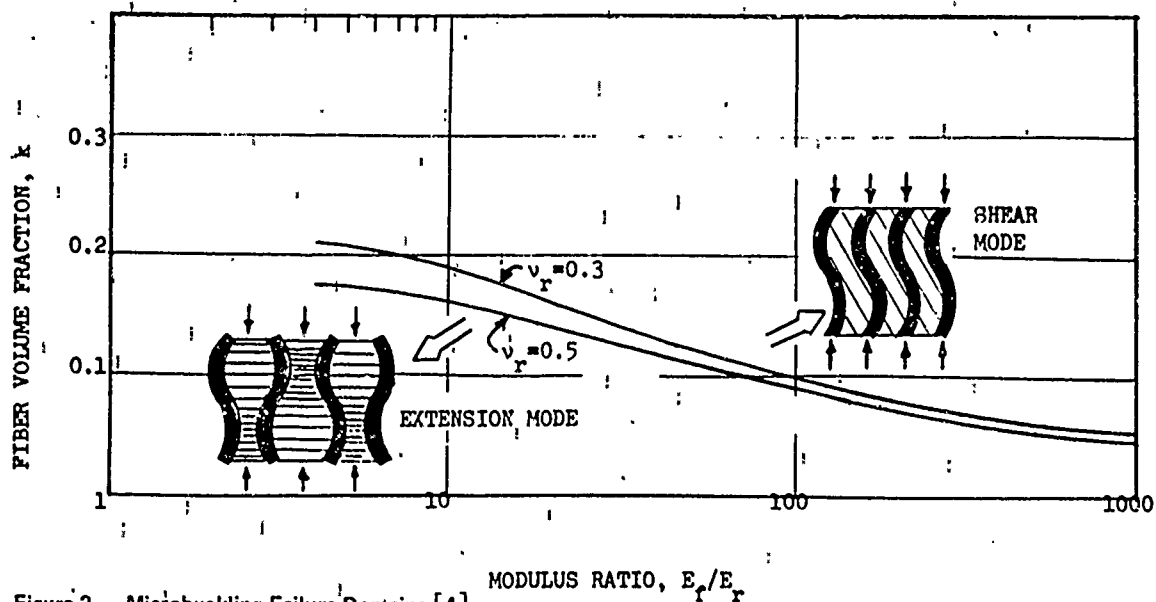


Figure 2. Microbuckling Failure Domains [4]

More recently Sadowsky, Pu, and Hussain [5] have performed a more rigorous analysis of the problem of microbuckling of composites. Their model consisted of an infinitely long circular fiber surrounded and bonded by matrix material of infinite extent. The stresses applied on the fiber by the matrix were derived from the three-dimensional, classical, linear mathematical theory of elasticity. Other assumptions made in their analysis were that:

- A. The volume percentage of fibers is small so that the mutual interference of fibers is negligible, and the matrix surrounding a fiber can be considered as infinitely large.
- B. The diameter of the fiber is very small in comparison to its length, so that the fiber may be treated as a linear fiber with infinite length.
- C. The constituents are homogeneous and isotropic and, therefore, the classical linear theory of elasticity applies.
- D. There is no twisting moment applied to the fiber by the matrix. The microfiber was therefore assumed to buckle in a plane similar to the case of Euler's column.

The results obtained by Sadowsky, et al. were obtained with and without couple stresses. No appreciable difference was found between the two for the case when  $E_f/E_r > 50$ . The equation for critical load on the fiber to cause microbuckling was given as

$$P_{cr} = \delta_f^* \pi r_o^2 E_f \quad (8)$$

where  $r_o$  is the fiber radius and  $\delta_f^*$  is the critical dimensionless relative contraction of the microfiber. The values of  $\delta_f^*$  as a function of  $E_f/E_r$  are given in Table I for the case of  $\nu_r = 0.4$  and when the couple stresses are ignored. As stated in Reference 5, the effect of  $\nu_r$  on  $\delta_f^*$  is negligible. Expressing Equation (8) in terms of composite stress

$$(\sigma_{CE})_3 = k \delta_f^* E_f \quad (9)$$

The solution for the problem of microbuckling of a single round fiber imbedded in a matrix has also been obtained by Herrmann, Mason, and Chan [6, 7]. A beam-on-elastic-foundation approach was used to solve the problem. Herrmann et al. give an "exact" and an "approximate" solution for the problem. In the exact solution, the foundation is considered as a three-dimensional continuous body. All the equations of elasticity for the matrix and all the displacement and force continuity requirements between the matrix and the fiber are satisfied. In the approximate solution, an approximate foundation model is used that does not completely satisfy the displacement and force continuity requirements between the matrix and the

Table I  
VALUES OF  $\delta_f^*$  (FOR  $\nu_r = 0.4$ )

$E_f/E_r$	10	30	50	80	100	300	500	800	1,000	5,000
$\delta_f^*$	0.355	0.188	0.142	0.106	0.095	0.052	0.038	0.030	0.025	0.010

fiber. In the approximate solution, the normal foundation reaction is considered as being of primary importance, and the modulus of foundation associated with rotation is assumed to be negligible.

The equation for the compressive force necessary to hold the fiber in the deformed shape is [ 6 ]

$$P = E_f I_f \beta^2 + \frac{k_2}{\beta} - k_1 \left( \frac{1}{\beta^2} + \frac{E_f I_f a_s}{A_f G_f} \right) \quad (10)$$

where

$I_f$  = Moment of inertia of fiber's cross section

$k_1$  = Modulus of foundation associated with extension

$k_2$  = Modulus of foundation associated with rotation

$a_s$  = Beam shear deformation coefficient of the fiber

$G_f$  = Shear modulus of the fiber

$A_f$  = Cross-sectional area of the fiber

$\beta = 2\pi/\ell$ , where  $\ell$  is the wave length of deformed fiber

The buckling load,  $P_{cr}$ , and the critical wave length,  $\ell_{cr} = 2\pi/\beta_{cr}$ , are determined by selecting  $\beta$  such that Equation (10) yields a minimum value of  $P$ . The terms  $k_1$  and  $k_2$  are very involved functions of  $\beta$ , which necessitates numerical minimization of Equation (10) to obtain the solution for  $P_{cr}$ . In the approximate solution obtained by Herrmann et al. [ 6, 7 ], it was assumed that  $k_2 = 0$ . The approximate expression for  $k_1$  was obtained as

$$k_1 = \frac{16\pi G_r (1 - \nu_r)}{2(3 - 4\nu_r) K_0(\beta r_o) + r_o \beta K_1(\beta r_o)} \quad (11)$$

where  $K_0(\beta r_o)$  and  $K_1(\beta r_o)$  are the modified Bessel functions of the second kind.

The most recent solution for the problem of microbuckling of unidirectional composites was obtained by Chung and Testa [8]. The solution presented in Reference 8 is rigorous; however, it is for a two-dimensional problem. The solution is obtained using the beam-on-elastic-foundation approach. In addition to presenting a rigorous solution, which requires use of numerical techniques to obtain the roots of the characteristic equation, Chung and Testa also present various approximate solutions, based also on the beam-on-elastic foundation approach. The approximate solution for the critical buckling strain in an extension mode was given as [8].

$$\delta_E = \frac{\alpha_1^2}{3} + \frac{4 \cosh^2 2\alpha_2 + 4\alpha_1^2 \sinh^2 2\alpha_2 + 4\alpha_1 (1 - \nu_r) \sinh 2\alpha_2 \cosh 2\alpha_2 - 8\alpha_1\alpha_2 (1 + \nu_r)}{\frac{2\alpha_1 E_f (1 + \nu_r)}{E_r} [(3 - \nu_r) \sinh 2\alpha_2 \cosh 2\alpha_2 - 2\alpha_2 (1 + \nu_r)]} \quad (12)$$

while the solution for the critical buckling strain in the shear mode was given as

$$\delta_S = \frac{\alpha_1^2}{3} + \frac{4 \sinh^2 2\alpha_2 + 4\alpha_1^2 \cosh^2 2\alpha_2 + 4\alpha_1 (1 - \nu_r) \sinh 2\alpha_2 \cosh 2\alpha_2 + 8\alpha_1\alpha_2 (1 + \nu_r)}{\frac{2\alpha_1 E_f (1 + \nu_r)}{E_r} [(3 - \nu_r) \sinh 2\alpha_2 \cosh 2\alpha_2 + 2\alpha_2 (1 + \nu_r)]} \quad (13)$$

where

$$\alpha_1 = \frac{\pi h}{\ell}$$

$$\alpha_2 = \frac{\pi c}{\ell}$$

$$\delta_S = -\frac{\sigma_f}{E_f} = -\frac{\sigma_r}{E_r}$$

$$\delta_E = -\frac{\sigma_f}{E_f} = -\frac{\sigma_r}{E_r}$$

$\ell$  is the buckle wave length, and  $h$  and  $c$  are defined in Figure 1. By assuming that the buckle wave length is long as compared to fiber spacing ( $2c \ll \ell$ ) and  $\nu_r = 0$ , Chung and Testa have shown that Equations (12) and (13) reduce to Equations (1) and (3), respectively (Rosen's equations).

For the case of short buckle wave lengths ( $2c > \ell$ ), Chung and Testa obtained the following single equation for buckling in the extensional and shear modes.

$$\delta = \left[ \frac{3E_r}{E_f(1+\nu_r)(3-\nu_r)} \right]^{\frac{2}{3}} + \frac{2E_r(1-\nu_r)}{E_f(1+\nu_r)(3-\nu_r)} \quad (14)$$

The comparison of solutions obtained by various authors is shown in Figures 3, 4, 5, and 6. Figure 3 shows the comparison of solutions of Sadowsky, et al. [5], Chung and Testa [8], Rosen [3], and Schuerch [4] for

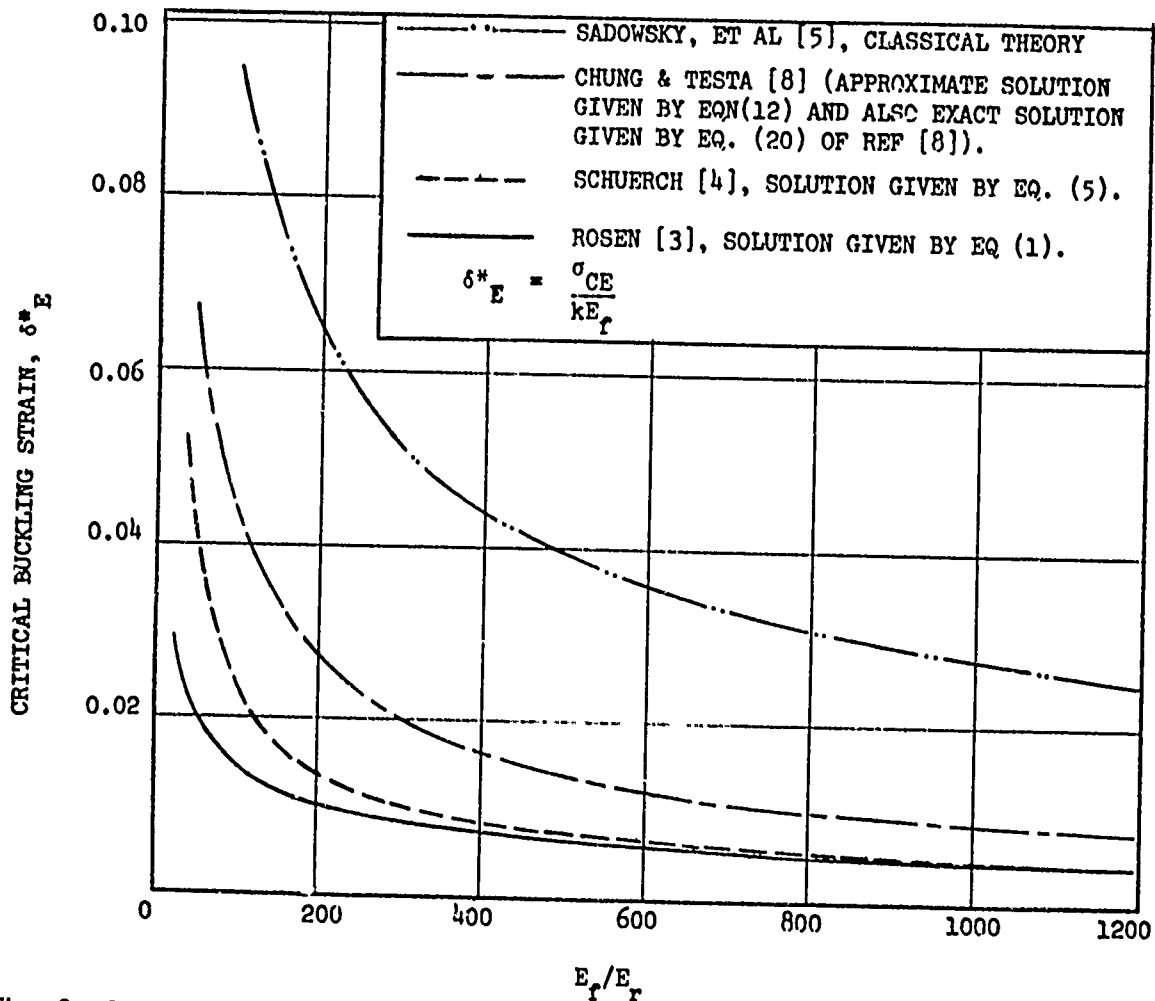


Figure 3. Comparison of Microbuckling Solutions for Composites With Low Fiber Volume Fraction ( $k = 1.64$  Percent)

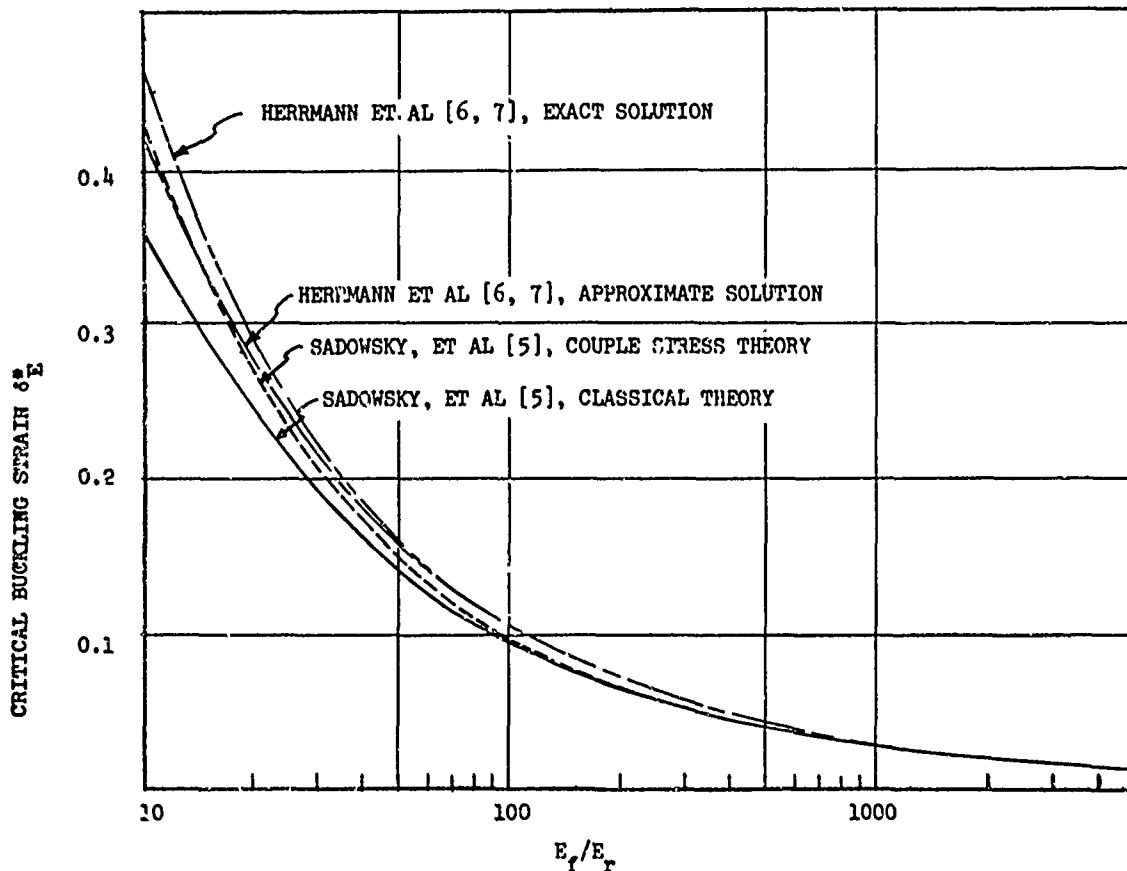


Figure 4. Comparison of Exact and Approximate Buckling Solutions of Sadowsky [5] and Herrmann [6, 7] for Composites With Low Fiber Volume Fractions

the critical buckling strain in unidirectional composites having low fiber volume fractions. The comparison of exact and approximate solutions of Sadowsky, et al. [5] and Herrmann, et al. [6, 7] is shown in Figure 4. For  $E_f/E_r > 100$ , the approximate solutions of Sadowsky, et al. [5] and Herrmann, et al. [6, 7] coincide with their exact solutions. Moreover, for  $E_f/E_r > 100$ , the solutions of [5], [6], and [7] show a reasonable agreement. The comparison of critical buckling wave lengths predicted from the results of [5] and [6] is shown in Figure 5. It is interesting to note that the buckle wave length can also be predicted quite accurately by the following equation

$$l_{cr} = 2\pi r_0 \left( \frac{E_f}{3E_r} \right)^{1/4} \quad (14)$$

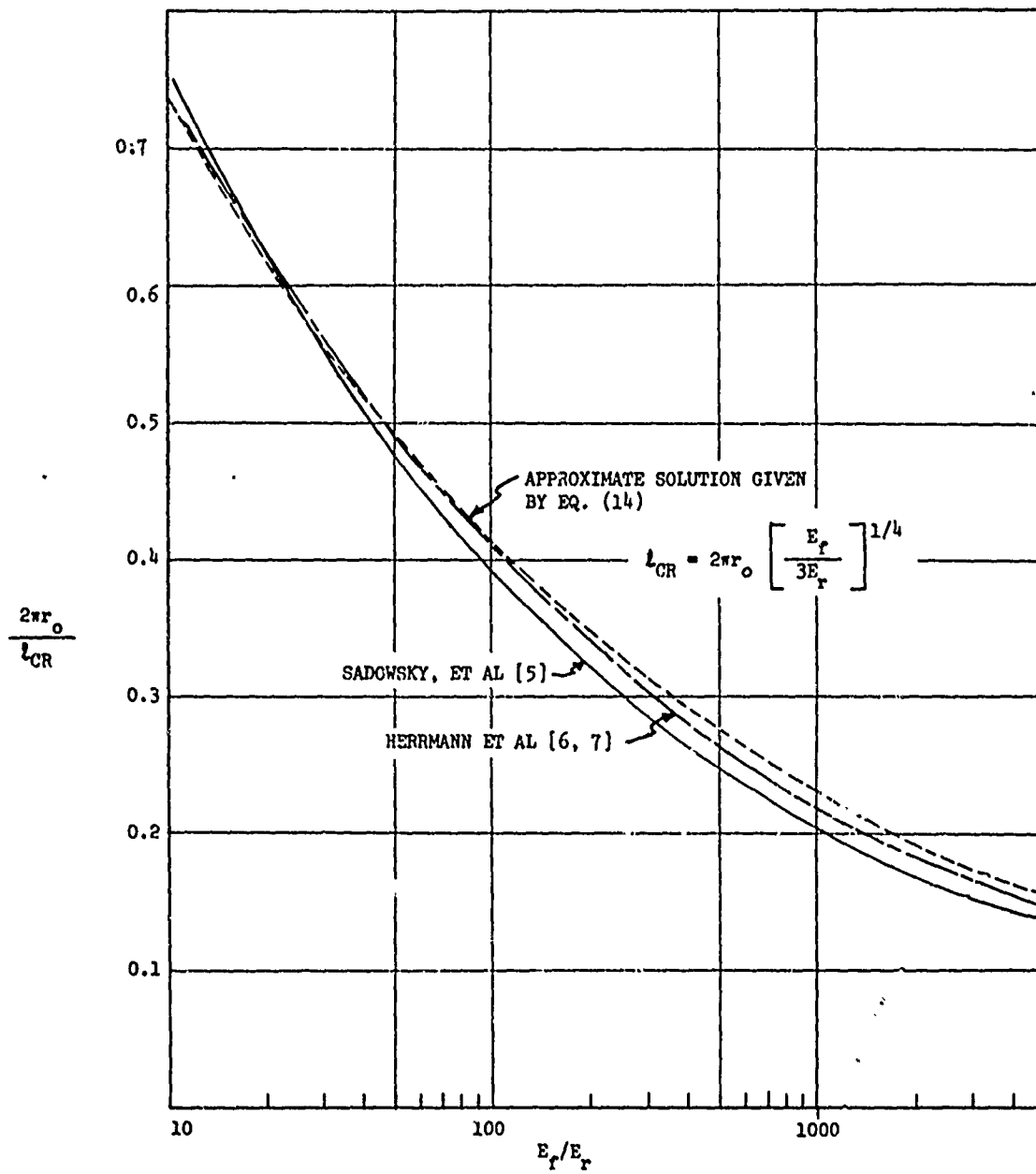


Figure 5. Comparison of Buckle Wave Lengths in Composites With Low Fiber Volume Fraction

which is plotted in Figure 5 as a dashed curve. Equation (14) was derived using Timoshenko's [2] column-on-elastic-foundation approach. The results shown in Figures 3, 4, and 5 are for composites with low fiber volume fractions so that buckling in an extension mode takes place. For composites with high fiber volume fractions ( $k \geq 20$  percent), the fibers buckle in the shear mode. The theories given in [3], [4], and [8] predict identical results, as shown in Figure 6. These results were obtained using a two-dimensional solution. A three-dimensional solution for buckling of composites with high volume fractions in the shear mode is not available in the literature.

As to the experimental work on microbuckling of composites, some results are reported by Schuerch [4], Chung and Testa [8], Lager and June [9], Narmco [10], and most recently by Moncunill de Ferran and Harris [11].

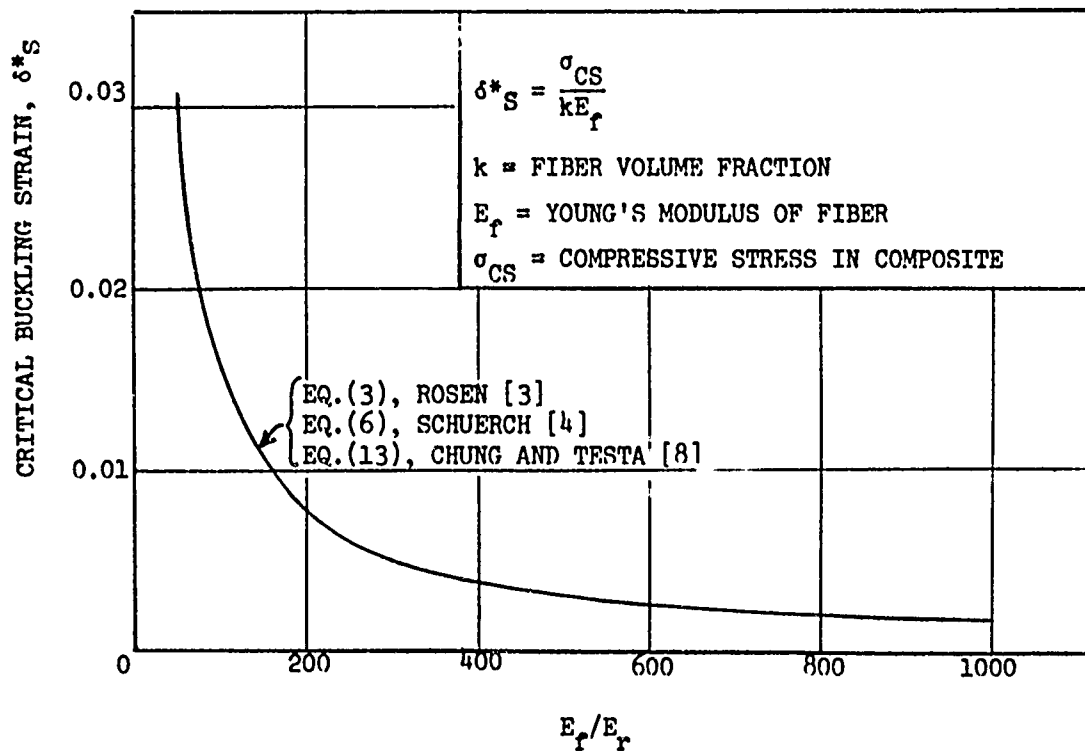


Figure 6. Comparison of Solutions for Buckling in the Shear Mode

Schuerch [4] performed compression tests on actual composites consisting of boron fibers in a magnesium matrix and showed a fair agreement between experimental results and theoretical results that assumed anelastic behavior of the matrix. Chung and Testa [8] performed compression tests on two-dimensional composite models consisting of thin glass fabric strips imbedded in an epoxy matrix. They obtained a fair correlation between the experimental results and theoretical results predicted by Equations (12) and (13), which apply to two-dimensional composites. Lager and June [9] performed compression tests on carefully prepared boron-epoxy composites. Comparison of their test data with theoretical results predicted by Equations (1) and (3) showed large differences between the theoretical and experimental results; the experimental results were  $\approx 60$  percent of the theoretical values. Consequently, they introduced what they called an "influence coefficient" of 0.63 in Equation (3) that produced test-theory correlation. Finally, Moncunill de Ferran and Harris [11] performed compression tests on composites consisting of steel wires in a polyester matrix. Their experimental results were also significantly lower than the theoretical results predicted by Equation (3). They attributed the low experimental values to the tendency of fibers to buckle in a helical mode rather than as beams on an elastic foundation.

The theoretical and experimental results obtained by various authors do not lead to any firm conclusions regarding the exact failure mechanism of unidirectional composites subjected to compressive loading, nor do they explain the abnormally low compressive strengths of composites such as graphite-epoxy.

## Section 2

### EXPERIMENTAL STUDIES ON MICROBUCKLING OF UNIDIRECTIONAL COMPOSITES

To establish if microbuckling is a valid failure mode for unidirectional composites subjected to compressive loading, and to gain a better understanding of the compression failure mechanism of these materials, experiments were performed on carefully prepared models consisting of rods imbedded in a resin matrix. Extensive tests were performed throughout the program to characterize the materials (rods and matrix) used for making the specimens. The test data on the properties of constituents were used to design multirod composite specimens. These were designed such that they would not fail by Euler column buckling (Figure 7).

#### CHARACTERIZATION OF CONSTITUENT MATERIALS

The reinforcing material selected consisted of extruded graphite rods with properties (degree of anisotropy) simulating those of Thornel graphite fibers. Two resins were selected to make composite models: soft, low-modulus resin (urethane) that would allow microbuckling of fibers, and a hard, high-modulus resin (Hysol) that would not. The compositions and the cure cycles for the two resins are shown in Table 1A of the Appendix. The following tests were performed on graphite rods: axial tension tests, axial compression tests, flexure tests, and transverse compression tests. Strength and modulus data were obtained. Young's modulus and Poisson's ratio were obtained for the soft resin. The data on hard resin were available from previous work.\* The average properties of the "fibers"\*\*\* and the resins are summarized in Tables II and III. Typical stress-strain curves for the two resins are shown in Figure 8. A typical compression stress-strain curve for the graphite rods\*\* is shown in Figure 9.

---

\*Compressive properties of the two resins were also measured during various phases of the program, and the results are described later on in this report.

\*\*The terms "fibers", "rods", and "reinforcement" are used interchangeably throughout this report.

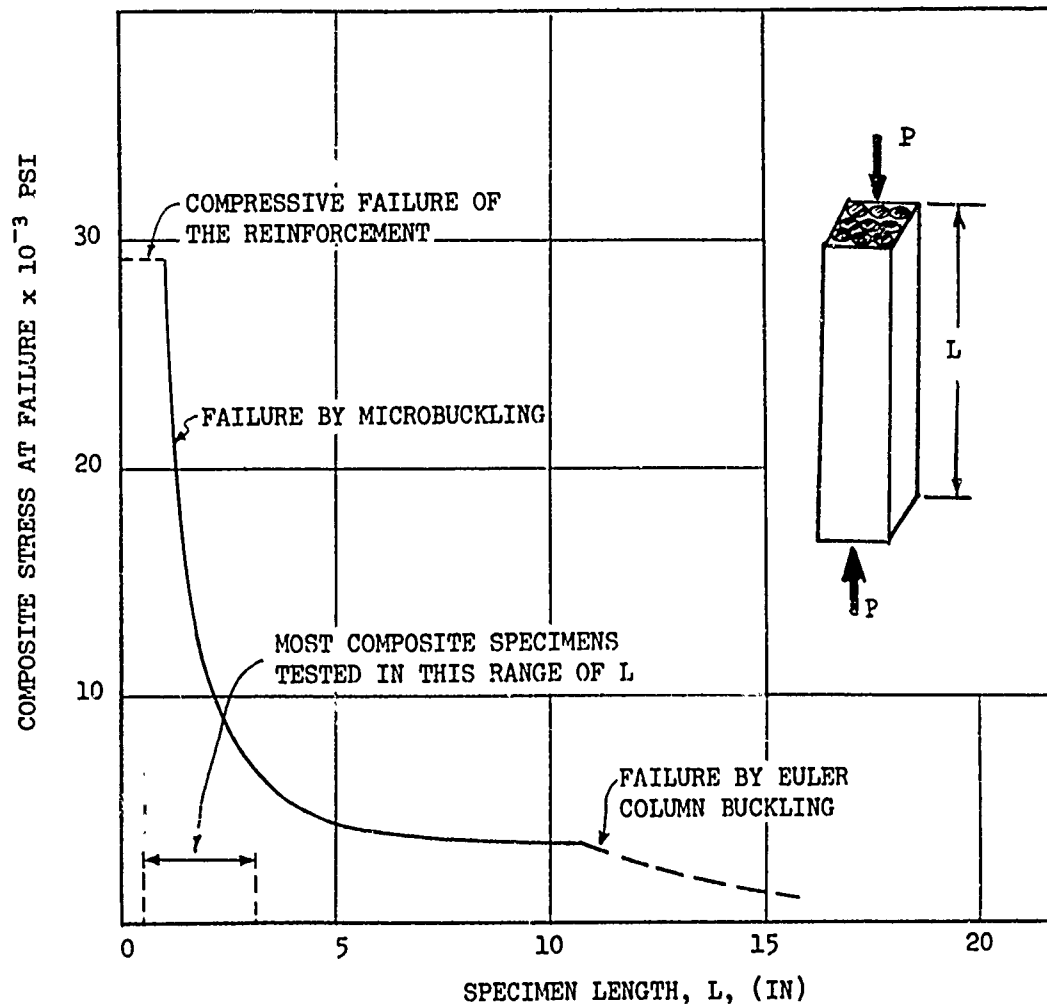


Figure 7. Failure Domains for Composite Compression Specimens

A graphite rod compression specimen prior to testing, and several failed specimens, are shown in Figure 10. Figure 11 shows a transverse compression specimen prior to testing, and a failed test specimen. The tensile specimens that are not shown consisted of graphite rods with built-up resin ends. The tensile specimen of this configuration worked quite satisfactorily, although in several instances the failure took place in the grips.

Table II

## AVERAGE PROPERTIES OF GRAPHITE RODS

Test Property	Axial Tension	Axial Compression	Flexure	Compression Transverse
Fiber Diameter, in.	0.077	0.0755	0.0760	0.0523*
Gage Length, in.	2	0.61	1 and 1.5	0.267
Strength x 10 <sup>-3</sup> psi	15.64	57.50	26.40	13.44
Young's Modulus x 10 <sup>-6</sup> psi	12.50	12.18	11.89	1.23
Number of Tests	5	8	11	6

\*Square Bars were machined from 0.076 in. diameter rods; five rods were stacked on top of each other.

Table III

## AVERAGE PROPERTIES OF RESINS

Material	Young's Modulus* x 10 <sup>-6</sup> psi	Poisson's Ratio	Shear Modulus** x 10 <sup>-6</sup> psi	Compression Strength x 10 <sup>-3</sup> psi	Tensile Strength x 10 <sup>-3</sup> psi
HYSOL	0.457 (C)	0.408	0.162	11.0	-
Urethane 4	0.00191 (T)	0.476	0.000647	-	0.641
Urethane 5	0.00102 (T)	0.467	0.000346	-	0.456

\* C and T denote that moduli were obtained from compressive (C) or tensile (T) tests.

\*\* Calculated by  $G = \frac{E}{2(1 + \nu)}$

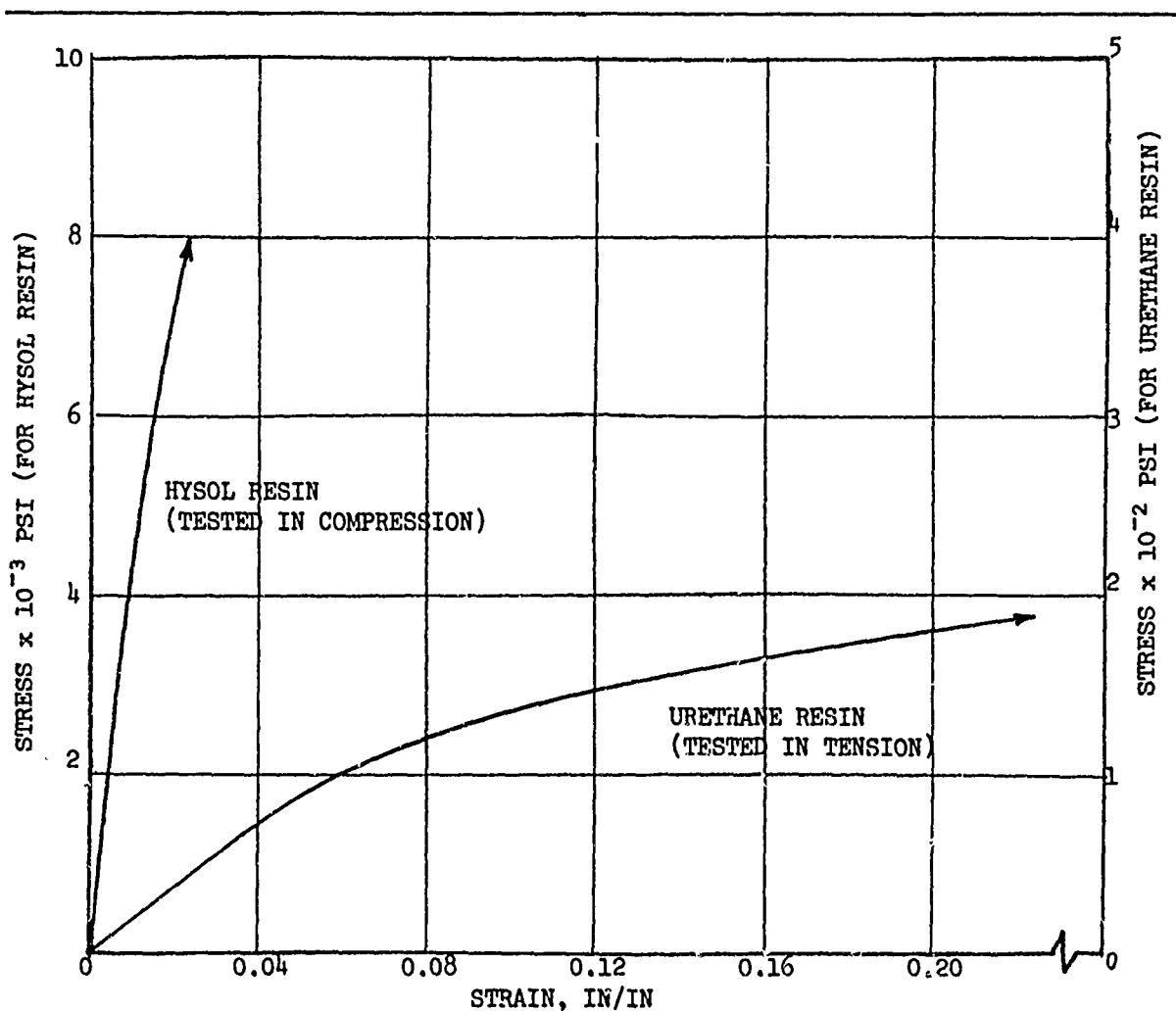


Figure 8. Typical Stress-Strain Curves for Resins

The transverse compression modulus was obtained from the type of specimen shown in Figure 11. Six specimens were tested. Values of the modulus ranged from  $0.91 \times 10^6$  psi to  $1.51 \times 10^6$  psi. The transverse compressive strength ranged from 12,740 psi to 13,900 psi. Thus the degree of anisotropy\* of the graphite rods was approximately 10.

\*Ratio of modulus in the axial direction to the modulus in transverse direction

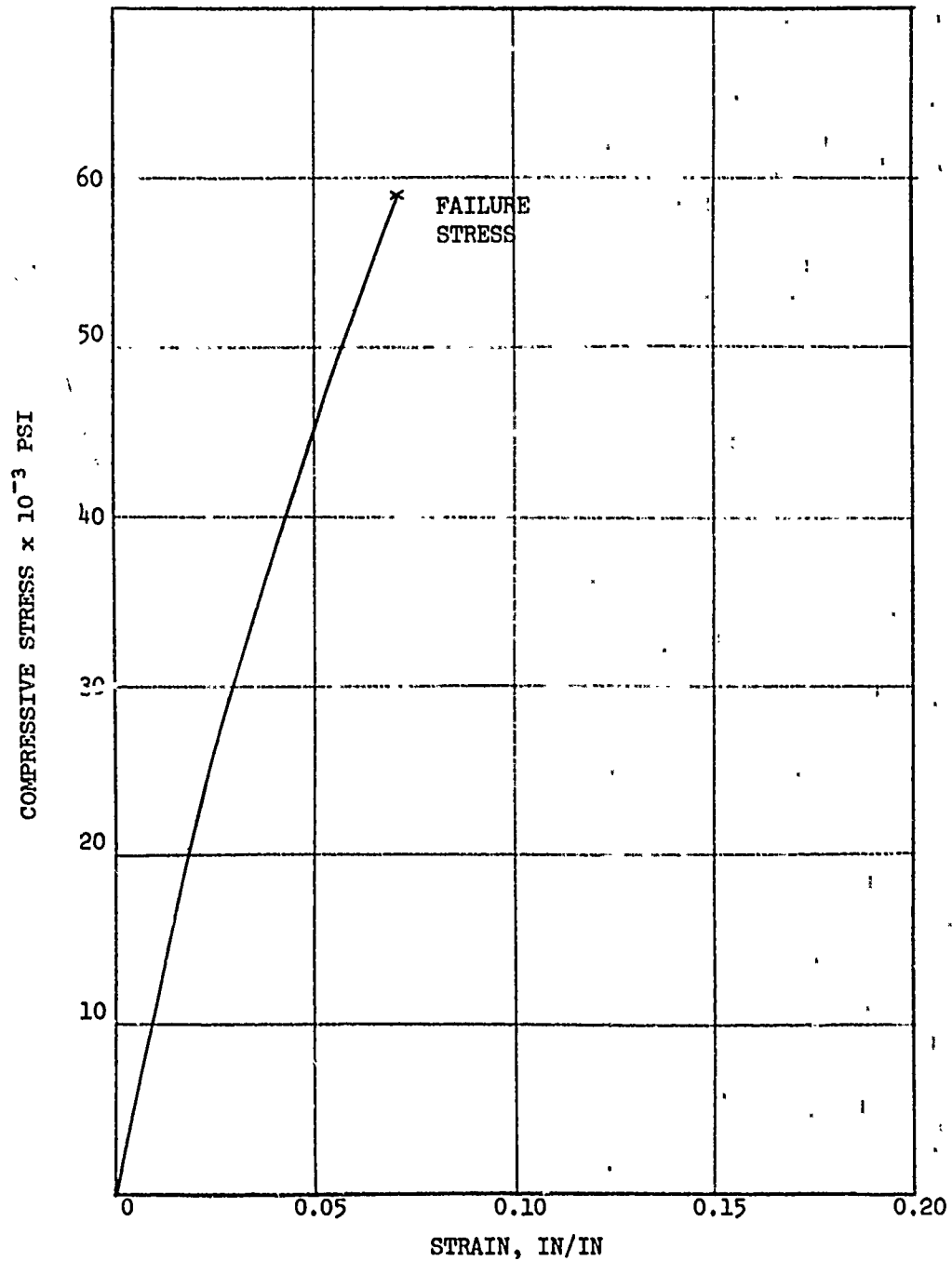


Figure 9. Typical Compressive Stress-Strain Curve for 0.076-In.-Diameter Graphite Rod

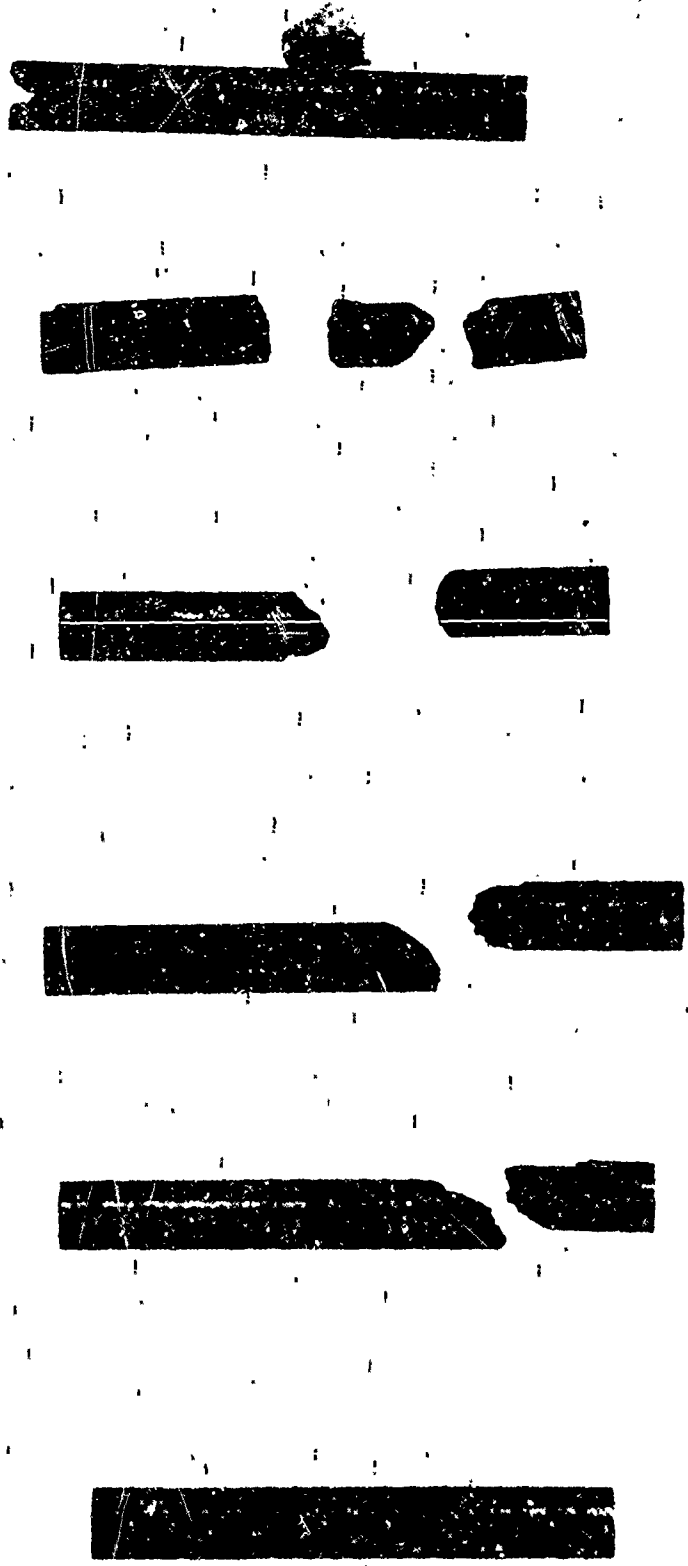


Figure 10. Graphite Rod Axial Compression Specimen and Several Failed Specimens (5X)

**NOTE: THE TRANSVERSE COMPRESSION TEST SPECIMENS CONSISTED OF FIVE SQUARE GRAPHITE RODS STACKED ON TOP OF EACH OTHER AND HELD TOGETHER IN THIS POSITION BY ADHESIVE TAPE. ARROWS INDICATE DIRECTION OF LOADING.**



**Figure 11. Transverse Compression Specimen and Specimen After Failure (5X)**

The Hysol resin properties were obtained from compression tests on resin blocks measuring 1 in. by 1 in. by 2.5 in. Conventional tensile coupons were used to obtain the properties of the urethane resins. Two specimens of each material were tested. The urethane resin was made from the same "batch" of material and cured at the same time as the composite compression models described later.

#### PRELIMINARY TESTING OF COMPOSITE MODELS

To establish trends in composite behavior, simple models of the type shown in Figure 12 were fabricated and tested in axial compression. The models consisted of five graphite rods imbedded in various resins. In addition to using Hysol and urethane as a matrix, several specimens were made with RTC resin (an epoxy cement used for bonding of strain gages). Its tensile modulus was measured to be  $E = 0.360 \times 10^6$  psi. The specimens were cut to various lengths and tested in a self-aligning compression fixture on an Instron testing machine. The pertinent information concerning these specimens, as well as the test data, are shown in Table 2A of the Appendix. The test data are also plotted in Figure 13. Comparison of test data with results predicted by Equation (3) showed drastic disagreement between the two. Further studies showed that in the models under consideration, the number of buckle wave lengths is not large, and therefore the term that contains the wave lengths cannot be ignored. Equation (4) was used to obtain the theoretical curve shown in Figure 13. The number of buckle wave lengths,  $m$ , was taken as one, which gives a minimum value of  $\sigma_f$ .

Some typical compressive failures (no microbuckling) of composites made with three resins are shown in Figures 14, 15, and 16. Figure 14 shows the failure of Specimen 7 of Table 2A, in which the matrix was urethane. Transverse failure of one fiber is quite obvious, as is also shear failure near the ends. Figure 15 shows the failure of a composite made with Hysol resin and designated as Specimen 3 in Table 2A. Figure 16 shows the failure of a composite specimen made with RTC resin. At failure, this specimen literally "blew up." One of the fibers failed in transverse tension, as shown in Figure 16. The clean appearance of the fibers after composite failure indicated poor fiber-matrix adhesion. The failure modes of rods in the composite

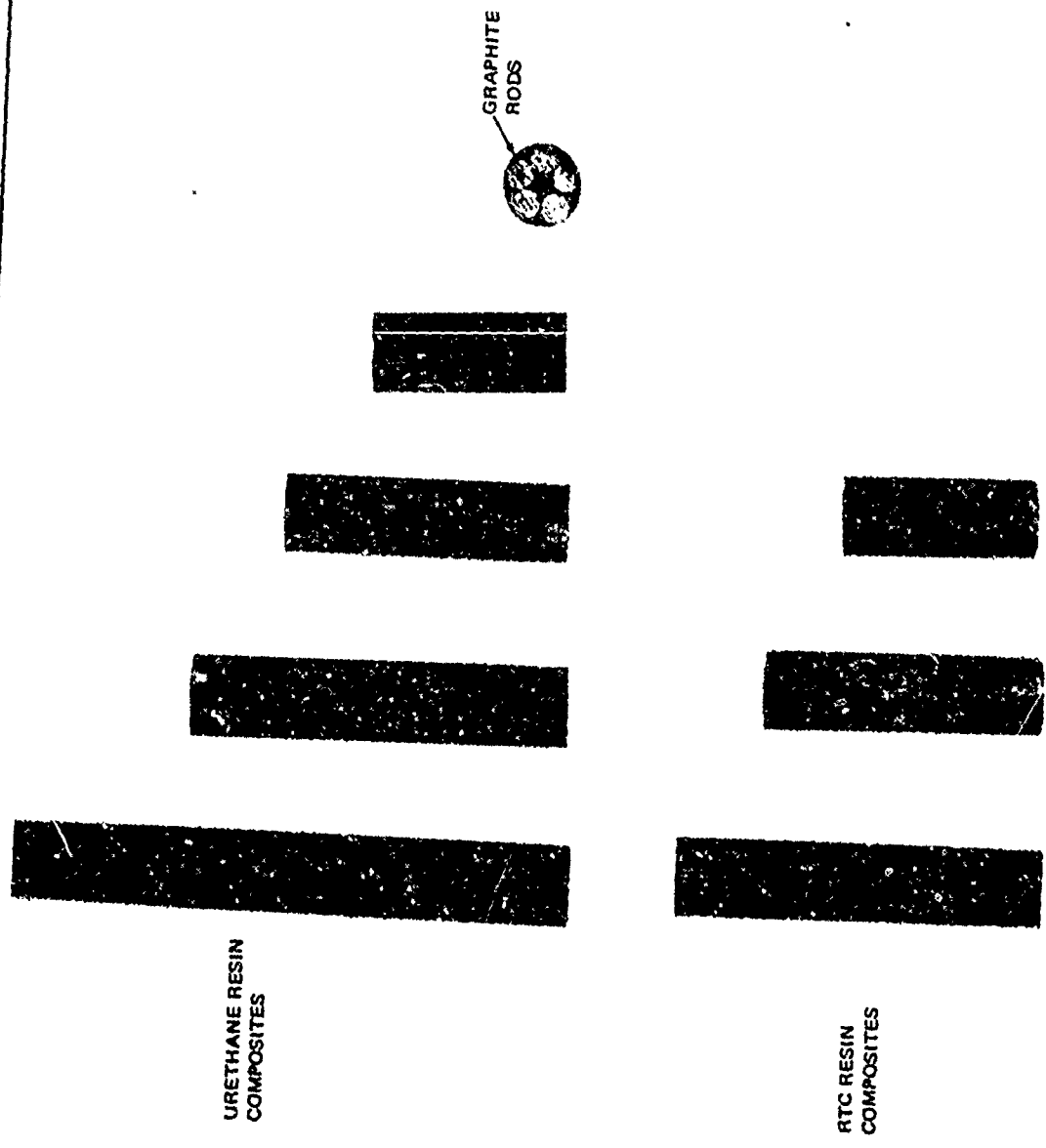


Figure 12. Five-Rod Compression Specimens (2X) (Urethane Resin Composites at Top, RTC Resin Composites at Bottom)

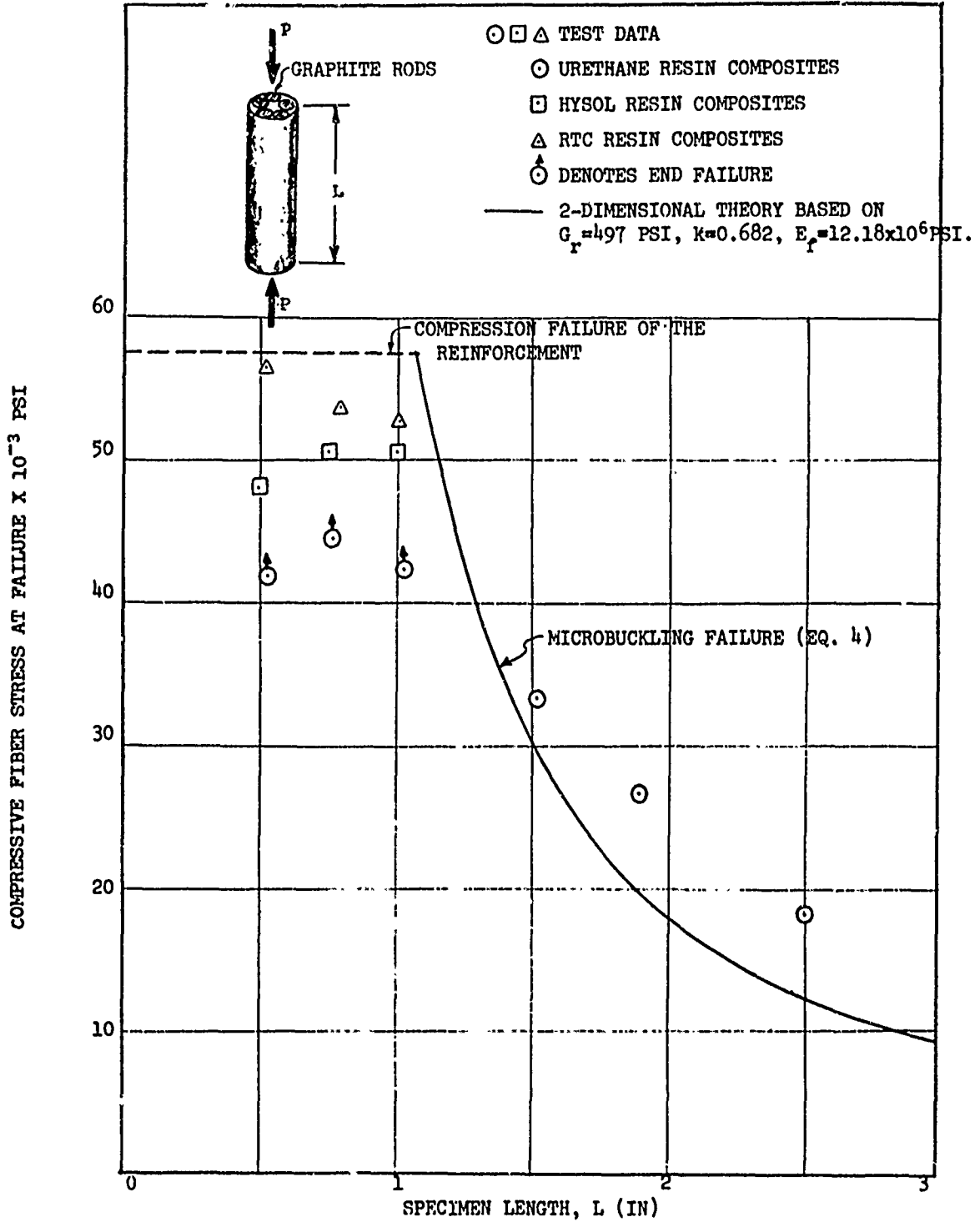


Figure 13. Test-Theory Correlation for Compressive Strength of Five-Rod Composite Specimens



SPECIMEN 7 FROM  
TABLE 2A

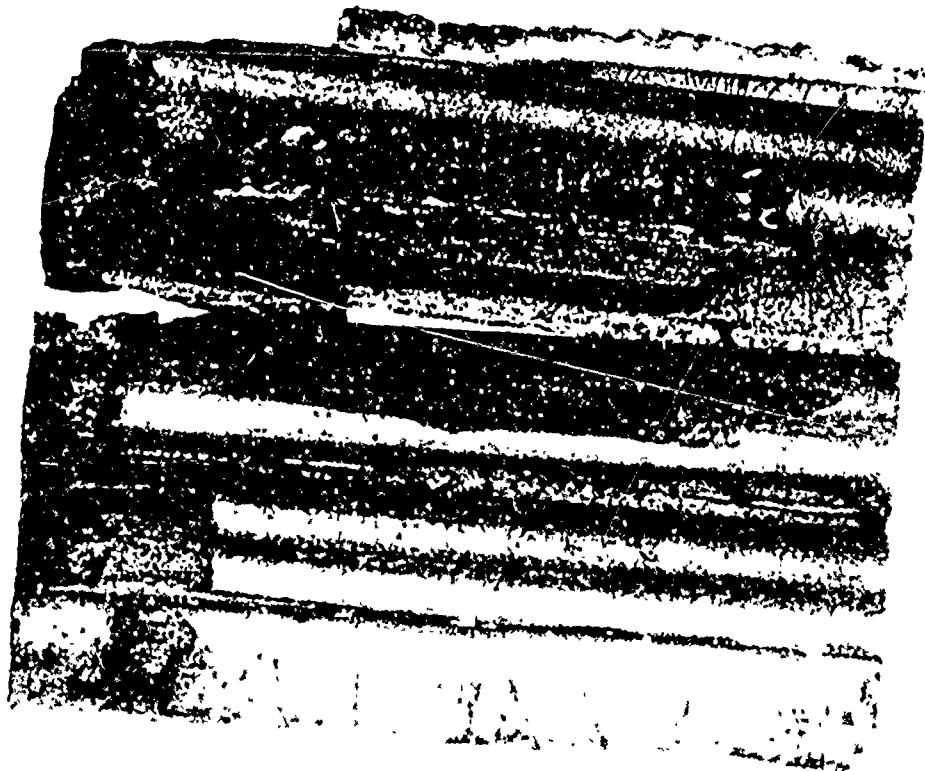
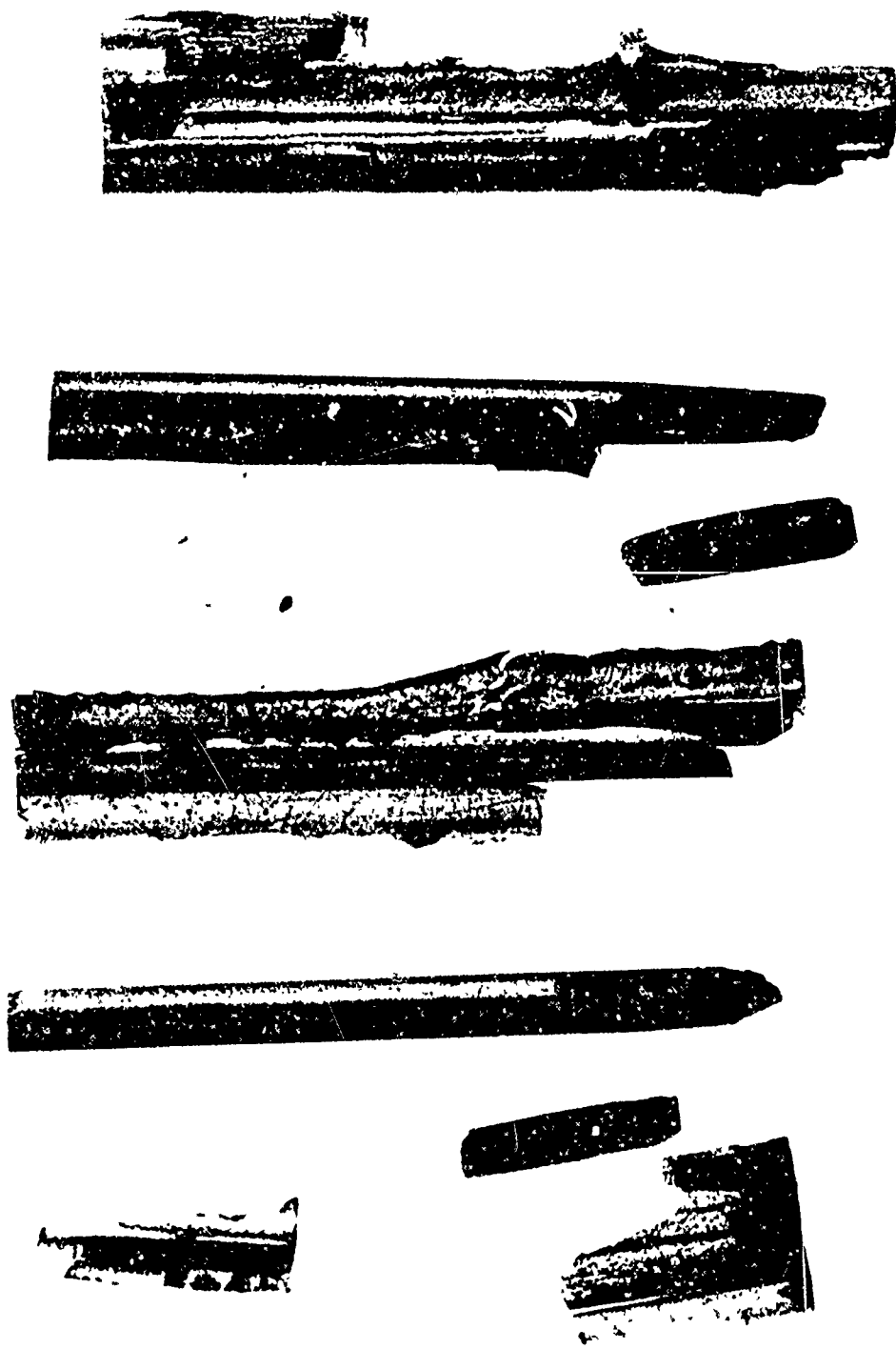


Figure 14. Compression Failure of Urethane Resin Composite Specimen (5X)



COMPOSITE SPECIMEN 3  
FROM TABLE 2A

Figure 15. Compression Failure of Hyzol Resin Composite Specimen 3 (5X)



NOTE: THE FIVE RODS ARE FROM A FIBER-RESIN COMPOSITE SPECIMEN (NO. 11) OF TABLE 2A.

Figure 16. Compression Failure of the RTC Resin Composite Specimen (5X)

specimen shown in Figure 16 are similar to failures of graphite rods that were tested individually (Figure 10). This indicates that the composite shown in Figure 16 failed by compressive failure of the reinforcement rather than by microbuckling, as is also apparent from Figure 13. The difference between the compressive failure of the reinforcement and failure by microbuckling can also be seen in Figure 17, which shows compressive load versus machine head travel for specimens of various lengths. The composite specimens that failed by compressive failure of the reinforcement have a linear, or nearly linear, load-deflection curve up to failure (Specimens 5, 6, and 7). Composites that failed by microbuckling have a "hook" in the load-deflection curve (Specimens 4, 8, and 9).

After performing the preliminary tests on circular, five-fiber composite models, the results were used to design nine-rod specimens for further, more accurate evaluation.

#### FINAL TESTING OF COMPOSITE MODELS

Two sets of composite models were fabricated: one set made with nine graphite rods in Hysol resin, and one made of nine graphite rods in urethane resin. \* To insure that the nine-rod composites were representative of multifiber composites, a 25-rod urethane resin composite was also fabricated. The nominal diameter of the rods was 0.076 in. The rod spacing was chosen to give a fiber volume fraction of  $k = 50$  percent. Except for the 25-rod composite specimen, the only geometric variable for the two sets of specimens was the length. Figure 18 shows several test specimens made of urethane. The Hysol resin specimens were identical to those shown in Figure 18. The specimens were tested in compression in a self-aligning fixture in an Instron test machine. The test results, as well as other pertinent data for the specimens, are shown in Table 3A of the Appendix. The key to the identity of specimens shown in Table 3A is as follows: designations 6a, 6b and 6c mean that three specimens were cut from composite bar No. 6. The failure loads enclosed by parentheses denote that the failure did not take

\*Each time a composite specimen was made, a resin casting was also made. The casting was cured at the same time as the composite, and its properties were measured. The cure cycle and the resin formulation were as shown in Table 1A of the Appendix.

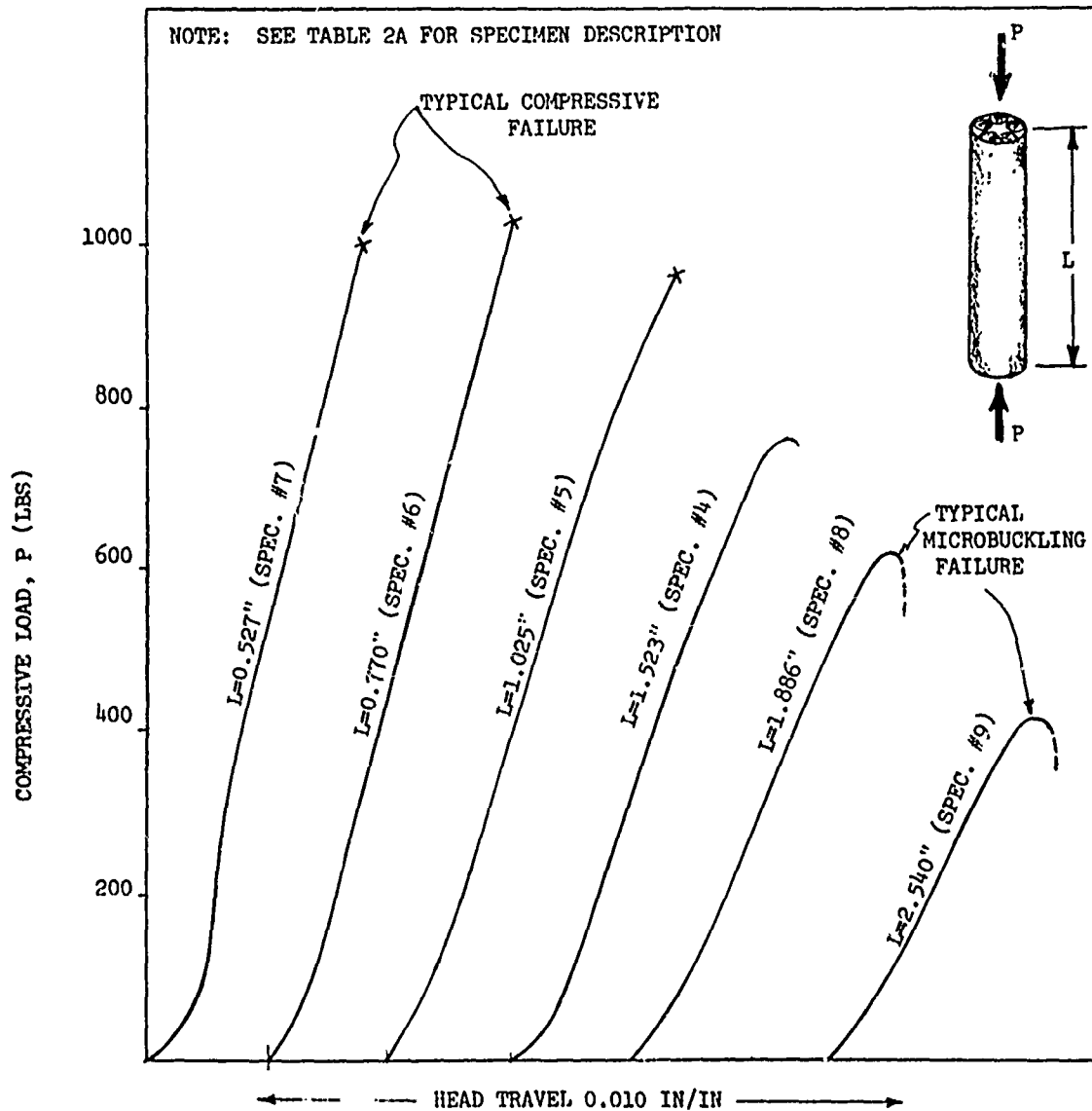
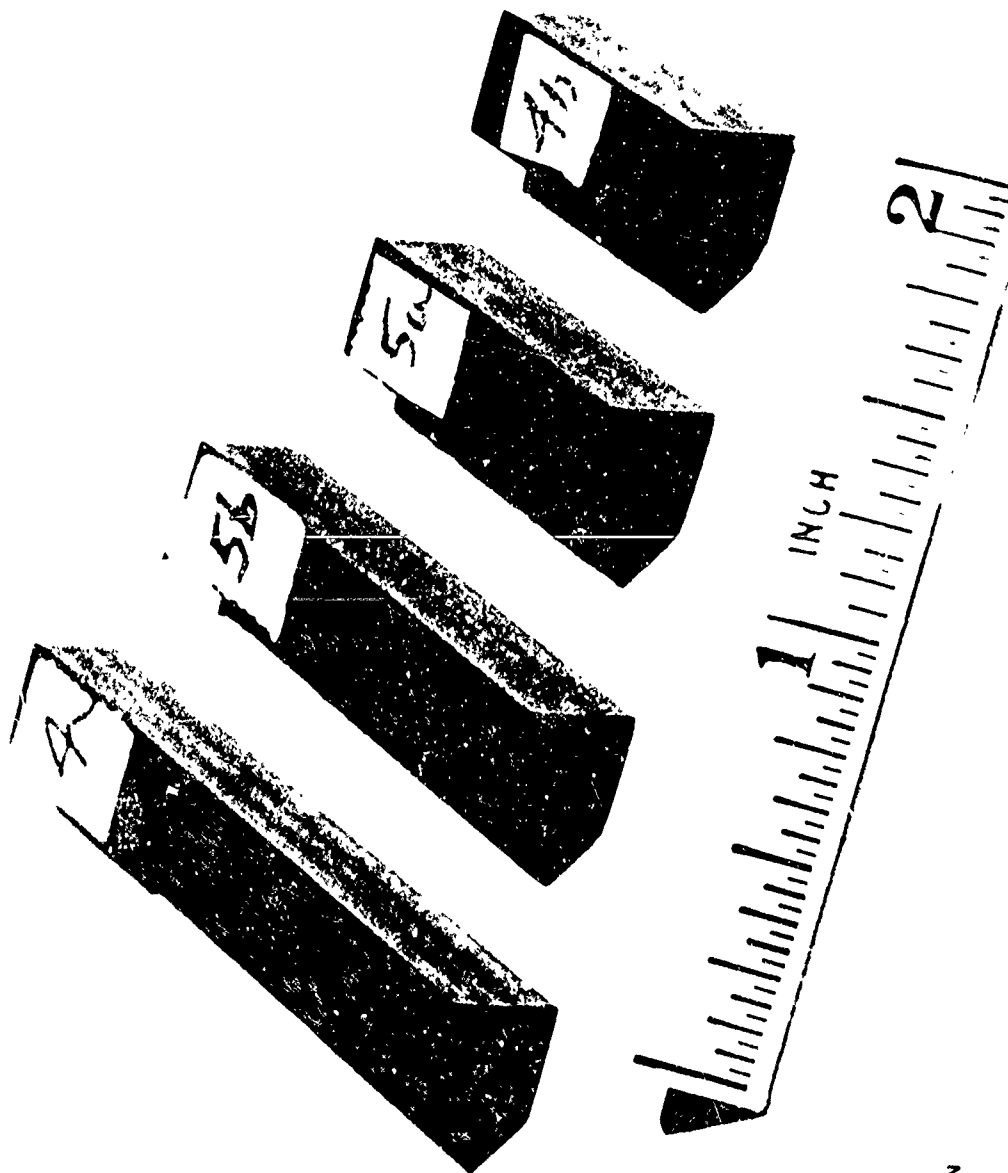


Figure 17. Compression Load Versus Machine Head Travel for Five-Rod Urethane Resin Composites

place in the test section but elsewhere — at the ends, for example. Young's modulus was measured for several specimens by means of a lightweight extensometer. The volume fractions of composites were calculated from the measured dimensions of the specimens and from the measured dimensions of the graphite rods. The results given in Table 3A are plotted in Figure 19. Fiber stress at failure is plotted as a function of the length of



(SEE TABLE 3A FOR  
DETAILED SPECIMEN  
DESCRIPTION)

Figure 18. Typical Nine-Rod Compression Specimens Made of Graphite Rods and Urethane Resin

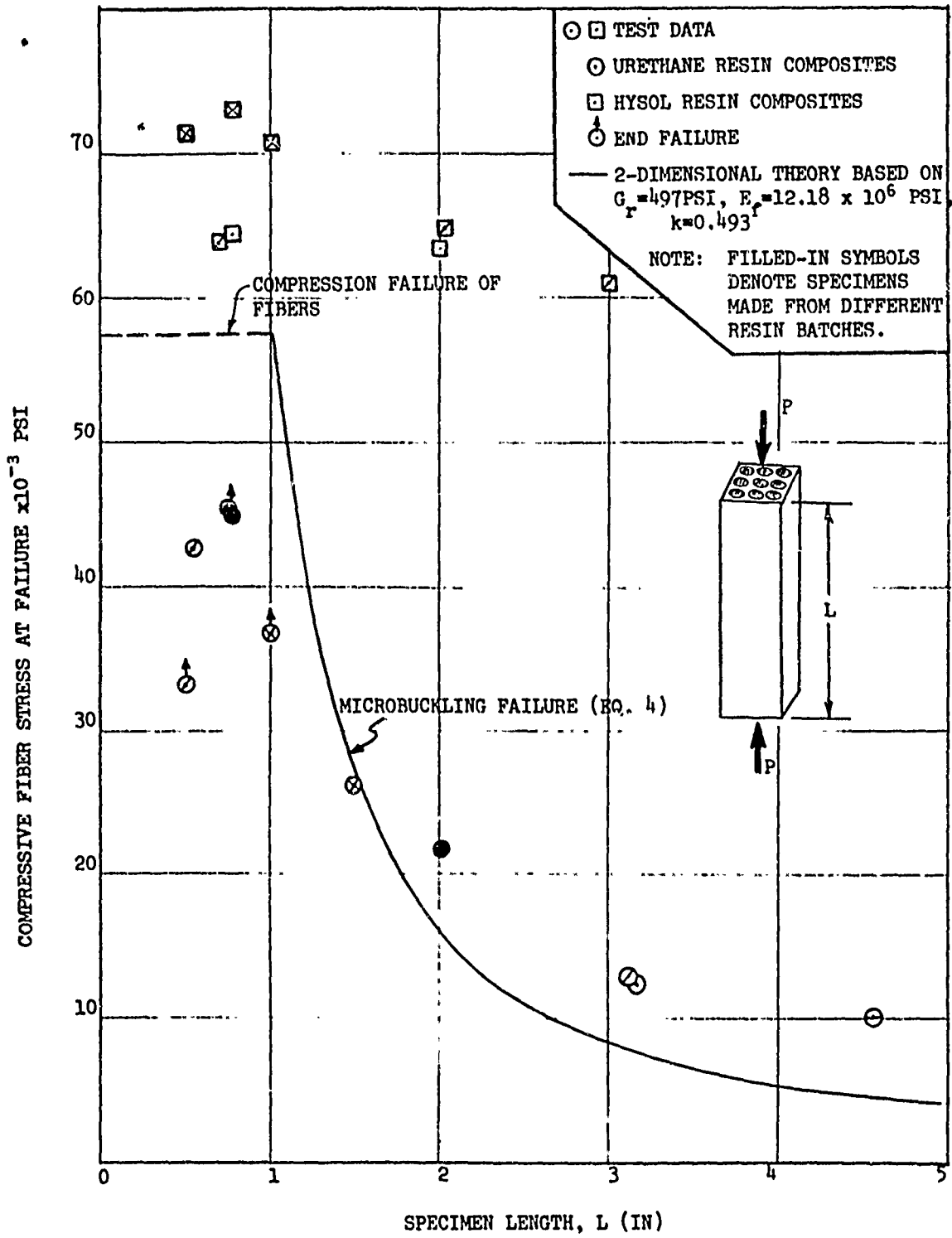


Figure 19. Test-Theory Correlation for Compressive Strength of Nine-Rod Composite Specimens

the composite specimen. The latter figure also shows theoretically predicted results. As before, the experimental results (in the microbuckling-critical region) are higher than the theory. This further indicates that the two-dimensional theory may not be adequate for determining the microbuckling failure of actual, three-dimensional composites. The application of the theory is, of course, approximate also from the standpoint that the theory is for isotropic fibers, while the test results are for composites made with anisotropic fibers. Nevertheless, the results do indicate that failure by microbuckling does take place—both theory and experiments show similar trends.

In the case of composites made of Hysol resin, the test data for which are also shown in Figure 19, failure was by compression failure of the reinforcement rather than by microbuckling. Moreover, in Hysol resin composites, the fiber stresses at failure were significantly higher than the measured compressive strengths of fibers by themselves (see Table II). \* The multi-axial internal stresses in the matrix could possibly account for this behavior. In addition to the data given in Table 3A, Figure 19 shows data points for Hysol resin composites, which are presented in Section 3 and Table 4A.

The 25-rod urethane resin composite, the test results for which are included in Figure 19, failed in a manner similar to the nine-rod composites and at approximately the same stress level (if we normalize test data with respect to L). Therefore, it appears that the test data for the nine-rod composites are representative of the test data for multifiber composites.

---

\*It is noted that the conversion of composite stresses to fiber stresses was made by means of the following equation based on one-dimensional, elementary considerations.

$$\sigma_f = \sigma_c \left[ \frac{1 - (E_r/E_c)(1 - k)}{k} \right]$$

where  $\sigma_c$  is the composite stress at failure and  $E_c$  is the modulus of the composite. This equation was used primarily to normalize the results with respect to k.

Figures 20 and 21 show the failed composite specimens made of urethane and Hysol resin, respectively. In testing short urethane specimens, it was found that the resin did not provide adequate support to the fibers and, in many cases, the fibers failed by end crushing (see Specimen 4b in Figure 20). Consequently, to eliminate this problem, the ends of several specimens were encapsulated in plastic cups filled with Hysol resin. The failures in the latter specimens were in the test section. Specimens made with Hysol resin failed in the test section, as shown in Figure 21. Figure 22 shows the 25-rod specimen after failure. It failed by microbuckling. It is noted that at failure, the graphite rods in this specimen failed; however the resin did not. Consequently, the resin was cut at the failure plane to show the detail of the fractured fibers.

Some typical stress strain-curves for specimens of various lengths are shown in Figure 23. Figures 24 and 25 show some typical load-versus-machine-head-travel curves for composites made of Hysol and urethane, and also for the 25-rod composite. From the results shown in Figures 23, 24, and 25, it is quite clear that compressive failure of the reinforcement is associated with a linear load deflection curve (or stress-strain curve) up to failure, while in the case when microbuckling took place, the curves became highly nonlinear at higher load intensities, as was shown previously in Figure 17.

It is important to note that the failures shown in Figures 20 and 22 are not microbuckling failures as such, but rather failures initiated by transverse deformations (formation of buckle waves) during microbuckling. Once microbuckling deformations take place, bending stresses are induced in the rods, and since the rods are brittle, they fail by bending, resulting in failures as shown in Figures 20 and 22. For the case of composites that are reinforced with brittle fibers and are of such a length that a number of buckle wave lengths can be formed in the test section, one would expect to observe a number of breaks of the fibers at equal-length intervals. This phenomenon was observed by Moncunill de Ferran and Harris [11].

NOTE: SPECIMENS 63, 4a, AND 5b FAILED BY MICROBUCKLING. SPECIMENS 5a AND 4b FAILED BY COMPRESSION (SEE TABLE 3A FOR SPECIMEN DESCRIPTION AND TEST DATA).

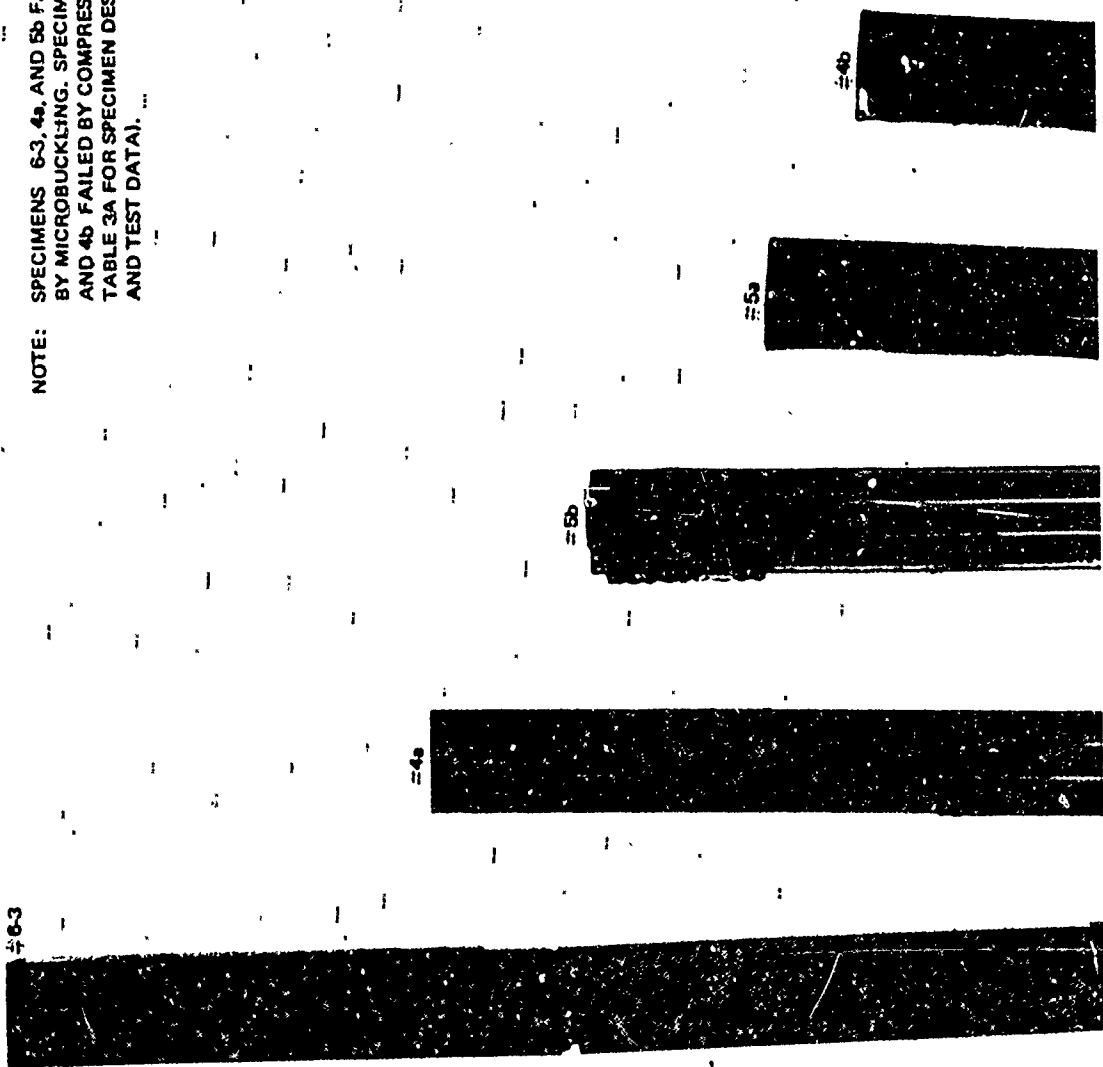


Figure 20. Urethane Resin Compression Specimens After Failure (2.5X)

NOTE: SPECIMENS FAILED BY  
COMPRESSION FAILURE OF  
THE REINFORCEMENT, OR  
END CRUSHING (SEE TABLE 3A  
FOR SPECIMEN DESCRIPTION  
AND TEST DATA).

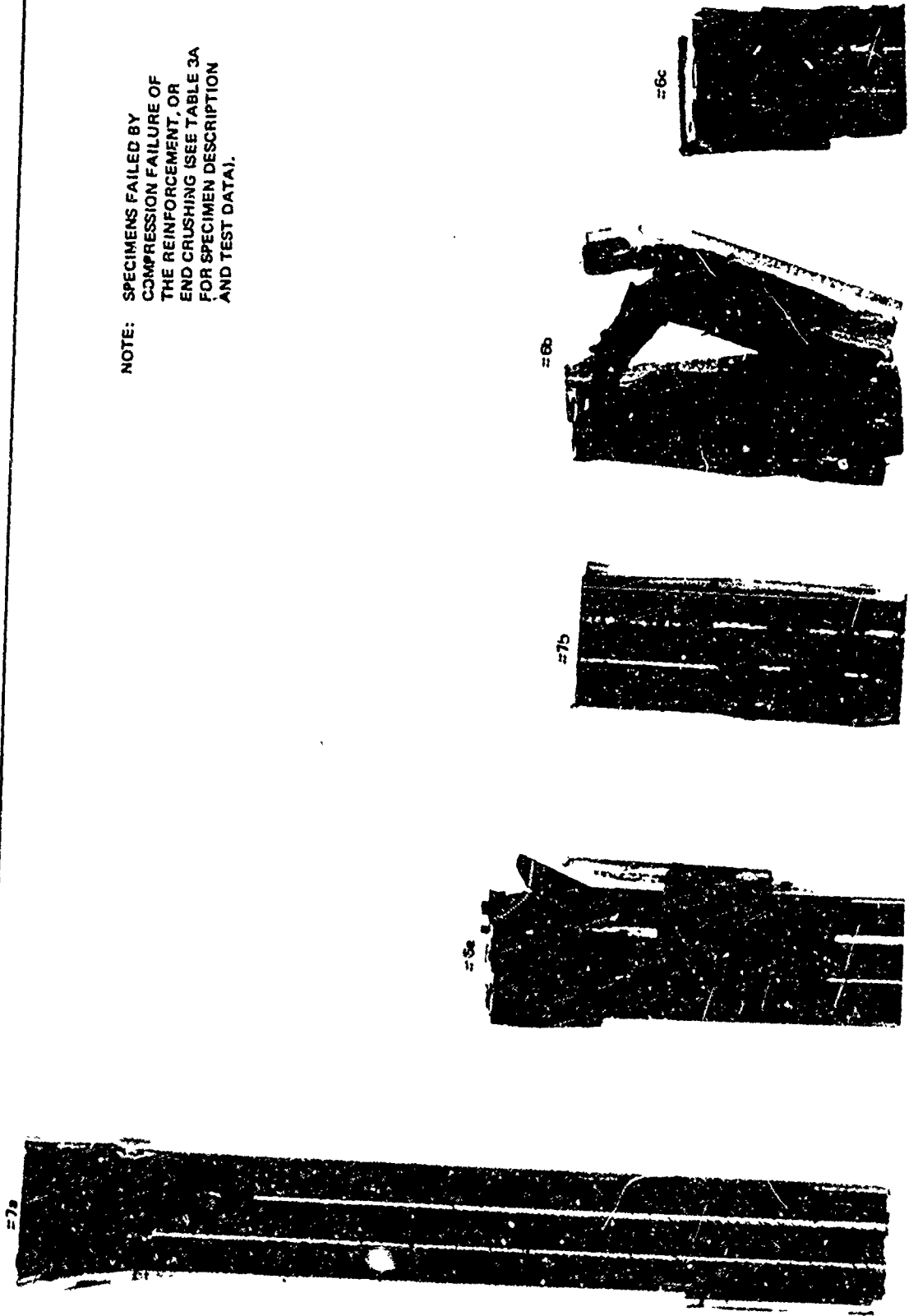


Figure 21. Nine-Rod Hysol Resin Compression Specimens After Failure (3X)



Figure 22. Twenty-Five-Rod Urethane Resin Composite Specimen After Failure

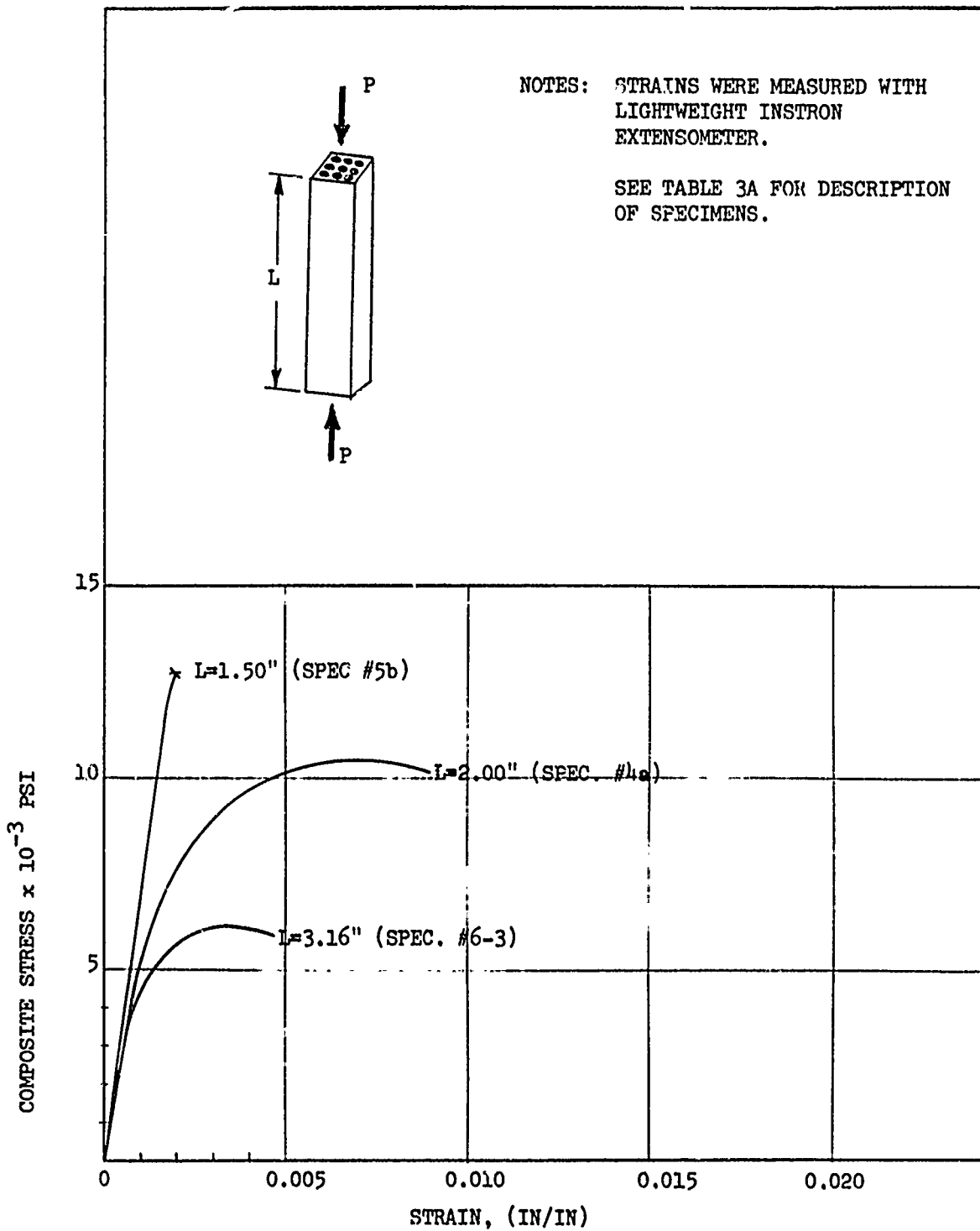


Figure 23. Typical Stress-Strain Curves for Urethane Resin Composites

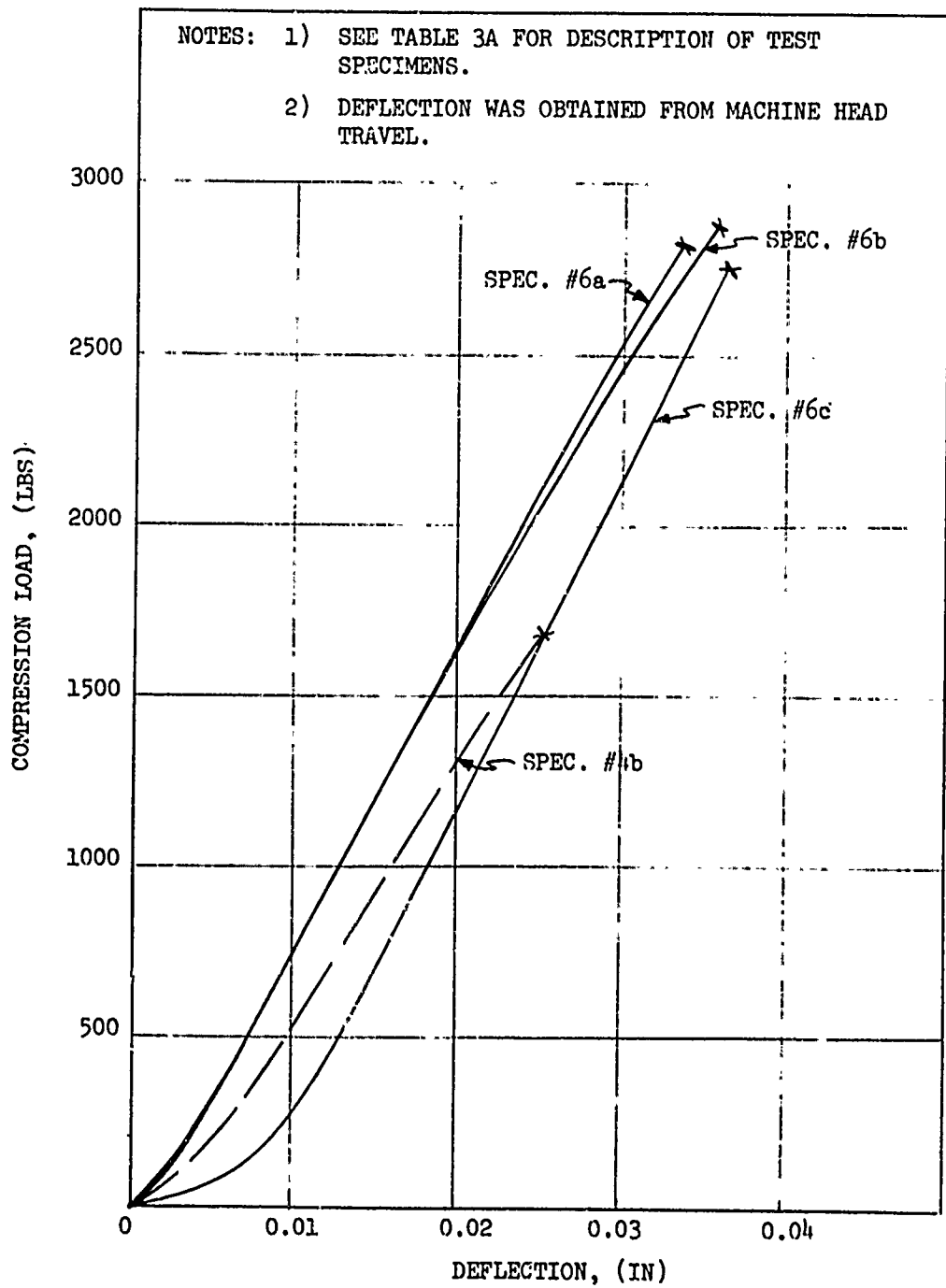


Figure 24. Load-Deflection Curves for Specimens That Did Not Fail by Microbuckling

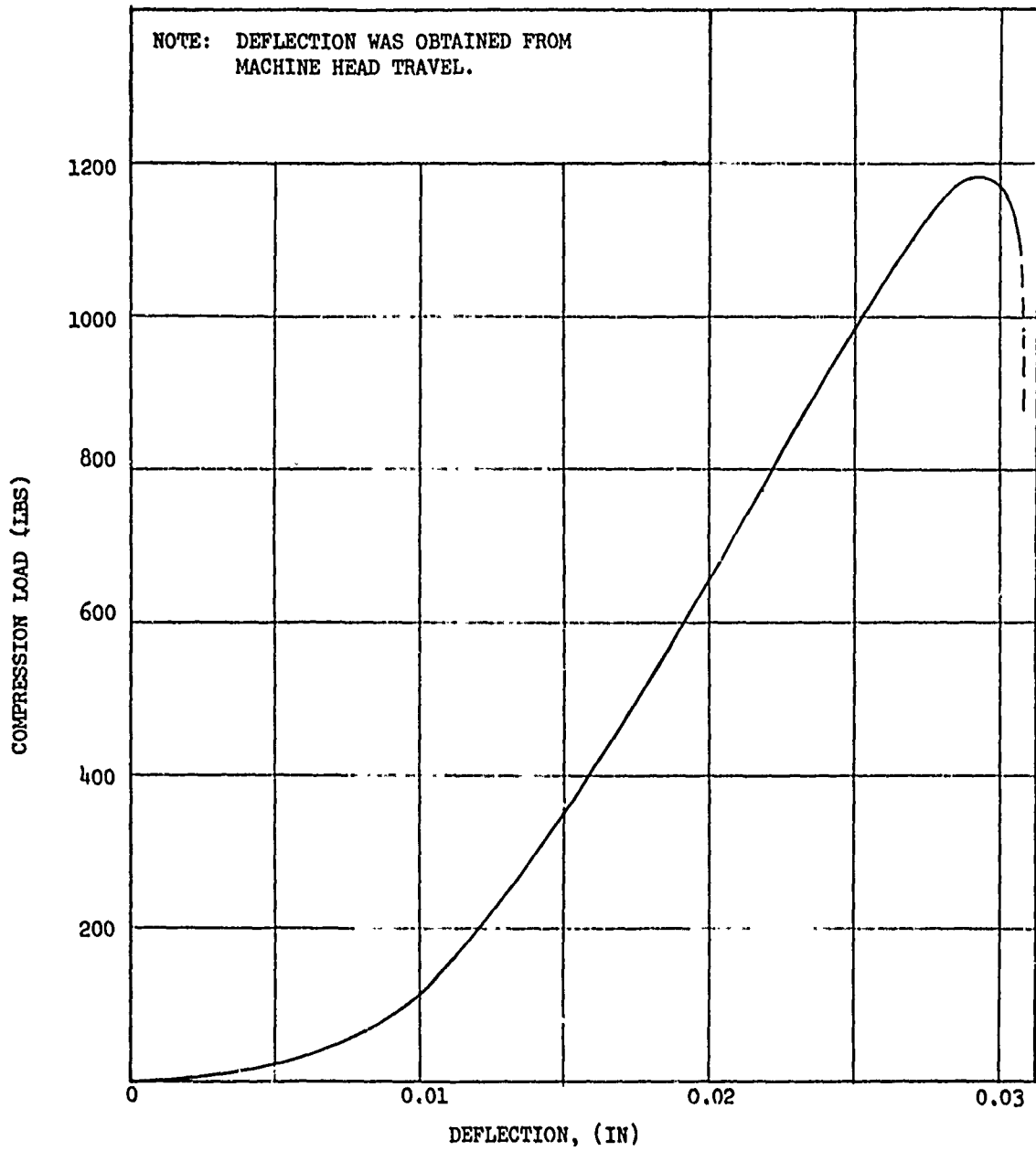


Figure 25. Load-Deflection Curve for Twenty-Five-Rod Graphite-Urethane Composite That Failed by Microbuckling

Section 3  
INFLUENCE OF FIBER DIAMETER ON COMPRESSIVE  
STRENGTH OF UNIDIRECTIONAL COMPOSITES

The amount of experimental data on the effect of fiber diameter on the compressive strength of filamentary composites is rather limited. Some results reported by Levenetz [12] are shown in Figure 26. The data show a significant amount of scatter. On the basis of results shown in Figure 26, Levenetz concluded that composites made with large-diameter (0.005-in.) fibers are stronger in compression than composites made with standard rovings (0.0003 in. diameter fibers). The following reasons were given for the improved compressive strengths of composites made with large-diameter fibers:

- A. Longer critical buckle wave length due to larger moment of inertia of the fiber
- B. Better collimation due to stiffer fiber
- C. Higher elastic modulus due to thermal history

The meaning of Item C is not clear. Item B does make sense, since in composites made of large-diameter fibers, there would be less likelihood of fiber crossovers. As to Item A, it appears questionable from the theoretical point of view for the following reason.

The relationship between fiber diameter,  $h$ , and the buckle wave length,  $\ell$ , is given by the following equation [3]\*

$$\ell = \frac{\pi h}{2} \left( \frac{E_f}{k_1} \right)^{1/4} \quad (15)$$

where  $E_f$  is the Young's modulus of the fiber and  $k_1$  is the foundation modulus. Thus, the buckle wave length increases linearly with the fiber diameter. This was shown experimentally in Reference 3 and is reproduced

---

\*Equation (15) applies to microbuckling in the extension mode. It is assumed here that the buckle wave length for the extension mode is the same as for the shear mode.

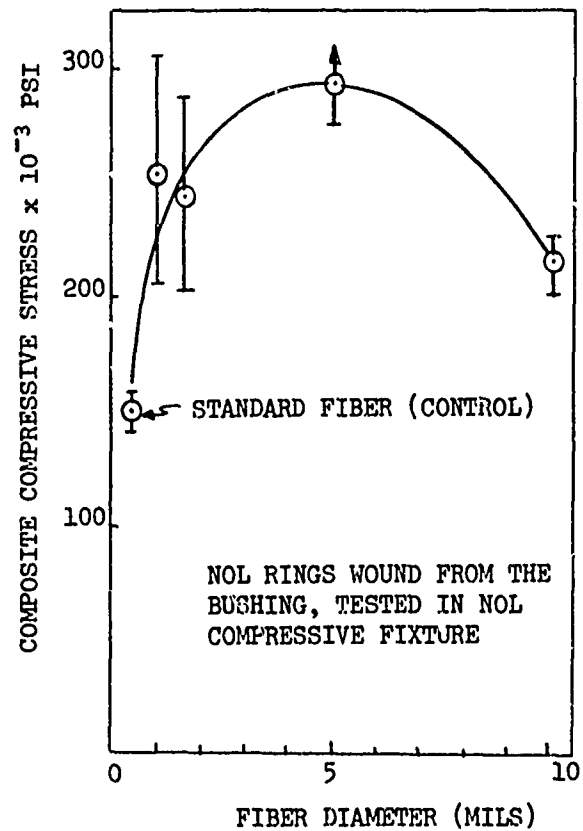


Figure 26. Compressive Strength Versus Fiber Diameter for Fiber Glass Composites [12]

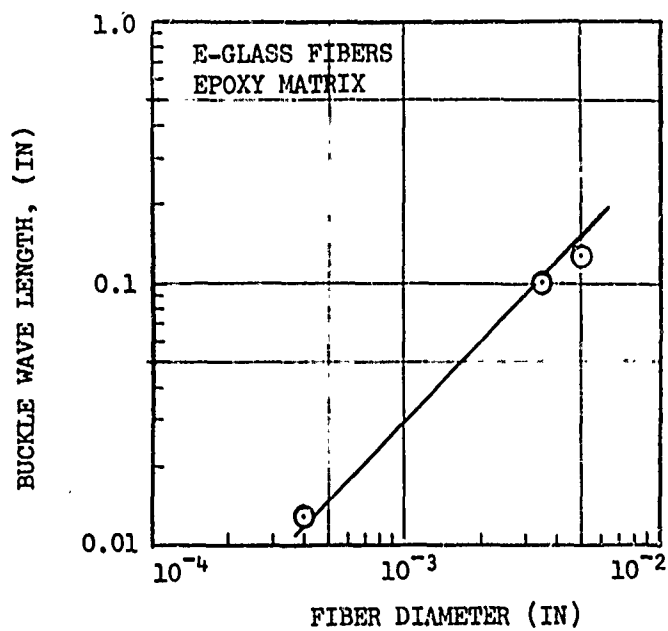


Figure 27. Experimental Results for Fiber Buckling Wave Length as a Function of Fiber Diameter [3]

in Figure 27. For practical composites ( $k > 20$  percent), the failure is governed by shear mode instability given by Equation (4). Combining Equations (4) and (15) and noting that  $l = L/m$  yields

$$(\sigma_{cs})_1 = \frac{G_r}{1-k} + \frac{k(k_1 E_f)^{1/2}}{3} \quad (16)$$

The above equation indicates that the fiber diameter does not influence the compressive strength of unidirectional composites,\* since none of the parameters entering in it is a function of the fiber diameter. For actual composites, the second term in Equation (16) is small as compared to the first and is generally ignored, thus giving

$$(\sigma_{cs})_1 = \frac{G_r}{1-k}$$

which obviously is independent of the fiber diameter. As to the effect of fiber diameter on the compressive strength of composites that do not fail by microbuckling, but by compression failure on the reinforcement, no test data have been found.

#### SCREENING TESTS ON CONSTITUENTS AND SPECIMEN PREPARATION

To establish experimentally the effect of fiber diameter on the compressive strengths of composites, a number of specimens with various-sized graphite rods were fabricated and tested.

To insure that the only variable was the fiber diameter, all rods for making the composite test specimens were machined from a batch of 0.079-in. - diameter extruded graphite rods. The nominal diameters of the machined rods were 0.030 in., 0.045 in., 0.060 in., and 0.079 in. Fifteen rods of each diameter were made. Their lengths were approximately 5.5 in. Aluminum molds for making nine-rod, 3-in. -long composite specimens with

---

\*This conclusion is contingent on the validity of the assumption given on the previous page.

$k = 0.50$  were then fabricated (Figure 28). The molds were used to make  $\approx 3$ -in.-long composite compression specimens. The excess lengths of the rods ( $\approx 2$  in.) were used to obtain the flexure strength and modulus of various-size rods. The flexure tests were performed to establish what effect machining had on the properties of the rods, and also as a rough indication of uniformity in material properties. Table IV summarizes the results of flexure testing.

As one would expect, machining did affect the strength of the rods and increased the scatter in test data. However, it did not affect the Young's modulus significantly.

The composite specimens with various-diameter rods were made using Hysol (rigid resin) as a matrix material. Hysol resin was selected so that the failure would be by compression failure of the reinforcement rather than by microbuckling. All specimens were prepared and cured at the same time using the resin formulation and cure cycle described in Table 1A of the Appendix. Resin castings were also made and cured at the same time as the composite specimens. Figure 29 shows several typical specimens with various-sized graphite rods, and also a resin test specimen. The nominal fiber content of the composite specimens was  $k = 0.50$ .

#### COMPRESSION TESTING OF RIGID RESIN COMPOSITES

Most of the compression tests were performed on composites with length-to-width ratios of 4 and 7. These dimensions were chosen well below the critical length for column instability. The pertinent information for the composites and the resin castings, as well as the test data, are summarized in Table 4A of the Appendix. The specimens were tested in an Instron test machine using a self-aligning fixture. The head speed of the machine was 0.02 in. per minute.

In the compression tests of graphite-Hysol composites, all the specimens failed by compression failure of the reinforcement material. Most of the

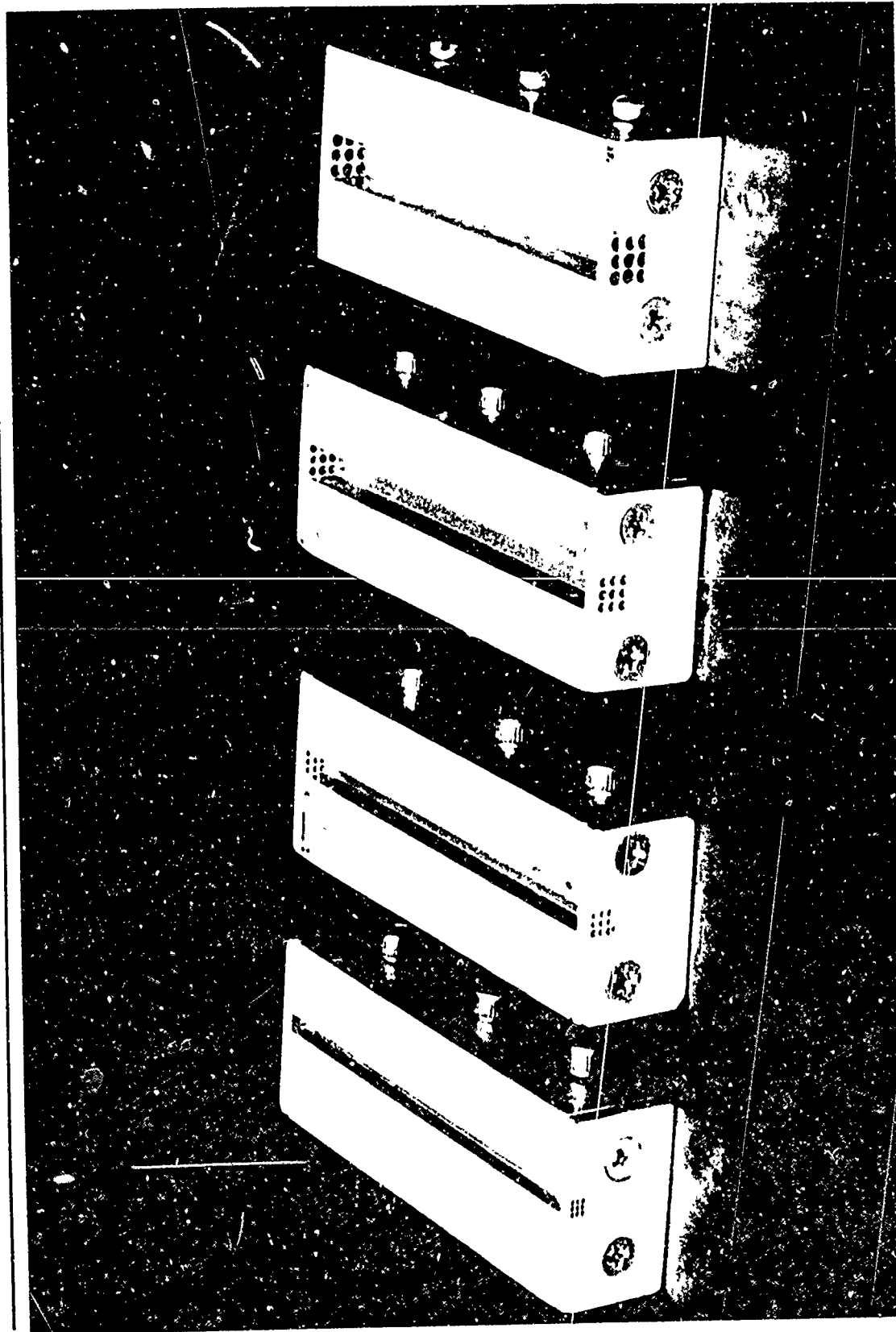


Figure 28. Aluminum Molds for Preparation of Composites

Table IV  
 EFFECT OF DIAMETER ON THE FLEXURE STRENGTH  
 AND MODULUS OF GRAPHITE RODS

Average Rod Diameter (in.)	Number of Specimens Tested	Average Flexure Strength x 10 <sup>-3</sup> psi	Average Flexure Modulus x 10 <sup>-6</sup> psi	Remarks
0.0297	8	26.15	13.22	Specimens machined from 0.079-in. - diameter rods. Span-to-depth ratio was 20:1.
0.0452	9	20.65	12.38	Same
0.0602	9	23.93	12.72	Same
0.0788	9	34.55	13.20	Specimens not machined. Span-to-depth ratio was 17:1.

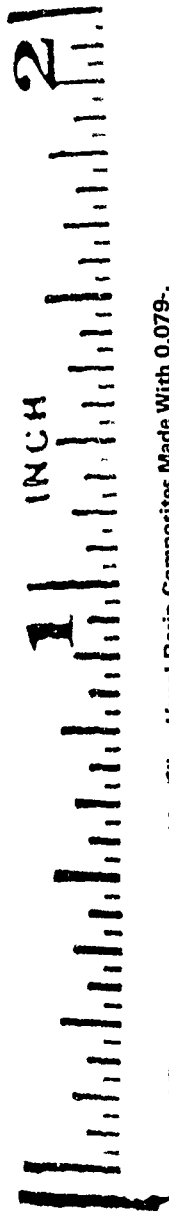


Figure 29. Resin Casting and Typical Unidirectional Graphite Fiber-Hycol Resin Composites Made With 0.079-, 0.060-, 0.045-, and 0.030-In.-Diameter Rods

failures were in the test section, except as noted in Table 4A. Shear failure of the fibers within the composite was a typical failure mode, similar to what was observed previously (Section 2). The test data given in Table 4A are plotted in Figures 30 and 31. Figure 30 shows the compressive strength of the composite and the fiber stress at failure of the composite as a function of fiber diameter. Figure 31 shows the effect of the length-to-width (L/W) ratio of the specimen and of the fiber diameter on the compressive strength of graphite-Hysol composites. From the results shown in Figures 30 and 31, it appears that the variation of fiber diameter from 0.030 to 0.079 in. does not have any significant influence on the compressive strength of graphite fiber-Hysol resin composites.

As was established previously (Section 2), the "effective" compressive strength (no microbuckling) of the fibers is increased by the rigid resin. The average compressive strength of graphite rods tested individually was 57,500 psi (Table II), while the average compressive fiber stresses at failure of composites described here were 65,000 psi.

Typical load-deflection and stress-strain curves for various composite specimens are shown in Figures 32 and 33. Figure 33 also shows the typical stress-strain curve for the Hysol resin.

#### COMPRESSION TESTING OF SOFT RESIN (URETHANE) COMPOSITES

In addition to the specimens and tests already described in Table 3A, a nine-rod composite containing 0.030-in. diameter graphite rods in urethane resin was fabricated and tested. When making the 0.030-in. diameter fiber composites, difficulties were encountered in making void-free specimens when using the cure cycle described in Table 1A. Therefore, the cure cycle was modified. The new cure cycle, described in Table 5A, did eliminate the problem of porosity. Moreover, it also affected the Young's modulus of the resin, which increased from approximately 1,460 psi to  $\approx 2,500$  psi. A typical compressive stress-strain curve for a urethane resin cured according to the modified cure cycle is shown in Figure 34. The pertinent data for the microbuckling specimens, the resin specimens, as well as the test results, are shown in Table 6A. The same test setup as

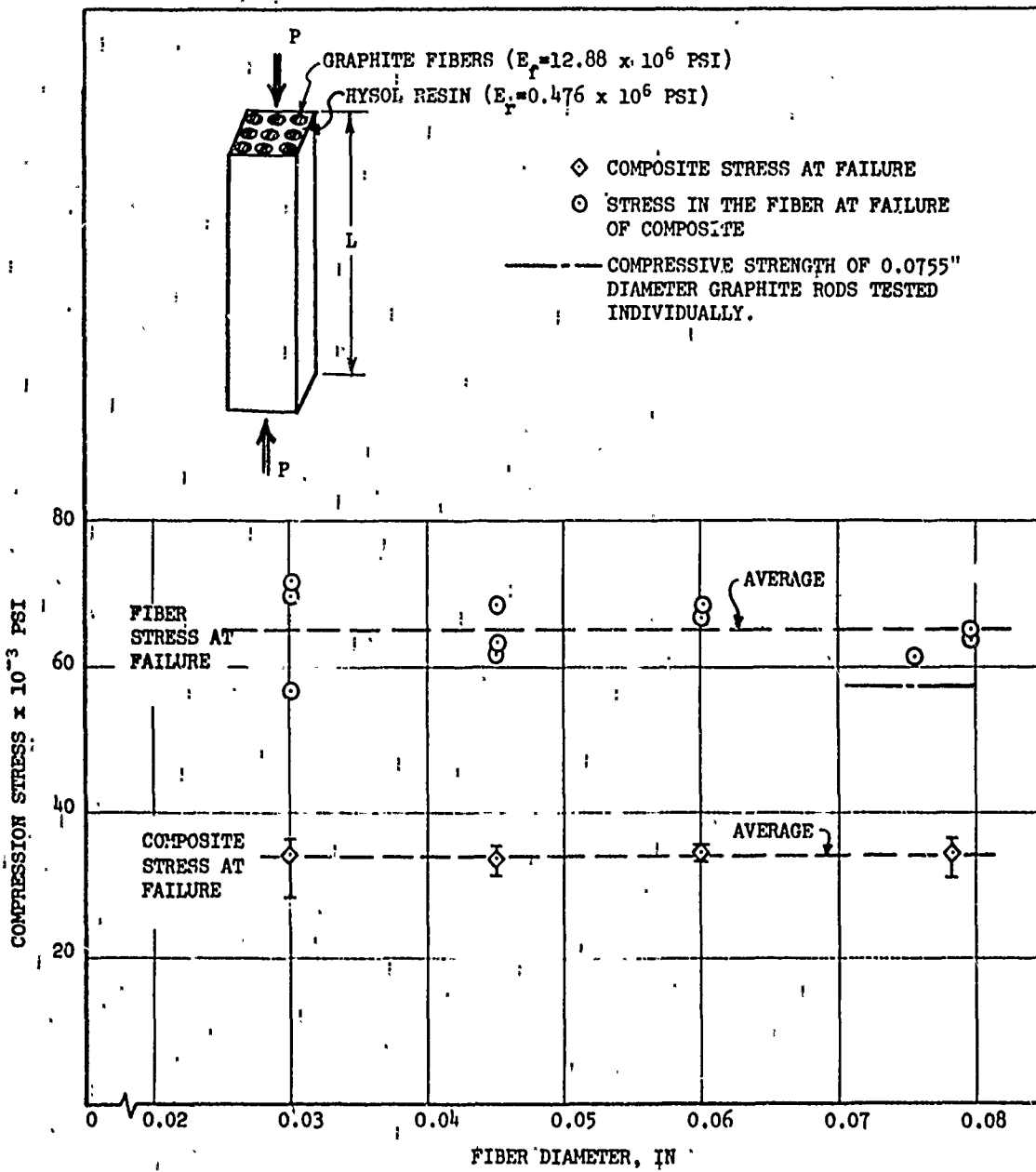


Figure 30. Effect of Fiber Diameter on the Compressive Strength of Composites and Fiber Failure Stress

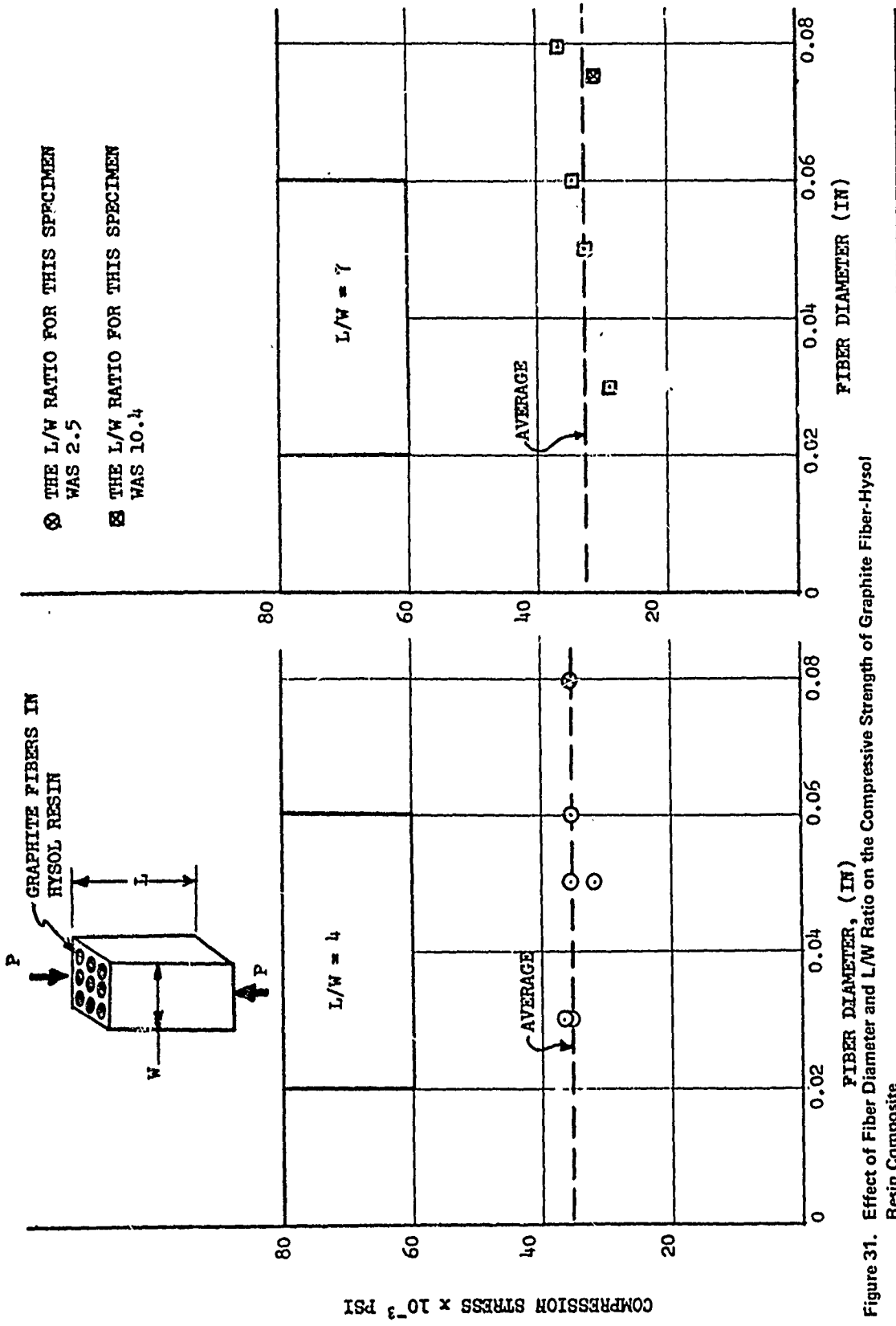


Figure 31. Effect of Fiber Diameter and L/W Ratio on the Compressive Strength of Graphite Fiber-Hysol Resin Composite

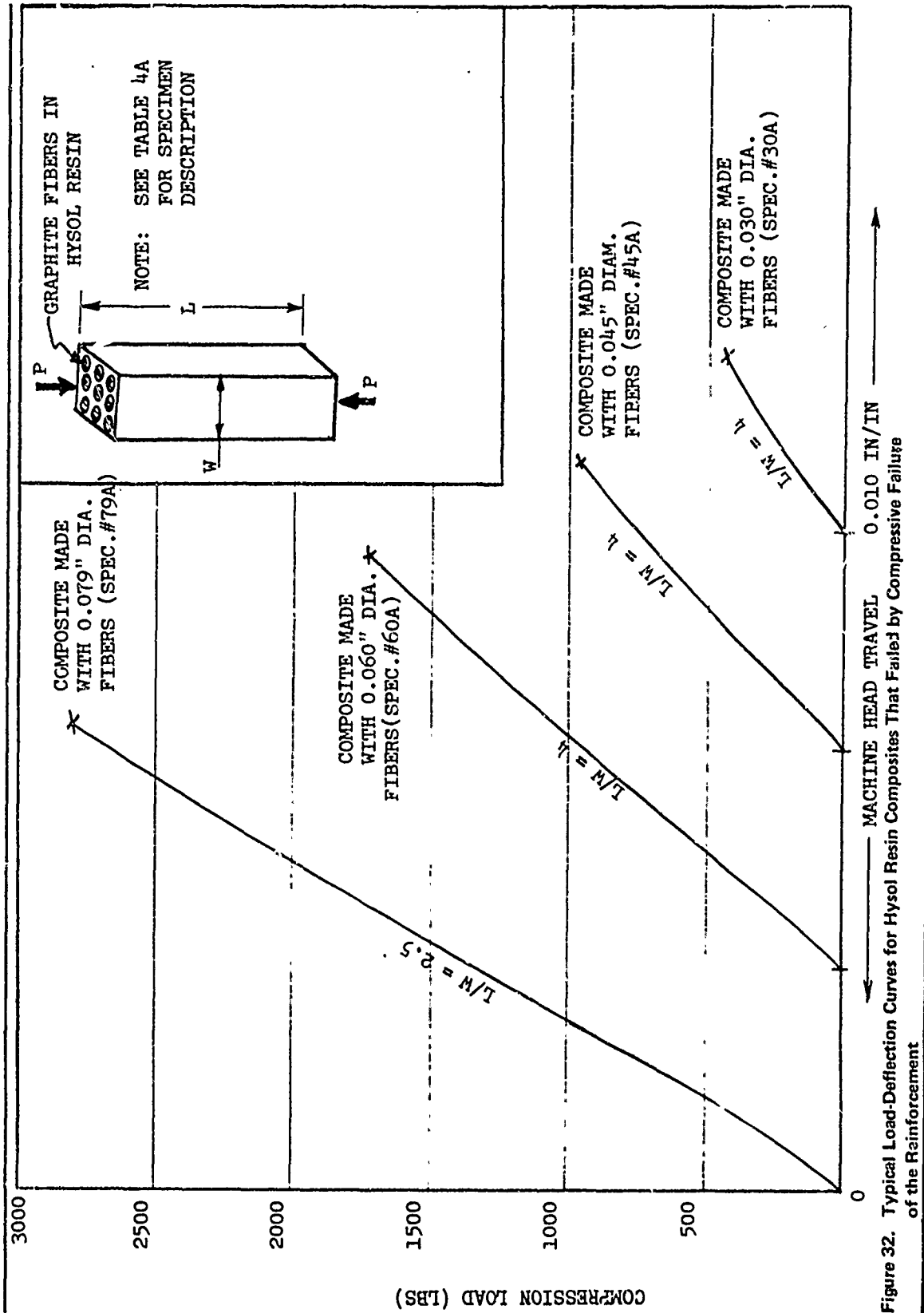


Figure 32. Typical Load-Deflection Curves for Hysol Resin Composites That Failed by Compressive Failure of the Reinforcement

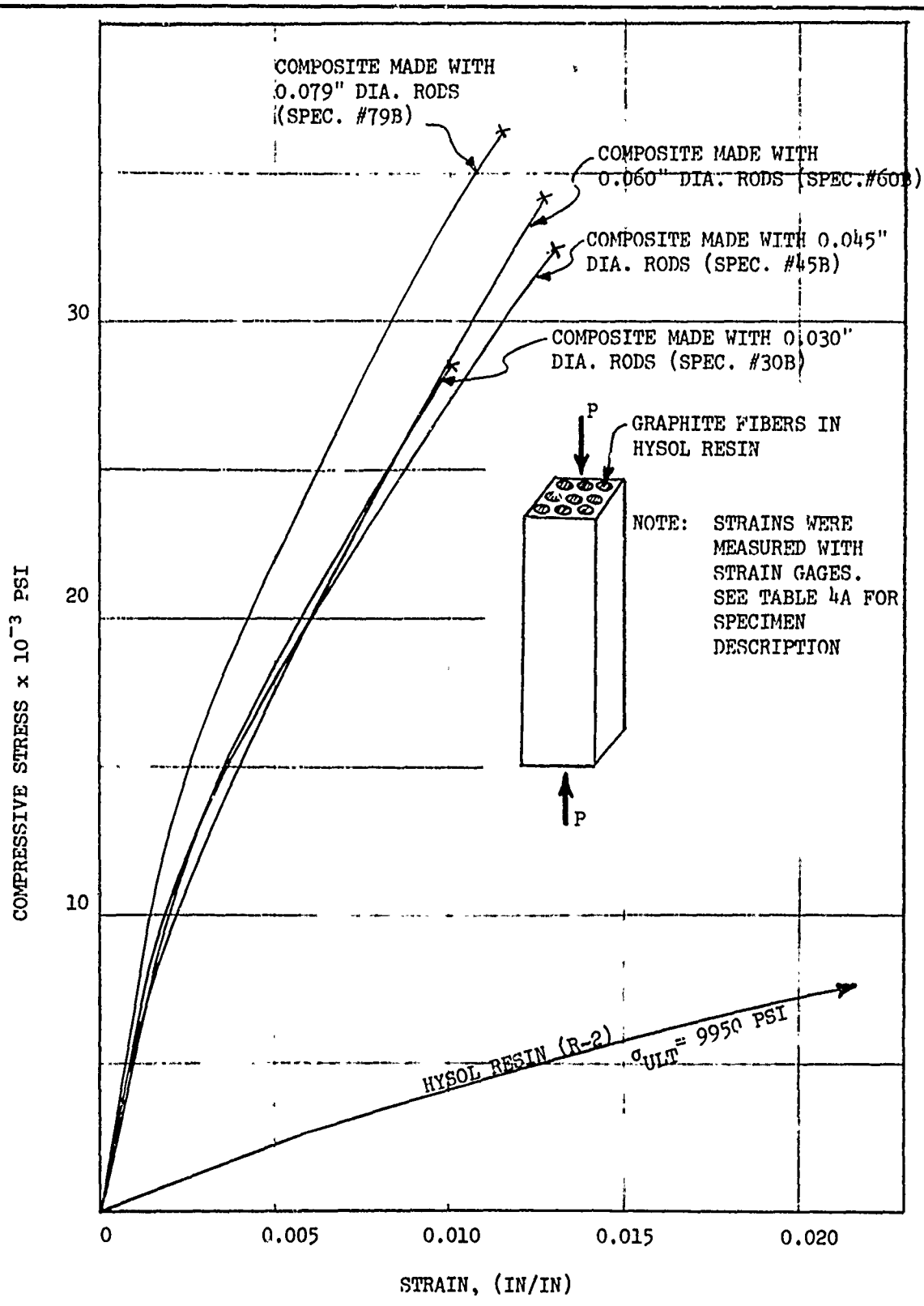


Figure 33. Typical Stress-Strain Curves for Hysol Resin Composites Subjected to Compressive Loading

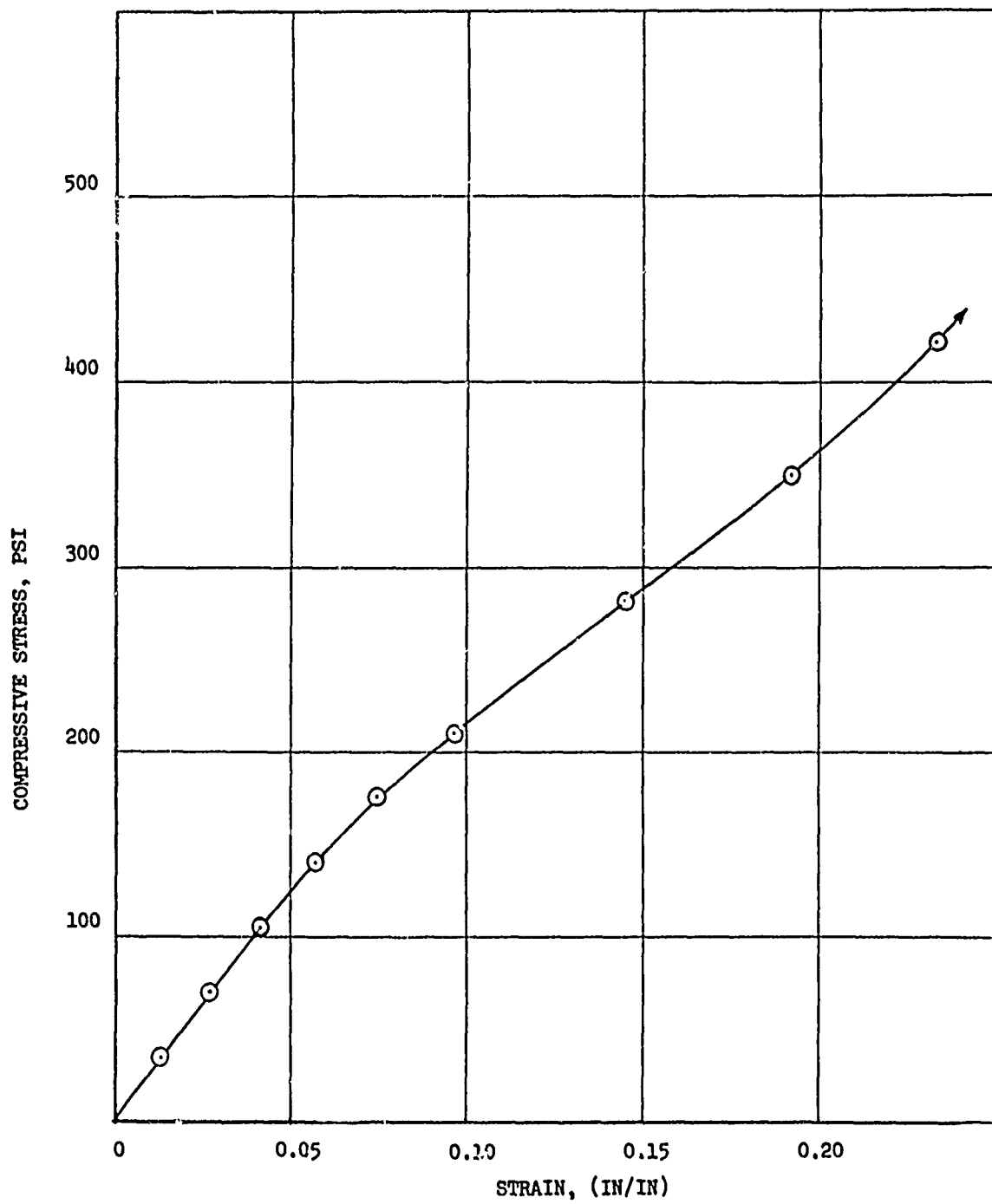


Figure 34. Typical Compression Stress-Strain Curve for Urethane Resin (Specimen R-3 of Table 6A)

described previously was used. Except for machine head travel, no precise strain or deflection measurements were made when testing the composite specimens. The load-deflection (machine head travel) curve was adequate to determine when failure by microbuckling took place. The deflection of the resin specimens was measured with a lightweight Instron extensometer. As before, the resin "batch" used to make the various composites was also used to make resin castings that were co-cured with the various composites.

A comparison between the experimental results reported here and in Section 2 and the theoretical microbuckling stresses predicted by Equation (4) is shown in Table V. As was already noted in Section 2, it appears that it does not make much difference in microbuckling if the composite contains nine-rods or 25-rods. The experimental results normalized with respect to the theoretical results are almost the same. The experimental microbuckling stress for 0.030-in. fiber-diameter composite, normalized with respect to the theoretical value, is lower than the normalized results for the 0.079-in. fiber-diameter composite. Since only one 0.030-in. fiber-diameter composite was tested, no conclusions can yet be made as to the effect of fiber diameter on the microbuckling of unidirectional composites. It is noted that for large-diameter fiber composites, the experimental results are consistently much higher than the values predicted from a two-dimensional theory [Equation (4)].

Table V  
 TEST-THEORY COMPARISON FOR COMPOSITE  
 MICROBUCKLING

Composite	Fiber Dia. (in.)	L/W (1)	Fiber Vol (%)	Composite Microbuckling Stress $\times 10^{-3}$ PSI			Remarks
				Test	Theory (2)	Test/Theory	
9-Rod Graphite-- Urethane Composite	0.030	11.1	48.8	5,460	4,476	1.220	New Data ( $E_{resin} = 2,380$ )
25-Rod Graphite-- Urethane Composite	0.0792	9.1	53.8	5,440	3,812	1.426	New Data ( $E_{resin} = 2,634$ )
9-Rod Graphite Composite (Spec No. 7-3d)	0.0784	10.9	53.4	6,870	4,607	1.490	Previous Data ( $E_{resin} = 1,664$ psi)
9-Rod Graphite-- Urethane Composite (Spec No. 6-3)	0.0747	11.1	48.3	6,030	4,186	1.440	Previous Data ( $E_{resin} = 2,263$ psi)

(1) L/W = Length of the Specimen Divided by the Width

(2) Based on Measured Resin Properties given in the Last Column and Previously Measured Average Poisson's Ratio of  $\nu = 0.472$ .

#### Section 4

### INFLUENCE OF CONSTITUENT PROPERTIES ON MICROSTABILITY OF UNIDIRECTIONAL COMPOSITES

Three different resins and two different types of reinforcing fibers were used to investigate the effect of constituent material properties on the microstability of unidirectional composites. The reinforcing materials included stainless steel wire and previously used graphite fibers. The resins used included urethane resin and two new resins with moduli of elasticity of 179,000 and 105,000 psi.

#### CHARACTERIZATION OF CONSTITUENT MATERIALS AND PREPARATION OF COMPOSITE SPECIMENS

Mechanical properties tests were performed to characterize the reinforcement and matrix materials. Tables VI and VII show the results and also give the pertinent information for the specimens and the tests that were performed. Figure 35 shows the typical stress-strain curves for the two resins designated as Epoxy A and Epoxy B. A typical stress-strain curve for the urethane resin was shown previously (see Figures 8 and 34).

Some difficulties were encountered in measuring the properties of Resin B. This was due to the resin having highly nonlinear stress-strain behavior, low modulus (thus prevent use of strain gages), and a high degree of creep. Mechanical extensometers and Instron head travel (corrected for machine compliances) were finally used to obtain the Young's modulus. The modulus values varied from approximately 80,000 to 120,000 psi. Both Resin A and Resin B have highly nonlinear stress-strain behavior, as shown in Figure 35.

The composite models made of graphite and steel rods contained nine rods each. The rods were arranged in a square array at a spacing corresponding to 50-percent fiber volume fraction. The composites were prepared in aluminum molds (shown in Figure 28). Each time that a composite was

**Preceding page blank**

Table VI  
MECHANICAL PROPERTIES OF  
REINFORCEMENT MATERIALS\*

Material	Material Description	Fiber Diameter (in.)	Young's Modulus x 10 <sup>-6</sup> psi			Remarks
			Tension	Compression	Flexure	
Stainless steel	Stainless steel QQW423; FS 302 Condition B wire	0.078	26.8(6)	- - -	26.7(4)	
Graphite	Extruded rods	0.078	12.50	12.18	11.89	See Table I

Table VII  
MECHANICAL PROPERTIES OF RESINS  
USED IN MODELS\*

Resin †	Formulation (parts by weight)	Average Young's Modulus x 10 <sup>-6</sup> psi			Poisson's Ratio
		Tension	Compression	Flexure	
Urethane	100 parts Hysol 2085 24 parts hardener 3562	- - -	0.001757(2)	- - -	0.472
Epoxy A	50 parts Epoxy 2795 61 parts Versamid 140	0.179(3)	0.178(5)	0.179(3)	0.399(3)
Epoxy B	50 parts Epoxy 2795 68 Parts Versamid 140	- - -	0.105(12)	- - -	(0.44)

\*Numbers in parentheses denote number of tests.

†The resin castings were made from the same resin batch and cured at the same time as the composite models. Resins A and B were cured at 120°F for 18 hr. Cure cycle for urethane resin is shown in Table 5A.

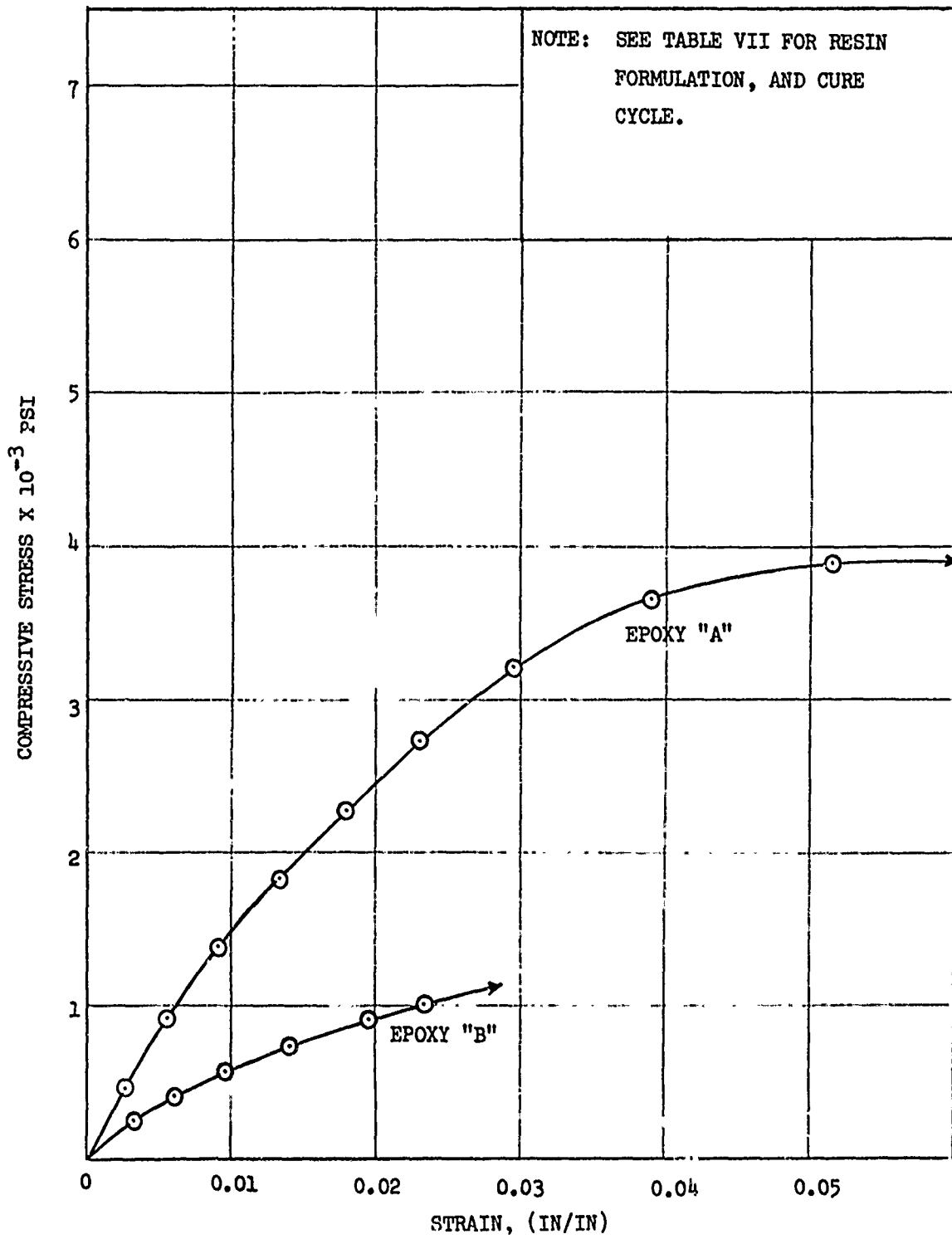


Figure 35. Compression Stress-Strain Curves for Resins A and B

prepared, a resin casting was made from the same resin batch as the composite and cured at the same time as the composite. The resin castings were used for measuring resin properties. The composite specimens were of square cross section and of two different nominal lengths,  $\approx 1.5$  in. and 2.5 in.

#### COMPRESSION TESTING OF COMPOSITES

All testing was performed in an Instron test machine provided with a self-aligning test fixture. The head speed of the machine was 0.02 in. per min. Pertinent information for the composites as well as the test data are summarized in Tables 7A, 8A, and 9A. Also included therein are remarks on failure type and location.

Typical load-deflection curves for the steel rod composites are shown in Figure 36 and 37. Figure 36 shows the load-deflection curve for the 1.5-in.-long specimen. Figure 37 shows a typical load-deflection curve for the 2.5-in.-long specimen and also the effect of repeated loading on microstability. Upon the first loading cycle the specimen, for which data are shown in Figure 37, did not exhibit any permanent damage. Subsequent loadings resulted in the load-deformation curves shown in Figure 37. Upon the fourth loading cycle, there was a slight bow in the specimen. The load-deflection curves for graphite fiber composites were similar to those shown in Section 2.

Two failure modes were observed in graphite fiber composites. As before, composites made with urethane resin (soft resin,  $E = 1,757$  psi) failed by microbuckling. Composites made with Resins A and B (moduli of  $179 \times 10^3$  psi and  $105 \times 10^3$  psi, respectively) failed by compression failure of the material and also by longitudinal cracking parallel to the direction of the fiber. Shear failure of the fibers was observed in most of the specimens. Typical failure modes of composites made of graphite fibers and Epoxy A are shown in Figure 38. Longitudinal splitting due to induced transverse tension and shear failures of fibers are readily seen. The recessed fibers at the end of the specimen indicate fiber matrix interface failure, probably caused by the sudden removal of the load when the specimens failed.

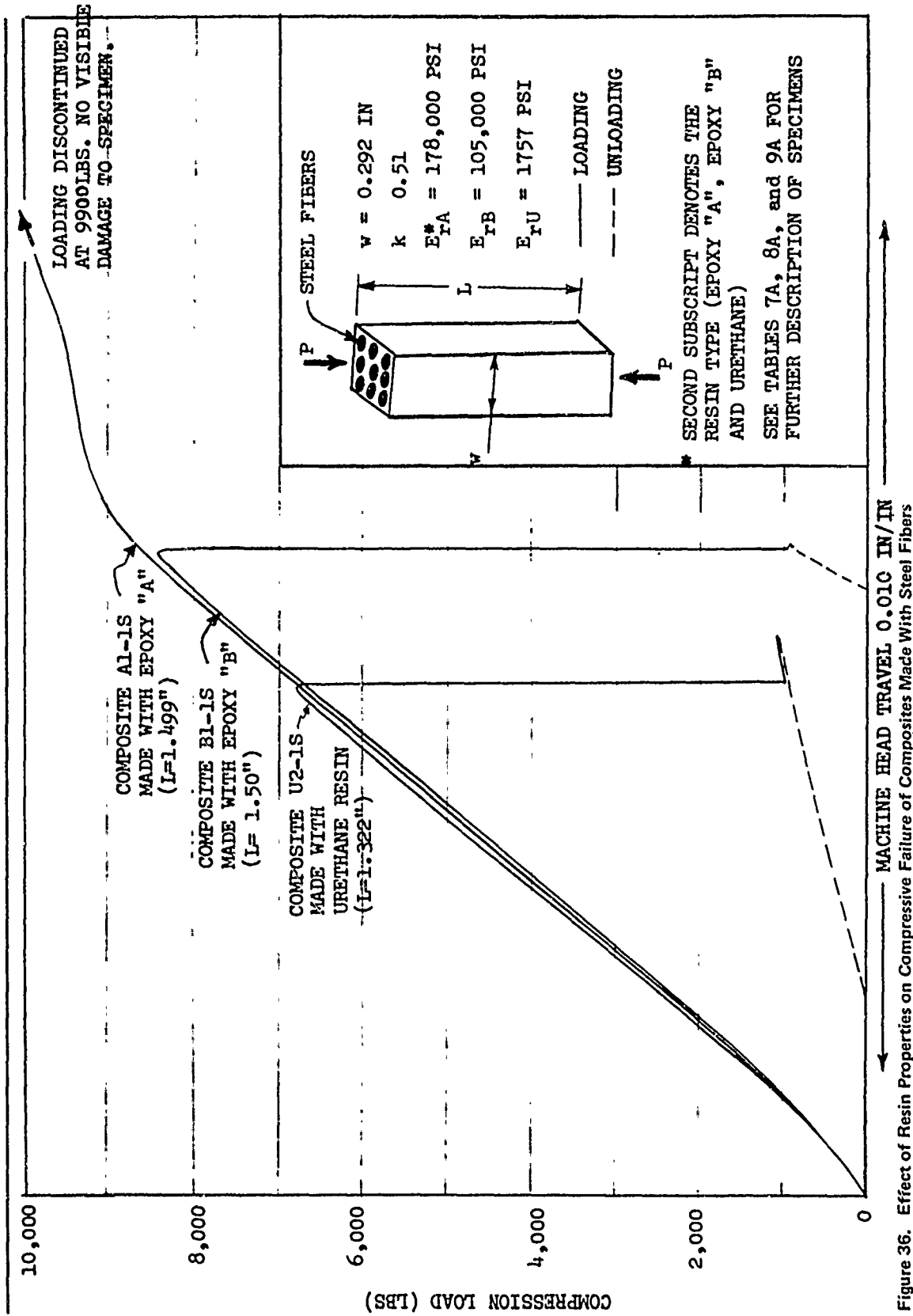


Figure 36. Effect of Resin Properties on Compressive Failure of Composites Made With Steel Fibers

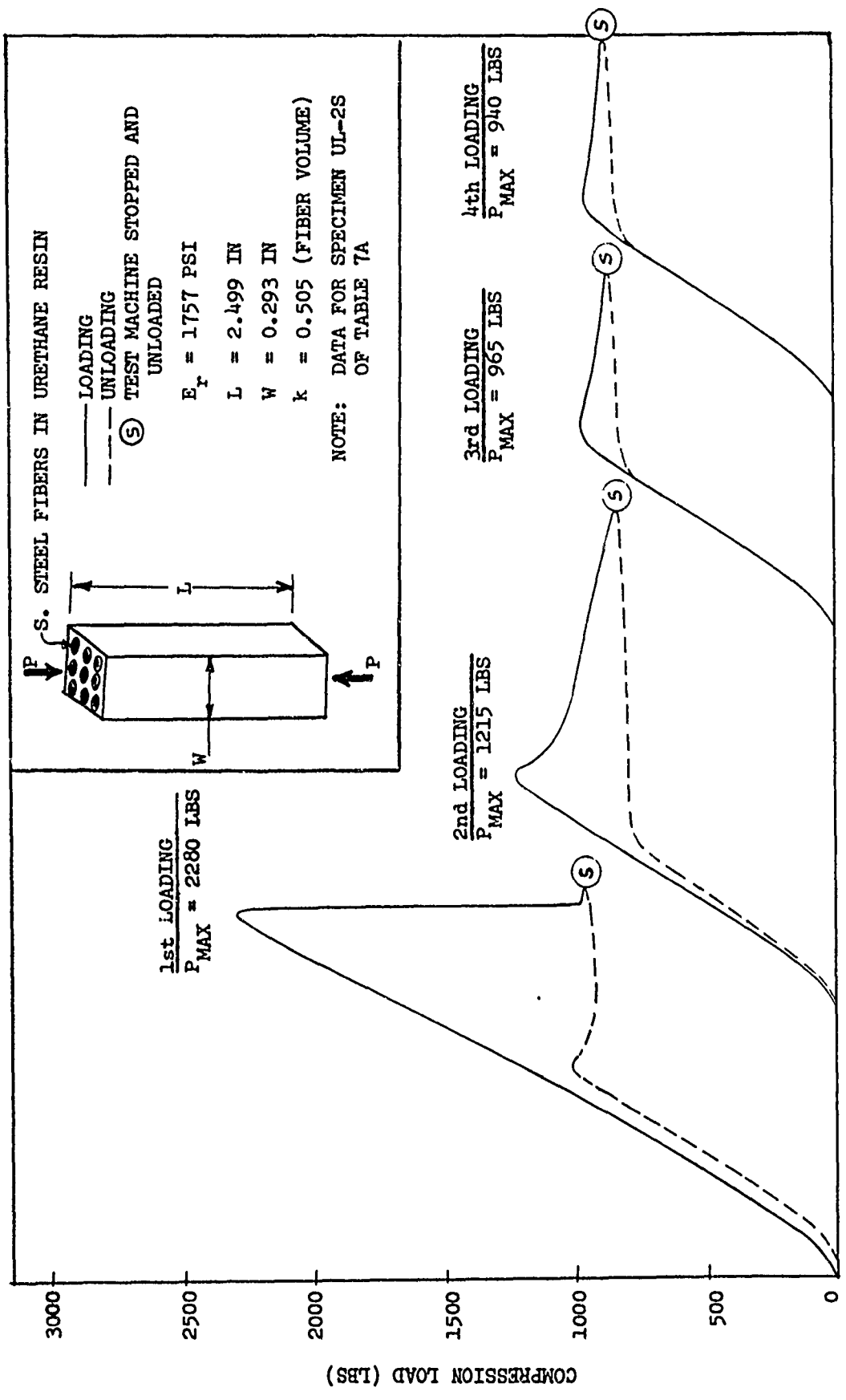


Figure 37. Effect of Repeated Loading on Microbuckling of Steel-Urethane Unidirectional Composites



A

Figure 38. Compression Failure Modes of Composites Made With Graphite Fibers and Epoxy A

Three failure modes were observed in composites made with steel rods: elastic microbuckling, inelastic microbuckling, and yielding of the reinforcement material. Some of the specimens that failed by inelastic microbuckling contained longitudinal cracks in the resin. The composites made with urethane (soft resin) failed by microbuckling. The composites made with Epoxy A and Epoxy B resins failed by elastic and inelastic microbuckling and also by compression yielding of steel rods. Several of the failed specimens are shown in Figure 39 and 40. Figure 39 shows the 1.5-in. -long specimens after failure. The excessive deformation in the first two specimens was caused by increasing the loading after failure by microbuckling. The third specimen shown in Figure 39 failed by yielding of the reinforcement. The load deflection curves for the three specimens shown in Figure 39 are shown in Figure 35. Figure 40 shows the 2.5-in. long specimens after failure. The failures shown are not microbuckling but are failures "triggered" by microbuckling deformations similar to what was described in Section 2. The fact that the failures shown in Figures 39 and 40 were not column buckling or bending failures can readily be seen from Figure 36. There, all the specimens were approximately of the same geometry and had approximately the same composite modulus in the fiber direction. Two of the specimens failed, however, by microbuckling, and one by compression yielding of the reinforcement.

The comparison of experimental and theoretical results is shown in Figures 41, 42, and 43. Equation (4) was used to predict the load at which microbuckling takes place.

As before, most of the experimental results on microbuckling fall above the theoretically predicted values. As shown in Figure 41, the test-theory correlation is much poorer for steel-urethane composites than it is for graphite-urethane composites. The effect of resin shear modulus on the compression strength of composites is shown in Figures 42 and 43. The experimental results are plotted there as a function of initial shear modulus. Due to the highly nonlinear stress-strain behavior of resins A and B (Figure 35), the effective shear moduli of the resins at the load that caused

SPECIMEN U2-16  
OF TABLE 7A



SPECIMEN A1-15  
OF TABLE 8A



SPECIMEN B1-18  
OF TABLE 8A



A

B

C

Figure 39. Failed Composite Specimens Made of S. Steel Fibers and Urethane (U), Epoxy B (B), and Epoxy A (A) Resins (L ≈ 1.5 IN.)



SPECIMEN A (C)  
OF TABLE 6A



SPECIMEN B (C)  
OF TABLE 6A



SPECIMEN U (C)  
OF TABLE 7A

U B A

Figure 40. Failed Composite Specimens Made of S. Steel Fibers and Urethane (U), Epoxy B (B), and Epoxy A (A) (L  $\approx$  2.50 In.)

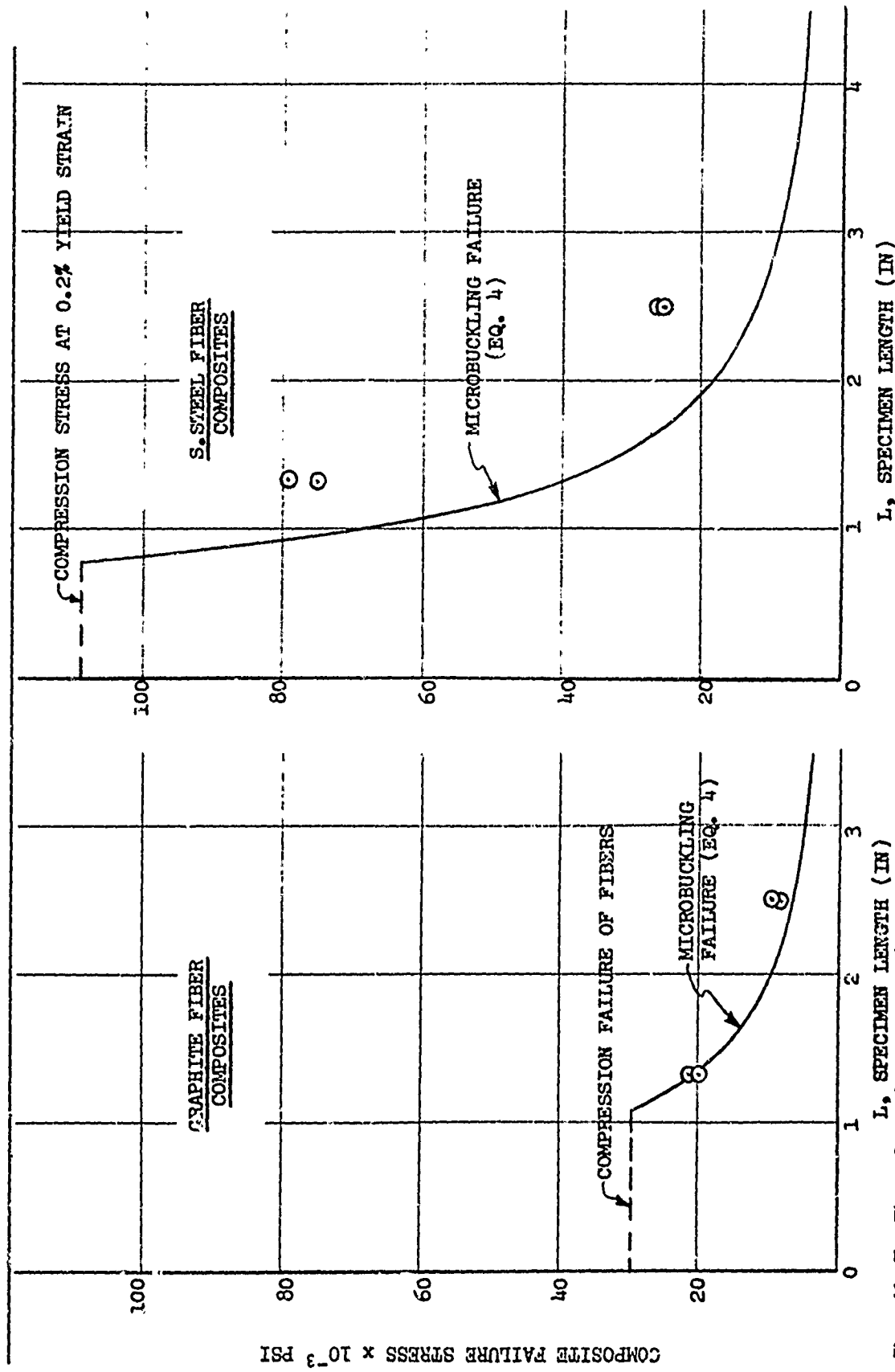


Figure 41. Test-Theory Comparison of Compressive Strength of Urethane Resin Composites Reinforced With Graphite and Stainless Steel Fibers

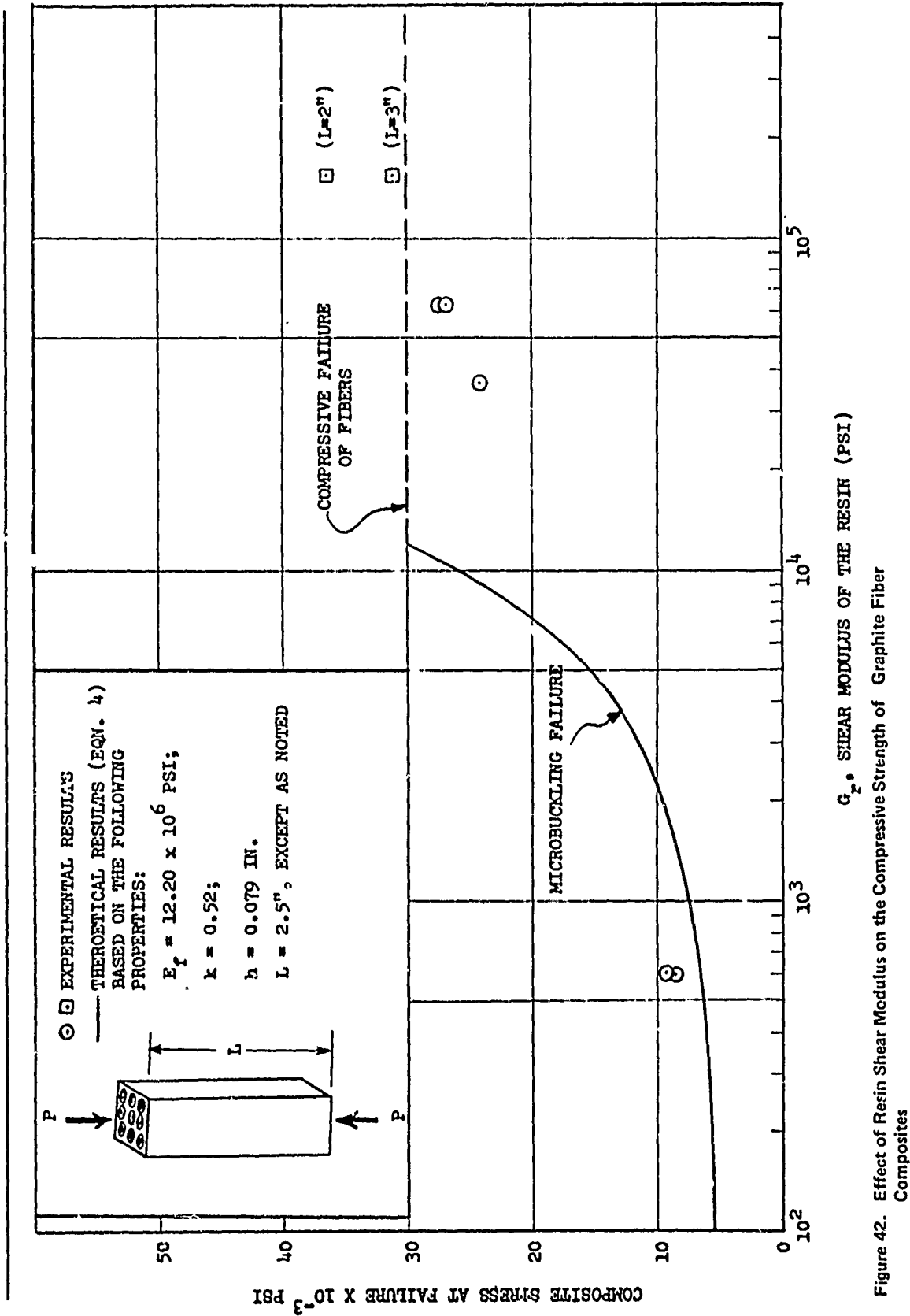


Figure 42. Effect of Resin Shear Modulus on the Compressive Strength of Graphite Fiber Composites

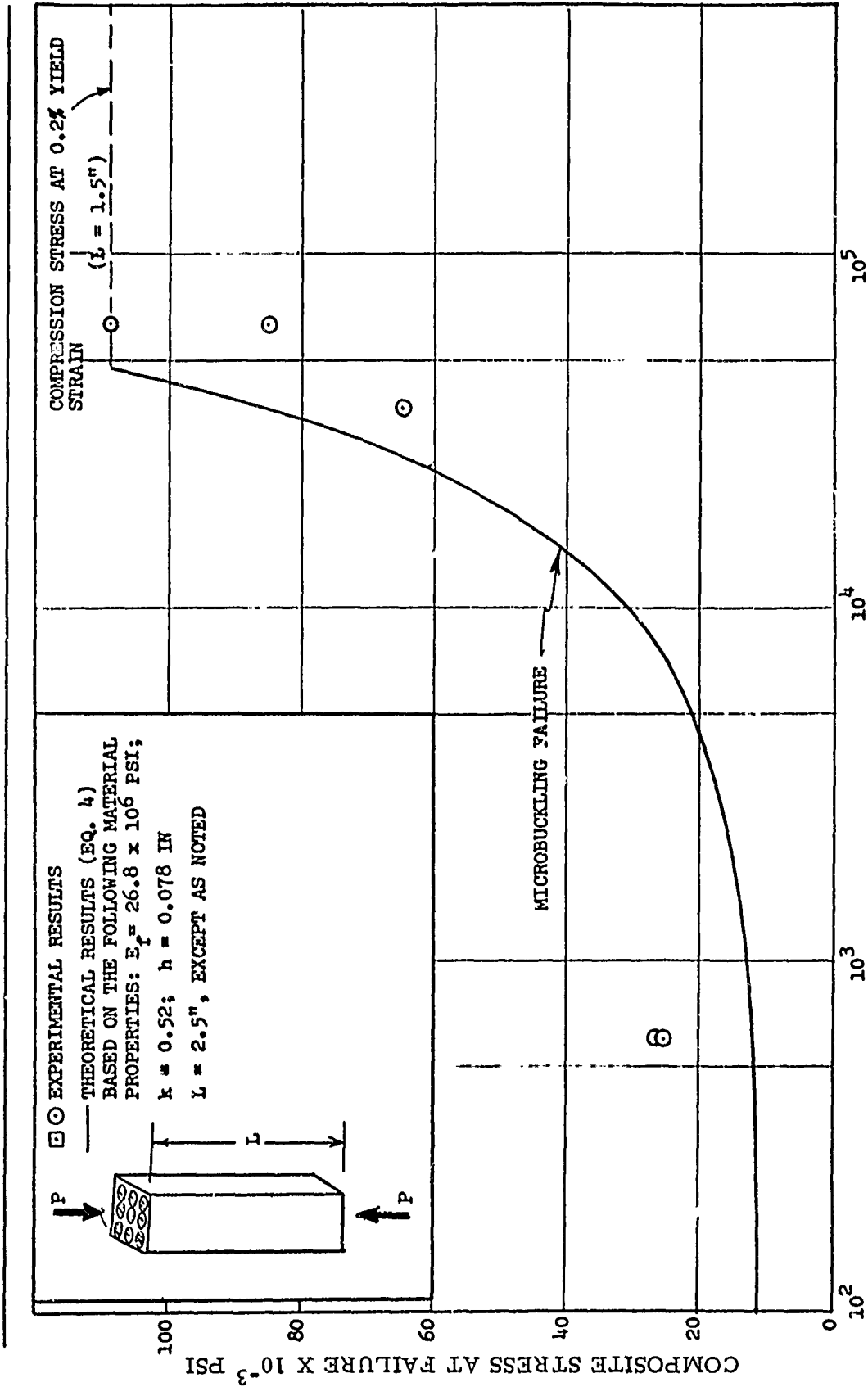


Figure 4. Effect of Resin Shear Modulus on the Compressive Strength of Stainless Steel Fiber Composites

microbuckling were much lower than the elastic shear moduli. Consequently, if one were to plot the experimental data as a function of shear moduli at failure, this would shift the experimental results to the left of the theoretical curve. Table VIII shows a comparison of experimental and preliminary theoretical results, assuming elastic and inelastic microbuckling.

One additional variable that was investigated briefly was the effect of initial fiber deformation on the compressive strength of composites. By repeated loading of the steel rod-urethane resin composites described in Table 7A, initial deformation was induced in the composites. The amount of deformation (bow) was measured, and the specimens were tested in compression. The test results are shown in Figure 44. Composite failure stress is plotted as a function of the initial deformation. The results show that the initial deformation of the reinforcement drastically reduces the compressive strength of the composite. These results could form a basis for explaining the low compressive strength, as compared to theoretical predictions, of actual composites such as graphite-epoxy.

Table VIII  
TEST-THEORY COMPARISON ASSUMING ELASTIC  
AND INELASTIC MICROBUCKLING

Specimen Designation	Composite Stress at Failure $\times 10^{-3}$ psi		
	Experiment	Theory	
		Elastic Microbuckling	Inelastic* Microbuckling
A1-2S	84.90	141.7	119.8
B2-2S	64.30	85.8	58.5

\* Assuming  $\nu_r = 0.5$

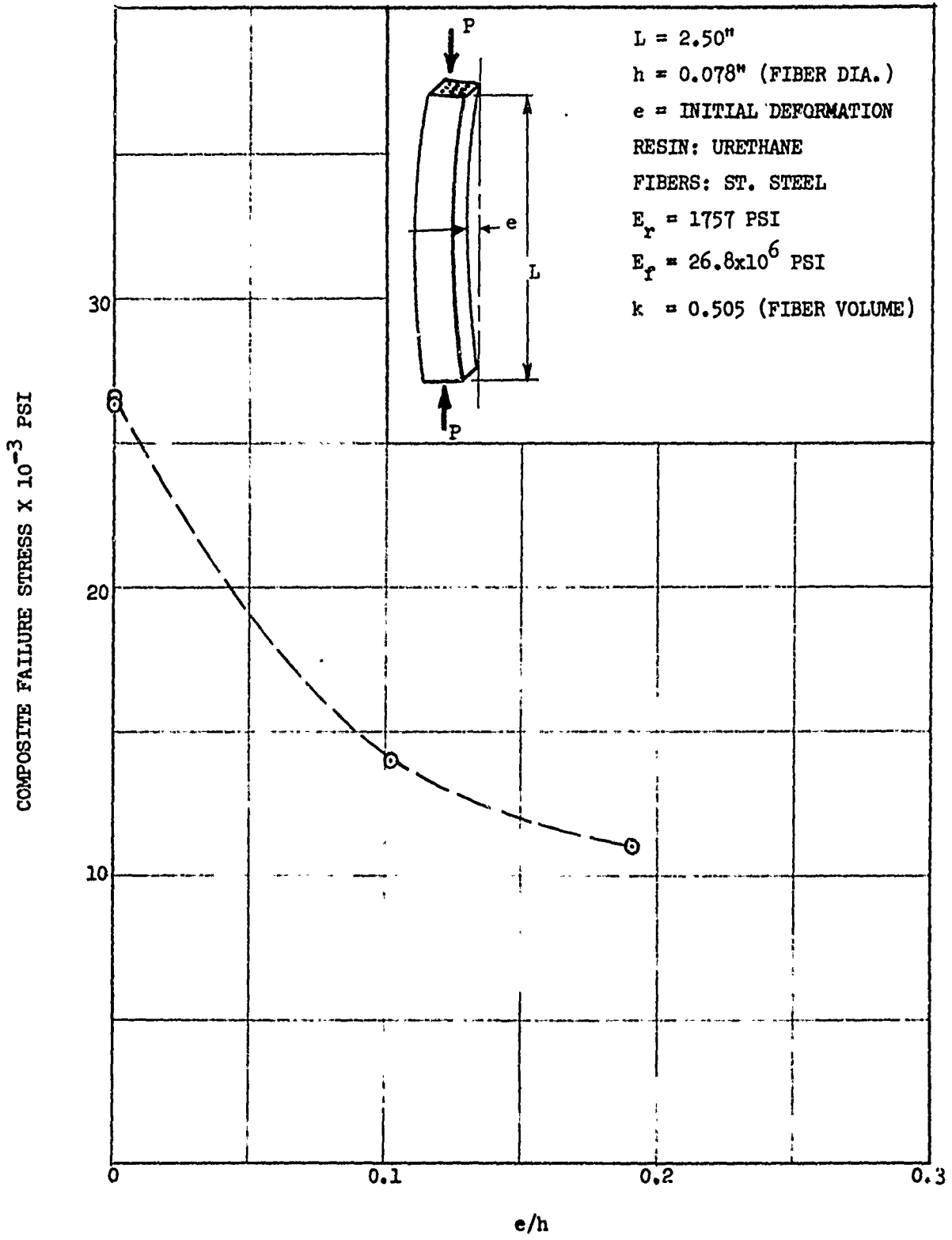


Figure 44. Effect of Initial Deformation on Microbuckling

Section 5  
FURTHER DISCUSSION OF RESULTS

For composites that failed by elastic microbuckling, the test data have been found to fall significantly higher than predicted by a two-dimensional microbuckling theory given by Equation (4). If there are a large number of buckle waves, Equation (4) reduces to

$$(\sigma_{cs})_1 = \frac{G_r}{1-k}$$

which is independent of the fiber properties. Intuitively one would expect that fiber properties should influence the microbuckling stress. Working under this assumption and also noting that  $G_r/(1-k)$  represents a shear modulus of a two-dimensional model composite, it appears reasonable to expect that the microbuckling of three-dimensional composites consisting of circular fibers should be governed by their shear modulus,  $G_{LT}$ ; that is, by the following equation

$$(\sigma_{CS}^*)_1 = G_{LT} + \frac{\eta^2 E_f k}{12} \left(\frac{mh}{L}\right)^2 \quad (17)$$

rather than by Equation (4). In Equation (17)

$$G_{LT} = f(G_r, G_f, k) \quad (18)$$

and can be obtained from various references [13, 14]. It is noted that  $G_{LT} > G_r/(1-k)$ .

A comparison of test data with results predicted from Equations (4) and (17) is shown in Figure 45. The test results shown in Figure 45 are for graphite-urethane composites and for graphite-Hysol composites and were

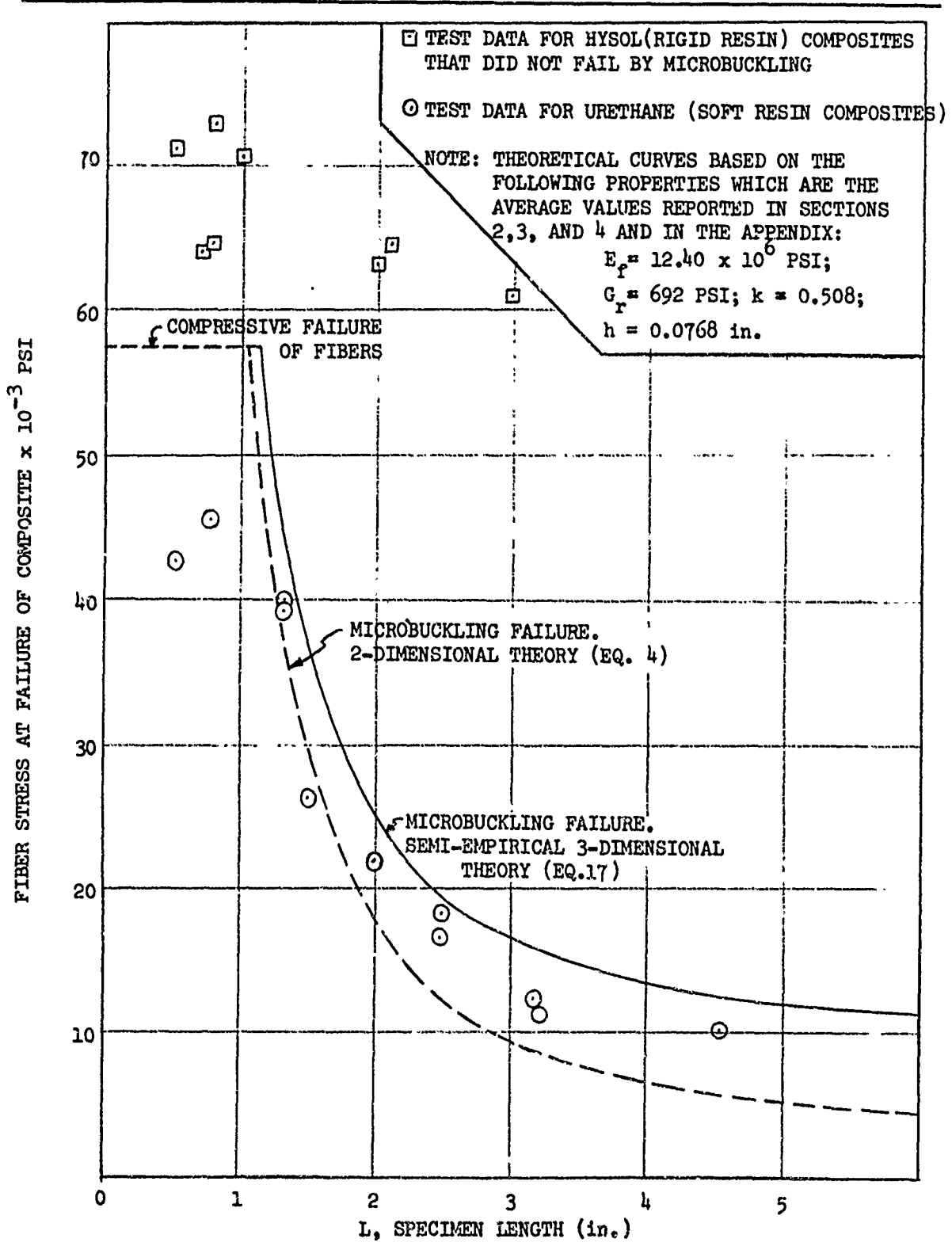


Figure 45. Comparison of Test Data for Graphite Fiber Composites With the Results Predicted by Two Dimensional and Semi-Empirical Three-Dimensional Microbuckling Theory

obtained from Tables 3A, 4A, 6A, and 7A. The theoretical curves shown in Figure 45 were based on the following properties:  $E_f = 12.40 \times 10^6$  psi,  $G_r = 692$  psi,  $k = 0.508$ , and  $h = 0.0768$  in. These are the average values for all the data reported in Sections 2, 3, and 4, and in the Appendix.

The theoretical results predicted by Equation (17) show a better correlation with the test data than the results predicted from Equation (4); the theory, Equation (17), is higher than the test data, as one would expect.

Figure 45 also shows the test data obtained from various tables for composites that did not fail by microbuckling but rather by compression failure of the reinforcement. The data are for composites consisting of graphite rods in Hysol (rigid resin) composites. It is interesting to note that for rigid resin composites, the fiber stresses at failure of the composites were significantly higher than the compressive strength of the fibers tested individually. On the other hand, for soft resin composites, the fiber stresses at failure of the composites were lower than the strength of fibers tested individually. The effect of resin properties on the fiber stresses at failure of the composites is shown in Figure 46.

The new, semi-empirical equation that is proposed for predicting the microbuckling stresses of composites, Equation (17), appears to contradict the experimental results that are reported in literature for actual composites [9, 11]. The experimental data obtained by Lager and June [9] and by Moncunill de Ferran and Harris [11] fall below the theoretical results predicted by Equation (4). They therefore proposed use of a correction factor  $K$  ( $K < 1$ ) in Equation (4), which would provide an improved test-theory correlation. If one compares Equations (4) and (17), however, the semi-empirical equation suggests use of  $K > 1$ . This apparent contradiction between the results for actual composites reported in the literature and the experimental results on model composites obtained in the present study has not yet been resolved. Factors that could explain the abnormally low (as compared to theoretical values) compressive strength of actual

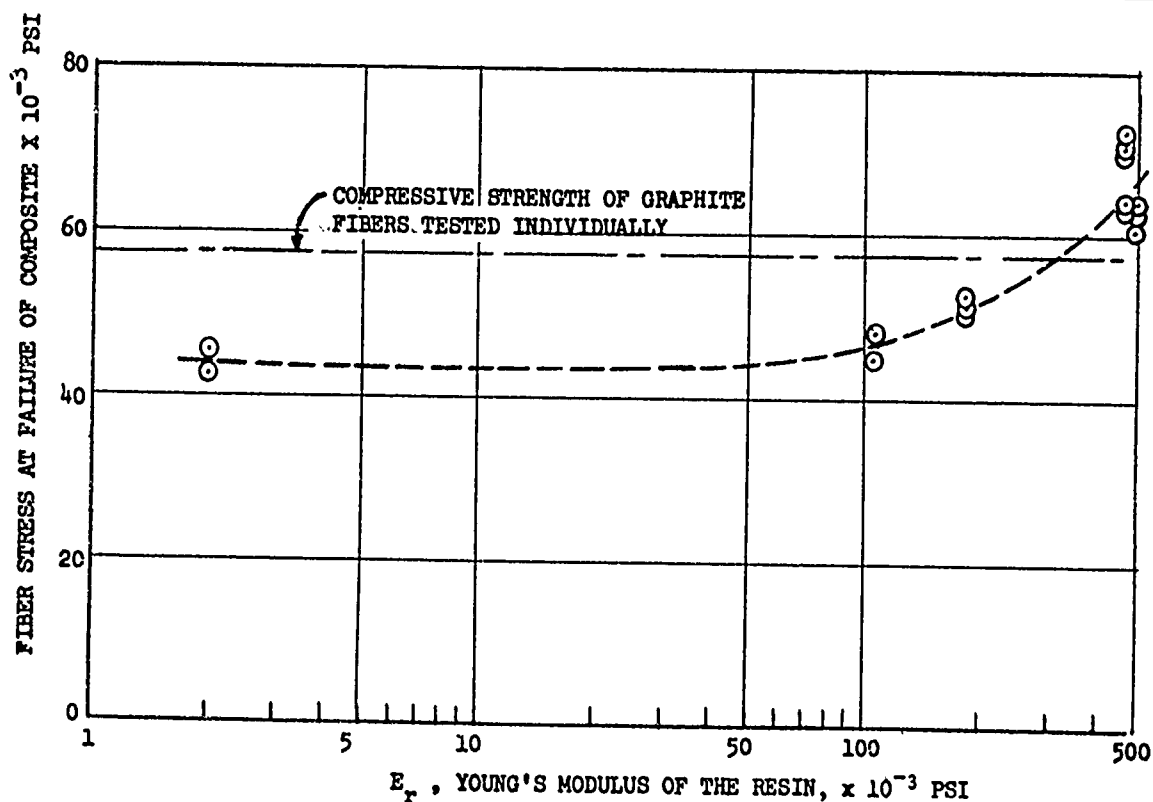


Figure 46. Effect of Young's Modulus of the Resin on the Non-Microbuckling Compressive Strength of Graphite Fibers at Failure of Composites

composites such as graphite epoxy are initial, prebuckling fiber deformations; poor fiber-matrix bond; effect of residual thermal stresses; porosity; fiber size effect; failure modes other than assumed in the analysis, helicoidal fiber buckling for example [11]; inadequate test methods; and possibly others.

Preliminary results shown in Figure 44 indicate that prebuckling deformations in the fibers drastically decrease the compressive strength of composites. The theoretical results of Herrmann, et al. [6, 7] confirm this conclusion to some extent. If the composite contained poorly bonded fibers, one would expect the fibers to debond at low load intensities. The shear modulus of a composite with debonded fibers would therefore be much lower than that of a composite in which the fibers were firmly bonded.

The decreased shear modulus due to fiber de-bonding would result in a decrease in microbuckling stress. Sadowsky, et al. [5] have shown theoretically, and Rosen [3] has shown experimentally that residual thermal stresses induced during cure can cause microbuckling of a single fiber imbedded in a matrix. The effect of residual thermal stresses on microbuckling of multifiber composites is not known at the present time. As to the effect of porosity, it is well known that porosity decreases the shear modulus of composites. Since the critical microbuckling stress is a function of the shear modulus, porosity will also decrease its value. As to the size effect, it has not yet been established conclusively what influence it has on microbuckling strength. It is noted, however, that whereas the compressive strength of composites made with 0.005-in. - diameter boron fibers is of the order of 300 to 450 ksi, the compressive strength of composites made with 0.0004-in. diameter graphite or glass fibers is of the order of 100 to 200 ksi.

As suggested in Reference 11 and also mentioned in Reference 5, there may be a lower-energy buckling mode, such as helicoidal fiber buckling, than the buckling mode assumed when using the beam-on-elastic-foundation approach. Finally, the test methods for actual composites cannot be ignored when trying to explain the low compressive strength as compared to theoretically predicted values. There are approximately half a dozen different test methods of various degrees of complexity, each giving somewhat different results.

Of the various explanations for the low compressive strength of actual composites as compared to theoretical results, the effect of prebuckling deformations coupled with size effect and improved test techniques deserve primary consideration.

Section 6  
CONCLUSIONS

The following conclusions are drawn from the work described in this report:

- A. The experimental results on composite models follow the same trend as predicted by the microbuckling theory. Microbuckling appears, therefore, to be a valid failure mode for unidirectional composites subjected to compressive loading parallel to the direction of the fibers.
- B. The experimental results for nearly perfect composite models consisting of resin reinforced with circular fibers are higher than the theoretical results predicted from a two-dimensional microbuckling theory. A semi-empirical microbuckling theory for three-dimensional composites shows an improved correlation with the test data.
- C. The compressive strength of composites is increased by increasing the shear modulus of the matrix and also by increasing the Young's modulus of the fibers.
- D. Resin properties influence the failure modes of unidirectional composites subjected to compressive loading parallel to the fiber direction. Composites made with low-modulus resin fail by microbuckling; composites made with intermediate-modulus resin fail by cracking parallel to the direction of the fibers (transverse tensile failure); composites made with high-modulus resin fail by compression failure of the fibers.
- E. At failure of a composite, the effective compressive fiber strength is increased by a high-modulus resin and decreased by a low-modulus resin, as compared to the compressive strength of fibers tested individually.

*Preceding page blank*

- F. For high-modulus resin composites designed to fail by compression failure of the reinforcement (no microbuckling), the variation of fiber diameter from 0.030 in. to 0.079 in. did not have any significant influence on the compressive strength of composites.
- G. Microbuckling failure can be elastic or inelastic, depending on the properties of constituents. Both types of failures were observed.
- H. Preliminary test data on the effect of prebuckling fiber deformations on the compressive strength of composites shows that the compressive stresses at which microbuckling takes place are reduced by 58 percent if the amplitude of prebuckling deformation is 20 percent of the fiber diameter.

12. B. Levenetz, Large Diameter Fiber Reinforced Plastic Composite Structures. Presented at the 20th Conference of the Society of Plastics Industry, Inc. Chicago, Illinois, February 1965, P. 9F.
13. D. F. Adams and D. R. Doner. Longitudinal Shear Loading of Unidirectional Composites. Journal of Composite Materials, Vol. 1, No. 1, January 1967, P 11.
14. L. B. Greszczuk. Interfiber Stresses in Filamentary Composites. MDAC Paper 4771, Presented at the AIAA/ASME 11th Structures, Structural Dynamics, and Materials Conference, Denver, Colorado, April 1970.

Appendix

COMPOSITE SPECIMEN TEST DATA

Table 1A

COMPOSITIONS AND CURE CYCLES FOR RESINS AND COMPOSITES

Soft Resin (Urethane)	Hard Resin (Hysol)
<ol style="list-style-type: none"> <li>1. Heat resin (Hysol 2085) to 248°F</li> <li>2. Deaerate</li> <li>3. Cool to 176°F</li> <li>4. Heat hardner (Hysol 3562) to 194°F</li> <li>5. Mix 100 pbw resin with 24 pbw hardner and deaerate</li> <li>6. Preheat mold to 176°F</li> <li>7. Cast mixed resin in the mold</li> <li>8. Cure at 284°F for 1.5 hr</li> <li>9. Postcure at 212°F for 4 hr</li> <li>10. Cool and remove from mold</li> </ol>	<ol style="list-style-type: none"> <li>1. Mix 100 pbw of resin (Hysol 2039) with 29 pbw of hardner (Hysol 3561)</li> <li>2. Deaerate</li> <li>3. Cast in mold</li> <li>4. Cure at 70°F for 72 hr</li> </ol>

Table 2A  
TEST RESULTS ON FIVE-FIBER COMPOSITE COMPRESSION SPECIMENS

Specimen Number	Resin	Average Fiber Dia. (in)	Specimen Dia. (in)	Specimen Length (in)	Fiber Volume k (%)	Failure Load (lbs)	Composite Failure Stress $\times 10^{-3}$ psi	Fiber Stress $\times 10^{-3}$ psi	Remarks on Failure
1	Hysol	0.0783	0.223	0.750	61.6	1240	31,710	50.5	Shear of fibers
2	Hysol	0.0783	0.223	0.500	61.6	1180	30,180	48.0	Shear of fibers
3	Hysol	0.0783	0.223	1.000	61.6	1240	31,710	50.5	Shear of fibers
4	Urethane	0.0793	0.210	1.523	69.7	895	23,260	33.4	Combined (Shear + ) at mid section
5	Urethane	0.0793	0.210	1.025	69.7	1020	29,500	42.4	(a) Columnar shear. Fiber Splitting
6	Urethane	0.0793	0.211	0.770	69.7	1085	31,000	44.5	(a)
7	Urethane	0.0793	0.215	0.527	69.7	1060	(29,200)	(41.9)	Mixed, one fiber split; some shear failure at ends
8	Urethane	0.0793	0.217	1.886	66.7	658	17,800	26.7	Center, Buckling
9	Urethane	0.0793	0.217	2.540	66.7	446	12,050	18.1	Center, Buckling
10	RTC	0.0797	0.214	1.010	70.3	1350	37,500	52.6	Shear; blew up
11	RTC	0.0797	0.215	0.754	70.3	1385	38,100	53.5	Shear & split fibers
12	RTC	0.0797	0.212	0.523	70.3	1413	40,100	56.4	Shear, blew up

(a) End crushing apparent before splitting fiber.

Table 3A  
COMPRESSION TEST DATA ON NINE-FIBER COMPOSITES

Resin	Specimen Designation	Dim. of Cross Section (in)	Specimen Length (in)	Fiber Dia. (in)	Fiber Vol.	Failure Load (Lbs)	Composite Failure Stress x10 <sup>-3</sup> psi	Fiber Stress x10 <sup>-3</sup> psi	Young's Modulus x10 <sup>-6</sup> psi	Failure Type
U R E T H A N E	4b	0.2865x0.288	0.779	0.0750	0.481	(1780)	(21.60)	(44.9)	-	End crushing
	4a	0.286 x0.287	2.00	0.0750	0.484	860	10.50	21.7	5.12	Center (microbuckling)
	5a	0.286 x0.289	1.00	0.0753	0.484	(1470)	(17.77)	(36.8)	6.19	End crushing
	5b	0.287 x0.289	1.50	0.0753	0.483	1050	12.68	46.20	7.04	Center (microbuckling) Some end crushing
	6-3	0.288 x0.283	3.163	0.0747	0.483	492	6.03	12.48	5.58	Center (microbuckling)
	7-3a	0.282 x0.288	0.527	0.0784	0.534	1850	22.80	42.7	-	Center, Shear*
	7-3b	0.282 x0.288	0.503	0.0784	0.534	(1440)	(17.75)	(33.2)	-	Cup failure
	7-3c	0.282 x0.288	0.777	0.0784	0.534	1970	24.26	45.5	-	Near end*
	7-3d	0.282 x0.288	3.116	0.0784	0.534	58	6.87	12.9	-	Microbuckling
	25K	0.478 x0.478	4.530	0.0792	0.533	1245	5.44	10.10	-	Microbuckling
	7b	0.287 x0.286	0.779	0.0732	0.462	2550	31.10	64.5	-	Center, Shear
	7a	0.287 x0.288	2.003	0.0732	0.457	505	50.30	63.4	5.01	Near End
S O L	6c	0.287 x0.287	0.505	0.0746	0.477	2920	35.40	71.4	-	Center, Shear
	6b	0.285 x0.286	0.778	0.0746	0.482	2980	36.60	73.1	-	Center, Shear
	6a	0.286 x0.287	1.002	0.0746	0.474	2880	35.20	70.7	-	Test Sect, Shear

The ends of these specimens were encapsulated in plastic cups filled with Hysol.

The properties of resins used to make the various urethane specimens were as follows:

Urethane 4: E 1910 psi; ν 0.476  
Urethane 5: E 1010 psi; ν 0.467  
Urethane 6-3: E 2263 psi;  
Urethane 7-3: E 1664 psi  
Urethane 25R: E 2634 psi

(The resin formulation and cure cycle for this resin and composites made with this resin are shown in Table 5A.)

Table 4A  
 COMPRESSION TEST DATA ON HYSOL RESIN--  
 GRAPHITE "FIBER" COMPOSITES

Material	Specimen Designation	Dimensions of Cross Section (in.)	Specimen Length (in.)	Average Filer Diam. (in.)	Fiber Volume (%)	Failure Load (lbs)	Composite Failure Stress x10 <sup>-3</sup> (psi)	Fiber (2) Stress at Failure x10 <sup>-3</sup> (psi)	Young's (1) Modulus x10 <sup>-6</sup> (psi)	Failure (3) Location and Other Information
Composite	30a	0.1135 x 0.1145	0.4566	0.03008	49.2	475	36,540	71,400	---	Test Section Test Section Test Section
	30b	0.1145 x 0.1125	0.4562	0.03008	49.7	460	35,660	69,200	---	
	30c	0.1135 x 0.1150	0.7988	0.03008	49.0	375	28,700	56,500	5.38	
	Average				49.3		33,600	5,700		
	45a	0.1702 x 0.1705	0.6802	0.04512	49.7	1,020	35,170	68,100	---	Test Section Near End Test Section
	45b	0.1700 x 0.1705	1.190	0.04512	49.6	940	32,550	61,700	5.81	
	45c	0.1705 x 0.1701	0.679	0.04512	49.6	920	31,800	61,700	---	
	Average				49.6		33,200	64,200		
	60a	0.2270 x 0.2270	0.905	0.06028	49.8	1,820	35,300	68,300	---	Test Section Near End
	60b	0.2255 x 0.2255	1.582	0.06028	50.2	1,750	34,200	65,500	5.72	
Average				50.0		34,750	66,900	---		
79a	0.2870 x 0.2868	0.7065	0.07956	54.3	2,950	35,840	64,000	---	Test Section Test Section Test Section	
79b	0.2860 x 0.2868	2.0095	0.07956	54.5	2,990	36,400	64,700	6.92		
79c	0.2864 x 0.2865	2.992	0.07560	49.2	2,550	31,060	61,000	---		
Average				52.7		34,400	63,200			
Resin	R-1	0.434 x 0.434	1.0004	---	0	1,660	8,855 (ULT)	---	0.467	v = 0.374
	R-2	0.433 x 0.433	1.5003	---	0	1,875	9,950 (ULT)	---	0.464	v = 0.363
	Average						9,400		0.476	v = 0.368

(1) Strain gages were used to measure Young's modulus and Poisson's ratio

(2) Calculated from the following approximate equation

$$\sigma_c = \frac{\sigma_f}{k} [1 - (E_r/E_c)(1 - k)]$$

Where  $\sigma_c$  = composite failure stress;  $E_r$  = Young's modulus of resin;  $E_c$  = Young's modulus of composite; k = fiber volume fraction

Table 5A

COMPOSITION AND MODIFIED CURE CYCLE FOR  
URETHANE RESIN AND URETHANE RESIN COMPOSITE

1. Heat resin (Hysol 2085) to 248°F
2. Deaerate
3. Cool to 176°F
4. Heat Hardner (Hysol 3562) to 194°F
5. Mix 100 pbw of resin with 24 pbw of hardner and deaerate
6. Preheat mold to 176°F
7. Cost mixed resin in mold
8. Leave at 70°F for 48 hr
9. Place in cold oven
10. Heat oven to 200°F
11. Cure at 200°F for 4 hr
12. Cool in oven and remove from mold

Table 6A  
TEST RESULTS ON RESINS AND ON MICROBUCKLING  
COMPRESSION SPECIMENS

Spec Number	Type of Material	Dim. of Cross Section (in.)	Specimen Length (in.)	Fiber Dia. (in.)	Fiber Vol (%)	Failure Load (lbs)	Composite Failure Stress $\times 10^{-3}$ psi	Fiber Stress to Failure $\times 10^{-3}$ psi	Young's Modulus (psi)	Failure Type
9R	9-Rod Graphite-Urethane Composite	0.113 x 0.115	1.266	0.030	48.8	71	5.450	11.190	---	Microbuckling
R-1	Urethane Resin For 9-Rod Composite	0.448 x 0.448	1.037	---	---	--	---	---	2,399	Not Tested To Failure
R-2	Urethane Resin For 9-Rod Composite	0.450 x 0.448	1.025	---	---	---	---	---	2,362	Not Tested To Failure
25R	25-Rod Graphite Urethane Composite	0.478 x 0.0478	4.350	0.0792	53.8	1,245	5.440	10.100	---	Microbuckling
R-3	Urethane Resin For 25-Rod Specimen	0.377 x 0.377	1.003	---	---	---	---	---	2,574	Not Tested To Failure
R-4	Urethane Resin For 25-Rod Specimen	0.379 x 0.379	1.003	---	---	---	---	---	2,694	Not Tested To Failure

Table 7A  
COMPRESSION DATA ON URETHANE RESIN COMPOSITES

Fiber Material	Specimen Designation	Dimensions of Cross Section (in.)	Specimen Length (in.)	Average Fiber Diameter (in.)	Fiber Volume (%)	Failure Load (lbs)	Composite Failure Stress x10 <sup>-3</sup> (psi)	Fiber Stress at Failure x10 <sup>-3</sup> (psi)	Young's Modulus x10 <sup>-6</sup> (psi)	Remarks on Failure Type and Location
Graphite Fibers	U1-1G	0.292 x 0.292	1.322	0.07917	51.9	1730	20,300	39,100	—	Center; microbuckling
	U1-2G	0.292 x 0.292	2.500	0.07917	51.9	810	9,500	18,300	5.63	Center; microbuckling
	U2-1G	0.292 x 0.292	1.322	0.07906	51.8	1755	20,600	39,800	—	Center; microbuckling
	U2-2G	0.292 x 0.292	2.498	0.07906	51.8	730	8,560	16,500	6.62	Center; microbuckling
S Steel Fibers	U1-1S	0.292 x 0.293	1.322	0.0782	50.5	6450	75,400	149,200	—	Microbuckling; permanent deformation
	U1-2S	0.292 x 0.293	2.499	0.0782	50.5	2280	26,650	57,800	—	Microbuckling; permanent deformation
	U2-1S	0.292 x 0.293	1.322	0.0782	50.5	6800	79,400	157,200	—	Elastic microbuckling
	U2-2S	0.292 x 0.293	2.500	0.0782	50.5	2250	26,300	52,100	—	Elastic microbuckling

Table 8A  
COMPRESSION DATA ON COMPOSITES MADE WITH EPOXY A

Fiber Material	Specimen Designation	Dimensions of Cross Section (in.)	Specimen Length (in.)	Average Fiber Diameter (in.)	Fiber Volume (%)	Failure Load (lbs)	Composite Failure Stress x10 <sup>-3</sup> (psi)	Fiber Stress at Failure x10 <sup>-3</sup> (psi)	Young's Modulus x10 <sup>-6</sup> (psi)	Remarks on Failure Type and Location
Graphite	A1-2G	0.288 x 0.288	2.501	0.07884	52.8	2250	27.20	50.90	5.88	Longitudinal cracks; shear failure of fibers near end
	A2-1G	0.288 x 0.288	1.499	0.07894	53.0	2350	28.40	53.00	—	Longitudinal cracks; shear failure of fibers near end
	A2-2G	0.288 x 0.288	2.499	0.07894	53.0	2270	27.40	51.10	6.15	Longitudinal cracks; shear failure of fibers near end
S. Steel	A1-1S	0.288 x 0.288	1.499	0.0780	51.8	9900	119.40	229.50	—	Yielding
	A1-2S	0.289 x 0.288	2.500	0.0780	51.6	7060	84.90	163.20	13.62	Elastic Microbuckling

Table 9A  
 COMPRESSION DATA ON COMPOSITES  
 MADE WITH EPOXY B

Fiber Material	Specimen Designation	Dimensions of Cross Section (in.)	Specimen Length (in.)	Average Fiber Dia. (in.)	Fiber Volume (%)	Failure Load (lbe)	Composite Failure Stress x 10 <sup>-3</sup> (psi)	Fiber Stress at Failure x 10 <sup>-3</sup> (psi)	Young's Modulus x 10 <sup>-6</sup> (psi)	Remarks on Failure Type and Location
"Graphite"	B1-1G	0.289 x 0.289	1.498	0.07918	53.0	2190	26.20	48.90	—	Longitudinal crack; shear failure of fiber near end.
	B1-2G	0.288 x 0.289	2.500	0.07918	53.1	(1500)	(18.03)	(33.60)	5.63	End crushing; some shear failure of fibers.
	B2-2G	0.288 x 0.290	2.50	0.0789	52.9	2000	24.05	45.00	5.17	Shear failure of fibers near end
S. Steel	B1-1S	0.289 x 0.288	1.50	0.0782	51.9	8400	101.00	195.00	—	Longitudinal cracks and possibly inelastic microbuckling
	B2-2S	0.288 x 0.288	2.499	0.0782	52.0	5350	64.30	123.60	16.15	Elastic microbuckling